

**CATALYTIC METHANE PARTIAL OXIDATION OVER SILICA AND SILICA  
SUPPORTED IRON PHOSPHATE**

**ARTHUR LAKES LIBRARY  
COLORADO SCHOOL OF MINES  
GOLDEN, CO 80401**

by

**Mohammad B. Al-Sahali**

ProQuest Number: 10796876

All rights reserved

INFORMATION TO ALL USERS

The quality of this reproduction is dependent upon the quality of the copy submitted.

In the unlikely event that the author did not send a complete manuscript and there are missing pages, these will be noted. Also, if material had to be removed, a note will indicate the deletion.



ProQuest 10796876

Published by ProQuest LLC (2019). Copyright of the Dissertation is held by the Author.

All rights reserved.

This work is protected against unauthorized copying under Title 17, United States Code  
Microform Edition © ProQuest LLC.

ProQuest LLC.  
789 East Eisenhower Parkway  
P.O. Box 1346  
Ann Arbor, MI 48106 – 1346

A thesis submitted to the Faculty and Board of Trustees of the Colorado School of Mines in partial fulfillment of the requirements for the degree of Doctor of Philosophy (Chemical and Petroleum-Refining Engineering).

Golden, Colorado

Date Dec 5, 2000

Signed: Mohammad Al-Sahali  
Mohammad B. Al-Sahali

Approved: Robert L. McCormick  
Dr. Robert L. McCormick  
Thesis Advisor

Golden, Colorado

Date 12/05/00

James F. Ely  
Dr. James F. Ely  
Professor and Head,  
Department of  
Chemical Engineering and Petroleum Refining

## ABSTRACT

Methane partial oxidation by molecular oxygen over silica and iron phosphate/silica catalysts has been studied in the temperature range of 848-898 K and at atmospheric pressure. Carbon monoxide, carbon dioxide, formaldehyde and water are the principal reaction products over both catalysts. Changes in product selectivity with methane conversion indicate two reaction pathways; a sequential route from methane to formaldehyde then to carbon monoxide in turn to carbon dioxide and a parallel route to carbon dioxide directly.

Reactions of intermediate species were also studied under atmospheric pressure but at lower temperatures because these reactants are too reactive at high temperature. It was found that silica and iron phosphate/silica catalysts affect the reactions in the same manner. Minor differences were found in the kinetic studies, which confirm that silica is the actual catalyst and iron phosphate is a promoter.

An inhibiting effect was discovered for carbon monoxide over both catalysts when carbon monoxide oxidation was carried out. It was proposed that the inhibition is caused by strong adsorption of carbon monoxide on the catalyst surface. This observation is connected to the positive oxygen dependence reported for methane partial oxidation over many catalysts. The competition between reaction products and oxygen for the active sites cause the high oxygen reaction order. In reoxidation reactions, the reaction dependence on

oxygen is usually assumed to be zero order and the hydrocarbons are first order. The rate-limiting step in these reactions is assumed to be the hydrocarbon activation. In this work, it was found that surface re-oxidation (oxygen chemisorption) occurs at a rate comparable to that of hydrocarbon activation. Over the iron phosphate/silica catalyst, methane activation and surface reoxidation occur at comparable rates. Actually active oxygen species are necessary for methane activation and oxygen adsorption is the rate-limiting step.

Methane oxidation pulse studies were also carried out to investigate the role of molecular and lattice oxygen in the reaction network. Lattice oxygen participation in the reaction was ruled out under the reaction conditions. The presence of gaseous oxygen is required for the reaction to proceed.

Pulse experiments helped identify the intermediate responsible for the direct path from methane to carbon dioxide. Formic acid was observed after a number of pulses, it seems that this intermediate builds up on the catalyst surface. It should be mentioned that this is the first time that formic acid has been detected in methane partial oxidation. Because of the direct correlation between the carbon dioxide and formic acid formation rates, it is proposed that formic acid is converted to carbon dioxide. Methanol, a suggested intermediate for the methane partial oxidation reaction, was not observed for silica or silica-supported iron phosphate.

The presence of iron phosphate on silica doubled the active site density. The population of the reduced sites on the catalyst surface during methane oxidation is significantly impacted by subsequent reactions of formaldehyde and carbon monoxide. Thus these reactions must be included in any kinetic model that explicitly includes surface sites.

In the modeling section, the surface reduction/oxidation state is extensively studied. The effect of the reaction products on the fraction of reduced sites was investigated. It was found that there is a relation between the catalyst activity and its fractional reduced density. Methane activation and surface reoxidation have been also examined. Over iron phosphate/silica, these two steps are more important than over silica.

## TABLE OF CONTENT

	Page
ABSTRACT .....	iii
LIST OF FIGURES .....	x
LIST OF TABLES .....	xvi
ACKNOWLEDGMENTS .....	xviii
DEDICATION .....	xix
<b>Chapter 1. INTRODUCTION</b> .....	<b>1</b>
1.1 Objectives and Scope of This Study .....	3
<b>Chapter 2. LITERATURE REVIEW</b> .....	<b>5</b>
2.1 Methane Conversion .....	5
2.1.1 Synthesis Gas Route .....	5
2.1.2 Direct Oxidation Route .....	6
2.2 Thermodynamic Stability .....	6
2.3 Direct Methane Partial Oxidation Catalysis .....	7
2.3.1 Vanadium and Molybdenum Oxides .....	8
2.3.2 Phosphate Catalysts .....	10
2.3.2.1 Vanadyl Pyrophosphate (VPO) Catalysts .....	10
2.3.2.2 Iron Phosphate (FePO <sub>4</sub> ) Catalysts .....	10
2.3.2.2.1 Macro-kinetics of Methane Oxidation Over Iron Phosphate Catalysts .....	11
2.3.2.2.2 The Effect of Catalyst Loading and Support .....	14
2.3.2.2.3 Catalyst Characterization .....	14
2.4 Silica as a Catalyst .....	16
2.5 Carbon Monoxide, Formaldehyde and Methanol Oxidation .....	17
2.5.1 Carbon Monoxide Oxidation .....	17
2.5.2 Formaldehyde Oxidation .....	18

2.5.3	Methanol Oxidation .....	18
2.6	Methane Oxidation Transient Studies .....	19
2.7	Characterization of the Catalyst Surface .....	21
2.7.1	Oxygen Chemisorption .....	21
2.7.2	Infrared Spectroscopy .....	22
2.8	Modeling Methane Partial Oxidation .....	25
2.8.1	Macro-kinetic Analysis of Methane Oxidation .....	25
2.8.2	Micro-kinetic Analysis of Methane Oxidation .....	26
2.9	Economics and Engineering .....	29
Chapter 3.	EXPERIMENTAL SECTION .....	35
3.1	Introduction .....	35
3.2	Experimental Setup and Procedure .....	36
3.2.1	Catalyst Preparation .....	36
3.2.1.1	Precipitated Silica .....	36
3.2.1.2	Silica Supported Iron Phosphate .....	36
3.2.2	Catalyst Testing .....	37
3.2.2.1	Continuous/Pulse Reactor Studies .....	37
3.2.2.2	Oxygen Chemisorption .....	43
3.2.2.3	Fourier Transform Infrared Spectroscopy (FTIR) .....	43
Chapter 4.	METHANE PARTIAL OXIDATION OVER SILICA .....	46
4.1	Flow Reactor Studies .....	46
4.1.1	Carbon Monoxide Oxidation .....	47
4.1.2	Formaldehyde Oxidation .....	50
4.1.3	Methanol Oxidation .....	54
4.1.4	Methane Oxidation .....	58
4.2	Pulse Reactor Studies .....	63
4.2.1	The Role of Gaseous and Lattice Oxygen .....	63
4.2.2	The Effect of Different Pretreatment on the Catalyst surface .....	65
4.2.3	Investigating Unknown Peak .....	65
4.3	Oxygen Chemisorption .....	68
4.4	In-situ IR Experiment .....	69
Chapter 5.	METHANE PARTIAL OXIDATION OVER SILICA	
	SUPPORTED IRON PHOSPHATE .....	75

5.1	Flow Reactor Studies .....	75
5.1.1	Carbon Monoxide Oxidation .....	76
5.1.2	Formaldehyde Oxidation .....	79
5.1.3	Methanol Oxidation .....	83
5.1.4	Methane Oxidation .....	87
5.2	Pulse Reactor Studies .....	92
5.2.1	The Role of Gaseous and Lattice Oxygen .....	92
5.2.2	The Effect of Different Pretreatment on the Catalyst surface .....	94
5.2.3	Investigating Unknown Peak .....	94
5.3	Oxygen Chemisorption .....	97
5.4	In-situ IR Experiment .....	97
Chapter 6.	DISCUSSION AND COMPARISON .....	103
6.1	Background and Objectives .....	103
6.2	Comparing SiO <sub>2</sub> and FePO <sub>4</sub> /SiO <sub>2</sub> .....	105
6.3	Chemisorbed Oxygen .....	110
6.4	Carbon Monoxide Inhibition .....	114
6.5	Enhanced Formaldehyde Yield .....	116
6.6	Adding Silver to Improve Surface Re-oxidation .....	117
6.7	Formic Acid Intermediate and the Reaction Network .....	120
Chapter 7.	MODELING METHANE PARTIAL OXIDATION .....	122
7.1	Introduction .....	122
7.2	Simple Model Comparison .....	124
7.2.1	Mars and Van Krevelen Model .....	124
7.2.2	Arena Model .....	125
7.3	Mathematical Models .....	126
7.3.1	Reactants Pressure Effect on $\theta_{red}$ .....	127
7.3.2	Products Pressure Effect on $\theta_{red}$ .....	129
7.4	Methane Oxidation over Silica .....	131
7.5	Methane Oxidation over Iron Phosphate/Silica .....	136
7.6	Rate Constants Sensitivity Analysis .....	140
Chapter 8.	CONCLUSION AND RECOMMENDATIONS .....	141
8.1	Conclusions .....	141
8.2	Recommendations .....	142

REFERENCES CITED .....	144
APPENDIX A: CO Adsorption Experiments over SiO <sub>2</sub> and FePO <sub>4</sub> /SiO <sub>2</sub> .....	150
APPENDIX B: Methane Partial Oxidation over Ag/SiO <sub>2</sub> and Ag-FePO <sub>4</sub> /SiO <sub>2</sub> .....	157
APPENDIX C: Experimental Data Used in Calculating Fractional Reduced Site Density .....	167
APPENDIX D Quadrature Method .....	170

## LIST OF FIGURES

	Page
Figure 1.1 Methane Conversion to Methanol and Formaldehyde .....	2
Figure 2.1 Catalysts Structure .....	15
Figure 2.2 Methane Partial Oxidation Over Silica Supported MoO <sub>3</sub> and V <sub>2</sub> O <sub>5</sub> .....	28
Figure 2.3 Methane Industrial Processes .....	31
Figure 2.4 Case Study for Methane Partial Oxidation Plant .....	33
Figure 3.1 Reactor System .....	38
Figure 3.2 Flow Reactor .....	39
Figure 3.3 Pulse Reactor .....	40
Figure 3.4 Reaction Chamber for In-situ IR Experiments .....	45
Figure 4.1 Effect of reactants partial pressure on carbon monoxide oxidation rate over silica. GHSV= 40000 h <sup>-1</sup> , P <sub>O<sub>2</sub></sub> =2-9 kPa@P <sub>CO</sub> =9 kPa, P <sub>CO</sub> =2.5-10 kPa @ P <sub>O<sub>2</sub></sub> =2.5 kPa, , and T=673 K .....	48
Figure 4.2 Arrhenius plot for carbon monoxide oxidation over silica. P <sub>CO</sub> = P <sub>O<sub>2</sub></sub> = 9 kPa and T=673-733 K .....	49
Figure 4.3 Effect of reactants partial pressure on formaldehyde oxidation rate over silica. GHSV= 25000 h <sup>-1</sup> , P <sub>O<sub>2</sub></sub> = 23-76 kPa @ P <sub>HCHO</sub> = 4 kPa, P <sub>HCHO</sub> = 4-15 kPa @ P <sub>O<sub>2</sub></sub> = 50 kPa and T= 648 K .....	51

Figure 4.4	Arrhenius plot for formaldehyde oxidation over silica. $P_{O_2} = 50$ kPa, $P_{HCHO} = 4.5$ kPa, and $T=648-723$ K .....	52
Figure 4.5	Product selectivity (%) as a function of formaldehyde conversion (%) for silica. GHSV= 5000-45000 $h^{-1}$ , $P_{O_2} = 50$ kPa, $P_{HCHO} = 4.5$ kPa, and $T= 623-673$ K .....	53
Figure 4.6	Effect of reactants partial pressure on methanol oxidation rate over silica. GHSV= 35000 $h^{-1}$ , $P_{O_2} = 18-63$ kPa @ $P_{CH_3OH} = 24$ kPa, $P_{CH_3OH} = 33-42$ kPa @ $P_{O_2} = 33$ kPa and $T= 723$ K .....	55
Figure 4.7	Arrhenius plot for methanol oxidation over silica. $P_{O_2} = 50$ kPa, $P_{CH_3OH} = 6$ kPa, and $T=673-773$ K .....	56
Figure 4.8	Product selectivity (%) as a function of methanol conversion (%) for silica. GHSV= 5000-45000 $h^{-1}$ , $P_{O_2} = 50$ kPa, $P_{CH_3OH} = 6$ kPa, and $T= 673-773$ K .....	57
Figure 4.9	Effect of reactants partial pressure on methane oxidation rate over silica. GHSV= 30000 $h^{-1}$ , $P_{O_2} = 9-40$ kPa @ $P_{CH_4} = 40$ kPa, $P_{CH_4} = 9-50$ kPa @ $P_{O_2} = 9$ kPa and $T= 873$ K .....	59
Figure 4.10	The effect of oxygen partial pressure on methane partial oxidation rate over silica. GHSV=30000 $h^{-1}$ , $P_{O_2}=9-40$ kPa @ $P_{CH_4}=40$ kPa .....	60
Figure 4.11	Arrhenius plot for methane oxidation over silica. $P_{O_2} = 20$ kPa, $P_{CH_4} = 40$ kPa, and $T=823-898$ K .....	61
Figure 4.12	Product selectivity (%) as a function of methane conversion (%) for silica. GHSV= 30000 $h^{-1}$ , $P_{O_2} = 20$ kPa, $P_{CH_4} = 40$ kPa, and $T= 823-898$ K .....	62
Figure 4.13	Mass spectral gas analysis of the effluent from pulse experiment Over $SiO_2$ at $T=873$ K and $P_{O_2}=P_{CH_4}= 40$ kPa .....	67
Figure 4.14	IR spectra of methanol oxidation over silica at $T=673$ K: a. Before oxidation, Ar was introduced for 1 hr. b. During reaction, $CH_3OH + O_2$ was introduced for 1 hr. c. After oxidation, Ar was introduced for 1 hr .....	71

Figure 4.15	IR spectra of methanol adsorption over silica at T=298 K: a. Before adsorption, Ar was introduced for 1 hr. b. During adsorption, CH <sub>3</sub> OH was introduced for 1 hr. c. After adsorption, Ar was introduced for 1 hr .....	72
Figure 4.16	IR spectra of methanol adsorption over silica at T=473 K: (B) Before adsorption, Ar was introduced for 1 hr. (C) During adsorption, CH <sub>3</sub> OH was introduced for 1 hr. c. After adsorption, Ar was introduced for 1 hr .....	73
Figure 4.17	IR spectra of methanol adsorption over silica at T=673 K: a. Before adsorption, Ar was introduced for 1 hr. b. During adsorption, CH <sub>3</sub> OH was introduced for 1 hr. c. After adsorption, Ar was introduced for 1 hr .....	74
Figure 5.1	Effect of reactants partial pressure on carbon monoxide oxidation rate over silica supported iron phosphate. GHSV= 40000 h <sup>-1</sup> , P <sub>O<sub>2</sub></sub> =2-9 kPa@P <sub>CO</sub> =9 kPa, P <sub>CO</sub> =2.5-10 kPa @ P <sub>O<sub>2</sub></sub> =2.5 kPa, , and T=673 K .....	77
Figure 5.2	Arrhenius plot for carbon monoxide oxidation over silica supported Iron phosphate. P <sub>CO</sub> = P <sub>O<sub>2</sub></sub> = 9 kPa and T=673-733 K .....	78
Figure 5.3	Effect of reactants partial pressure on formaldehyde oxidation rate over silica supported iron phosphate. GHSV= 25000 h <sup>-1</sup> , P <sub>O<sub>2</sub></sub> = 23-76 kPa @ P <sub>HCHO</sub> = 4 kPa, P <sub>HCHO</sub> = 4-15 kPa @ P <sub>O<sub>2</sub></sub> = 50 kPa and T= 648 K .....	80
Figure 5.4	Arrhenius plot for formaldehyde oxidation over silica supported iron phosphate. P <sub>O<sub>2</sub></sub> = 50 kPa, P <sub>HCHO</sub> = 4.5 kPa, and T=648-723 K .....	81
Figure 5.5	Product selectivity (%) as a function of formaldehyde conversion (%) for silica supported iron phosphate. GHSV= 5000-45000 h <sup>-1</sup> , P <sub>O<sub>2</sub></sub> = 50 kPa, P <sub>HCHO</sub> = 4.5 kPa, and T= 623-673 K .....	82
Figure 5.6	Effect of reactants partial pressure on methanol oxidation rate over silica supported iron phosphate. GHSV= 35000 h <sup>-1</sup> , P <sub>O<sub>2</sub></sub> = 18-63 kPa @ P <sub>CH<sub>3</sub>OH</sub> = 24 kPa, P <sub>CH<sub>3</sub>OH</sub> = 33-42 kPa @ P <sub>O<sub>2</sub></sub> = 33 kPa and T= 723 K .....	84

Figure 5.7	Arrhenius plot for methanol oxidation over silica supported iron phosphate. $P_{O_2} = 50$ kPa, $P_{CH_3OH} = 6$ kPa, and $T=673-773$ K .....	85
Figure 5.8	Product selectivity (%) as a function of methanol conversion (%) for silica supported iron phosphate. $GHSV= 5000-45000$ $h^{-1}$ , $P_{O_2} = 50$ kPa, $P_{CH_3OH} = 6$ kPa, and $T= 673-773$ K .....	86
Figure 5.9	Effect of reactants partial pressure on methane oxidation rate over silica supported iron phosphate. $GHSV= 30000$ $h^{-1}$ , $P_{O_2} = 9-40$ kPa @ $P_{CH_4} = 40$ kPa, $P_{CH_4} = 9-50$ kPa @ $P_{O_2} = 9$ kPa and $T= 873$ K .....	88
Figure 5.10	The effect of oxygen partial pressure on methane partial oxidation rate over silica supported iron phosphate. $GHSV=30000$ $h^{-1}$ , $P_{O_2}=9-40$ kPa @ $P_{CH_4}=40$ kPa .....	89
Figure 5.11	Arrhenius plot for methane oxidation over silica supported iron phosphate. $P_{O_2} = 20$ kPa, $P_{CH_4} = 40$ kPa, and $T=823-898$ K .....	90
Figure 5.12	Product selectivity (%) as a function of methane conversion (%) for silica supported iron phosphate. $GHSV= 30000$ $h^{-1}$ , $P_{O_2} = 20$ kPa, $P_{CH_4} = 40$ kPa, and $T= 823-898$ K .....	91
Figure 5.13	Mass spectral gas analysis of the effluent from pulse experiment Over $FePO_4/SiO_2$ at $T=873$ K and $P_{O_2}=P_{CH_4}= 40$ kPa .....	96
Figure 5.14	IR spectra of methanol oxidation over silica supported catalyst at $T=673$ K: a. Before oxidation, Ar was introduced for 1 hr. b. During reaction, $CH_3OH + O_2$ was introduced for 1 hr. c. After oxidation, Ar was introduced for 1 hr .....	99
Figure 5.15	IR spectra of methanol adsorption over silica supported iron phosphate catalyst at $T=298$ K: a. Before adsorption, Ar was introduced for 1 hr. b. During adsorption, $CH_3OH$ was introduced for 1 hr. c. After adsorption, Ar was introduced for 1 hr .....	100

Figure 5.16	IR spectra of methanol adsorption over silica supported iron phosphate catalyst at T=473 K: a. Before adsorption, Ar was introduced for 1 hr. b. During adsorption, CH <sub>3</sub> OH was introduced for 1 hr. c. After adsorption, Ar was introduced for 1 hr .....	101
Figure 5.17	IR spectra of methanol adsorption over silica supported iron phosphate catalyst at T=673 K: a. Before adsorption, Ar was introduced for 1 hr. b. During adsorption, CH <sub>3</sub> OH was introduced for 1 hr. c. After adsorption, Ar was introduced for 1 hr .....	102
Figure 6.1	The effect of oxygen partial pressure on methane oxidation rate over silica and silica supported catalyst. GHSV=30000 h <sup>-1</sup> , P <sub>O<sub>2</sub></sub> =9-40 @ P <sub>CH<sub>4</sub></sub> = 40 kPa .....	112
Figure 6.2	CO <sub>2</sub> production rate as a function of the reactants partial pressure Over silica and silica supported catalyst. GHSV=40000h <sup>-1</sup> , P <sub>O<sub>2</sub></sub> =2-9 kPa @ P <sub>CO</sub> =9 kPa, P <sub>CO</sub> =2.5-10 kPa @ P <sub>O<sub>2</sub></sub> =2.5 kPa and T=673 K .....	115
Figure 6.3	Product selectivity (%) as a function of methane conversion (%) for Ag-FePO <sub>4</sub> /SiO <sub>2</sub> . GHSV= 12000-60000 h <sup>-1</sup> , P <sub>O<sub>2</sub></sub> = 17-26 kPa, P <sub>CH<sub>4</sub></sub> = 34-52 kPa, P <sub>CH<sub>4</sub></sub> /P <sub>O<sub>2</sub></sub> = 2, and T= 823-898 K .....	119
Figure 7.1	Methane partial oxidation over silica at T=873K: (B) Fractional density of reduced sites versus inlet reactants pressure. (C) Log-log plot to find $\theta_{red}$ dependence on P <sub>CH<sub>4</sub></sub> and P <sub>O<sub>2</sub></sub> .....	133
Figure 7.2	Methane partial oxidation over silica at T=873K: (A) Fractional density of reduced sites versus products pressure. (B) Log-log plot to find $\theta_{red}$ dependence on P <sub>CH<sub>4</sub></sub> and P <sub>O<sub>2</sub></sub> .....	134
Figure 7.3	Comparing $\theta_{red}$ when using the reactants and products pressure Models over SiO <sub>2</sub> .....	135
Figure 7.4	Methane partial oxidation over iron phosphate/silica at T=873K: (A) Fractional density of reduced sites versus inlet reactants pressure. (B) Log-log plot to find $\theta_{red}$ dependence on P <sub>CH<sub>4</sub></sub> and P <sub>O<sub>2</sub></sub> .....	137

Figure 7.5	Methane partial oxidation over iron phosphate/silica at T=873K:	
	(A) Fractional density of reduced sites versus products pressure.	
	(B) Log-log plot to find $\theta_{\text{red}}$ dependence on $P_{\text{CH}_4}$ and $P_{\text{O}_2}$ .....	138
Figure 7.6	Comparing $\theta_{\text{red}}$ when using the reactants and products pressure	
	Models over $\text{FePO}_4/\text{SiO}_2$ .....	139

## LIST OF TABLES

	Page
Table 2.1 Kinetic Parameters and Yields for CH <sub>4</sub> Oxidation over Bulk and Silica supported FePO <sub>4</sub> .....	13
Table 2.2 Results Reported for the Methanol, Dimethyl Ether, Formaldehyde and Carbon Monoxide Oxidation/Hydration Reactions .....	20
Table 2.3 Cost of Transporting Fuel as a Function of Distance .....	30
Table 4.1 Methane Partial Oxidation in the Presence and Absence of Gas-phase Oxygen in Pulsed Reaction Experiment over SiO <sub>2</sub> .....	64
Table 4.2 Pulse Study Results for Methane Partial Oxidation over Silica at 873 K .....	66
Table 5.1 Methane Partial Oxidation in the Presence and Absence of Gas-phase Oxygen in Pulsed Reaction Experiment .....	93
Table 5.2 Pulse Study Results for Methane Partial Oxidation over Silica supported Iron Phosphate at 873 K .....	95
Table 6.1 Comparison of Results over Silica and Silica Supported Iron Phosphate .....	106
Table 6.2 Comparison of Turnover Frequency (TOF) for Silica and Silica Supported Iron Phosphate .....	107
Table 6.3 Results Reported for the Total Active Site Density on Silica and Silica Supported Catalysts .....	109
Table 6.4 Comparing Conversion-Selectivity and Reaction Rates for Different Catalysts .....	118

Table 7.1 Comparing Methane Reaction Rate (mol/(s.g)) for Different Models at T=600 C .....	126
Table 7.2 Kinetic Parameters for Methane Partial Oxidation .....	131

## ACKNOWLEDGMENTS

In the name of **ALLAH**, the Beneficent, the Merciful I started and ended this work that I hope it achieved its objectives. I am most grateful to Colorado School of Mines especially its library for their valuable help.

I wish to express my thanks and appreciation to my thesis advisor Dr. Robert L. McCormick for his helpful comments and valuable advice. I would like to thank Dr. Robert M. Baldwin for letting me use his mass spectrometer. I would also like to thank my committee members Dr. J. Douglas Way, Dr. Gaerne Fairweather and Dr. Baki Yarar.

The effort of Dr. Andrew Herring and Dr. Gokhan Alptekin in teaching me how to use most of the experimental devices is deeply appreciated. Thanks are extended to my friends for their support.

Finally, I would like to express my sincere appreciation to my family for their support and encouragement. Profound gratitude to my wife and children for their sacrifices that made this work possible.

**Dedicated to my Mother and Father**

## CHAPTER 1

### INTRODUCTION

Methane is the major component of natural gas and a by-product of oil production and refinery operations. Natural gas is currently utilized by direct delivery using pipelines and tankers or chemically converting methane to liquid fuels and chemicals. Methane is a low-cost carbon source with high energy content, therefore it is used primarily as a fuel. It is a highly symmetrical and stable molecule, and its direct conversion to other useful chemicals is not yet feasible because of the high C-H bond energy. The purpose of the work performed here is to more deeply understand the elementary reaction steps in catalytic methane oxidation to methanol and formaldehyde. Methane conversion to methanol and formaldehyde can be accomplished by two catalytic methods, via synthesis gas and direct oxidation. Figure 1.1 shows a block flow diagram for these two methods.

In the direct oxidation process, obtaining a high selectivity to methanol and formaldehyde is critical. Unfortunately these reaction products are much more reactive than methane and can be easily converted to carbon monoxide and carbon dioxide over most catalysts. By understanding the methane activation step, it may be possible to devise catalysts that are active at lower temperatures. Lower temperature should lead to improved selectivity.

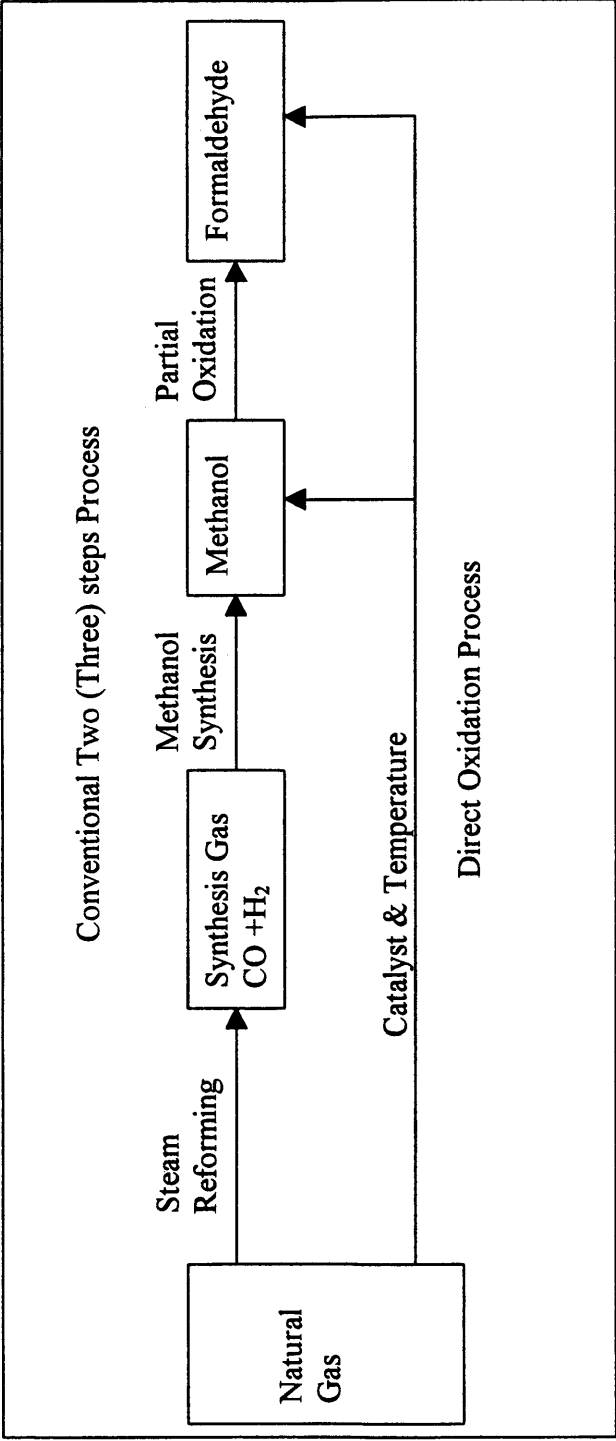


Figure 1.1 Methane Conversion to Methanol and Formaldehyde

However it is also important to fundamentally understand the reactions that convert desired products to carbon oxides in order to devise catalysts that are less active for these reactions.

### **1.1 Objectives and Scope of this Study**

The first objective of this work is to study the reactions that convert the desired products to carbon oxides and to fully understand their reaction network and macro-rates in order to devise catalysts that are less active for total oxidation. Also, investigating the oxidation of desired intermediates is necessary to evaluate model parameters (reactions rate constants) and the data collected can be used for model fitting and analysis.

Another goal is to reveal the role of silica and iron phosphate surfaces in methane partial oxidation and the interaction between the two surfaces for the supported catalyst.

A more specific objective is to identify the active sites and how these active sites activate methane and oxygen. Studying the rate-limiting step (thought to be methane activation) in methane partial oxidation is another goal. Understanding if this step is affected by product inhibition, or if there is a methane to oxygen pressure ratio at which the rate controlling step changes, are questions to be considered in this work.

To these ends, the oxidation of methanol, formaldehyde, CO, as well as methane has been studied over silica and silica-supported iron phosphate in a continuous reactor. Product yields as well as global reaction kinetics have been determined. A pulsed reactor has been used to investigate the role of gaseous versus lattice oxygen in methane

oxidation. The catalyst surface was examined by oxygen chemisorption to measure the number of surface sites, as well as via in-situ IR experiments. A simple model of the effect of methane oxidation and subsequent reactions on the fraction of oxidized surface sites was developed. A number of important new observations relevant to the kinetics and mechanism of oxidation reactions in this system are reported.

## CHAPTER 2

### LITERATURE REVIEW

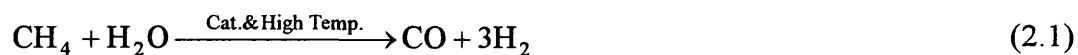
#### 2.1 Methane Conversion:

Methane is converted to formaldehyde and methanol through two techniques, either reforming methane to synthesis gas first, then converting the synthesis gas to methanol or by directly transforming methane to methanol and formaldehyde via one step process.

##### 2.1.1 Synthesis Gas Route

In practice, methane is converted to formaldehyde through a three-step process involving steam reforming at high temperature, methanol synthesis and partial oxidation of methanol to formaldehyde, Pitchai and Klier (1986). This three-step process occurs as follow:

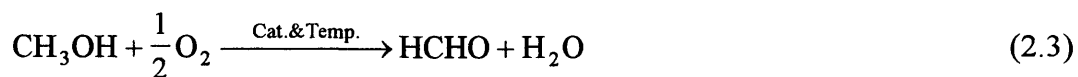
1. Steam Reforming:



2. Methanol Synthesis:



3. Methanol Partial Oxidation:



The steam-reforming step is highly endothermic and in practice oxygen is also fed to the reactor in step 1. Exothermic partial oxidation reactions provide heat for the reforming steps. This process is practiced on an extremely large scale all over the world.

### 2.1.2 Direct Oxidation Route

Unlike this multistage process, the direct conversion of methane to formaldehyde or methanol is an exothermic one-step process. The selective oxidation of methane can give either:



or



This processing approach has not been commercialized because of low product yield and very high process temperatures.

## 2.2 Thermodynamic Stability

Although methane partial oxidation to formaldehyde and methanol is thermodynamically feasible, the total oxidation of methane to carbon oxides is even more favored. The driving force for conversion of methane to various products is better presented in terms of Gibbs free energy, Pitchai and Klier (1986), as shown below:

Reaction	$\Delta G_{700K}^{\circ}$ kJ / mole
$\text{CH}_4 + \frac{1}{2}\text{O}_2 \rightarrow \text{CH}_3\text{OH}$	-111
$\text{CH}_4 + \text{O}_2 \rightarrow \text{HCHO} + \text{H}_2\text{O}$	-290
$\text{CH}_4 + \frac{3}{2}\text{O}_2 \rightarrow \text{CO} + 2\text{H}_2\text{O}$	-543
$\text{CH}_4 + 2\text{O}_2 \rightarrow \text{CO}_2 + 2\text{H}_2\text{O}$	-800

At the high temperatures used for this reaction, suppression of the subsequent oxidation of oxygenated products and the simultaneous direct oxidation of methane to carbon oxides is necessary if high product yields are to be obtained. To utilize methane selectively, a catalyst and reaction conditions are required to facilitate the formation of oxygenates without further oxidizing them.

### 2.3 Direct Methane Partial Oxidation catalysis:

A working catalyst for methane selective oxidation should possess dehydrogenation and oxygen insertion abilities. The dehydrogenation step is necessary to activate methane while oxygen insertion is needed to form oxygenates like formaldehyde and methanol. It has been shown that for saturated hydrocarbons, the first step in activating the molecule is the dissociation of the C-H bond in a manner similar to the production of hydrocarbon free radicals, Kung (1986), for methane this can lead to surface methoxide groups. There is evidence that high partial pressure steam may suppress sequential oxidation, Alptekin

(1998), and hydration of surface intermediates by surface hydroxyls may improve selectivity to methanol. Thus, catalysts such as phosphates that possess a hydration function may also be desirable.

### **2.3.1 Vanadium and Molybdenum oxides:**

The vast majority of studies into the catalytic partial oxidation of methane concentrated on metal oxides. Research has focused on molybdenum and vanadium based oxides as catalysts for methane partial oxidation to methanol and formaldehyde. Among the different supports studied, silica was found to be the most effective in increasing formaldehyde yield, Alptekin (1998) and Parmaliana et al. (1994). Comparing silica supported  $V_2O_5$  and  $MoO_3$ , it was found that  $V_2O_5/SiO_2$  is more active and selective. That was explained by the higher density and stability of the reduced vanadium ions, which are able to activate gas-phase oxygen, Parmaliana et al. (1994). For example, over the silica-supported  $V_2O_5$ , formaldehyde selectivity was high (>50%) at methane conversions approaching zero (<2%). Over  $MoO_3/SiO_2$  formaldehyde production was less than over the precipitated silica-support. Methanol production over these catalysts was negligible.

The nature of interaction between the metal oxide and the silica is still not clear, but it appears that low loading of metal oxides on silica produce more formaldehyde. In a recent study, Sun et al. (1997), it was proved that metal oxides are well dispersed as

isolated islands over silica. These islands are proposed to be the active sites for methane and oxygen activation.

Metal oxide catalysts have the ability to be reduced and re-oxidized. Thus metal oxide catalytic behavior is explained by a re-dox mechanism. In this mechanism, the oxidized catalyst is reduced by hydrocarbon molecules, which are oxidized. Then the reduced catalyst is re-oxidized by oxygen from the gas phase completing the catalytic cycle. When at steady state, the rate of these two steps must be the same, although either step can be rate limiting.

Mars and Van Krevelen (1954) developed a model to describe the kinetic behavior of the partial oxidation of several aromatic hydrocarbons over vanadium oxide catalysts. No assumptions were made about the oxygen form on the catalyst surface. The rate expression developed by Mars and Van Krevelen is:

$$-r_{\text{HC}} = \frac{1}{\left(\frac{1}{k^*P_{\text{O}_2}^n}\right) + \left(\frac{1}{kP_{\text{HC}}}\right)} \quad (2.6)$$

If  $k^*P_{\text{O}_2} \gg kP_{\text{HC}}$ , then  $-r_{\text{HC}} = kP_{\text{HC}}$  and the hydrocarbon activation is the rate limiting step. If on the other hand,  $k^*P_{\text{O}_2} \ll kP_{\text{HC}}$ , then  $-r_{\text{HC}} = k^*P_{\text{O}_2}$  and in this case oxygen activation is the controlling step.

### **2.3.2 Phosphate Catalysts:**

#### **2.3.2.1 Vanadyl Pyrophosphate (VPO) Catalysts:**

A catalyst employed industrially for the partial oxidation of an alkane is vanadyl pyrophosphate. It is used in the selective oxidation of n-butane to maleic anhydride. Moreover, moderate to high selectivity in the oxidation of ethane and propane over VPO are reported, Ai (1986) and Michalakos et al. (1993). McCormick et al. (1997), investigated methane partial oxidation over VPO but only very low yield of formaldehyde was achieved. The same group studied VPO promoted with several transition metals and a positive effect on formaldehyde selectivity was observed for the iron promoted catalyst. These experiments, along with work by Wang and Otaska (1995) and (1997), showing significant activity and yields to oxygenated products for methane oxidation over iron phosphate, led us to also examine iron phosphate.

#### **2.3.2.2 Iron Phosphate (FePO<sub>4</sub>) Catalysts:**

An extensive study of methane selective oxidation over iron phosphate catalysts was made by Alptekin (1998). In his thesis, the effect of reaction conditions, including co-feeding of steam, on methane oxidation activity and selectivity were examined over FePO<sub>4</sub> and FePO<sub>4</sub> supported on silica and other supports, in a continuous flow reactor. It was shown in this work that supporting FePO<sub>4</sub> on silica produced the highest space-time yield of the desired oxygenates. In addition, iron phosphate structure and the effect of iron phosphate loading on reactivity and selectivity were investigated.

Most of the work done by Alptekin (1998) on iron phosphate based catalysts falls into two categories, the global kinetics of methane selective oxidation in a flow reactor, or catalyst characterization. The global kinetic studies are helpful in setting up experiments for examining reaction intermediates and in collecting data to be compared with a micro-kinetic model. Catalyst characterization is needed to identify the active sites for the different reactants and to understand the structure and the chemistry of the catalyst.

#### **2.3.2.2.1 Macro-kinetics of Methane Oxidation over Iron Phosphate Catalysts:**

The partial oxidation of methane to methanol and formaldehyde by molecular oxygen was investigated over crystalline and silica-supported iron phosphate at atmospheric pressure and in the temperature range 723-973 K, Alptekin et al. (1998).

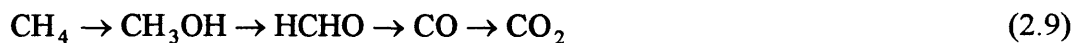
For unsupported  $\text{FePO}_4$ , the global reaction network is as follows (oxygen and water molecules are not shown):



This network suggests that formaldehyde is a primary reaction product and carbon monoxide is secondary product. It also indicates the presence of a direct oxidation path to carbon dioxide. Using a simple power-law rate model for conversion of methane to all reaction products, the reaction orders were calculated to be  $0.66 \pm 0.07$  for methane and  $0.45 \pm 0.05$  for oxygen with an activation energy of  $174 \pm 9$  kJ/mole, as reported by

Alptekin et al. (1998b). The maximum space-time yield of formaldehyde obtained by Alptekin for unsupported FePO<sub>4</sub> was 59 g/kg.h.

Supporting FePO<sub>4</sub> on precipitated silica caused an appreciable improvement in the catalytic activity and selectivity and quantifiable amounts of methanol were observed. Alptekin obtained formaldehyde and methanol yields of 285 and 11 g/kg.h, respectively. The selectivity/conversion pattern at low methane-to-oxygen ratios (~2) suggests a sequential reaction network:



However, the possibility that methanol and formaldehyde are formed in separate, parallel paths cannot be ruled out:



At high methane-to-oxygen ratios (>10) and low methane conversions (<3%) the reaction network is identical to that proposed for unsupported FePO<sub>4</sub> in reactions (2.7) and (2.8), i.e., includes direct conversion of methane to carbon dioxide. Reaction orders were calculated to be 0.61±0.07 and 0.28±0.03, respectively, for methane and oxygen and the overall reaction activation energy was found to be 149±4 kJ/mole. The catalyst used in evaluating the kinetic parameters was 5 wt. % FePO<sub>4</sub> on silica. Alptekin et al. (1998) list reaction orders and Arrhenius parameters for bulk iron phosphate and silica supported iron phosphate in Table 2.1.

Table 2.1 Kinetic Parameters and Yields for CH<sub>4</sub> Oxidation Over Bulk and Silica Supported FePO<sub>4</sub>. Arrhenius parameters obtained at CH<sub>4</sub>:O<sub>2</sub>=2.

Catalyst	Reaction Order		H <sub>2</sub> O	Activation Energy, kJ/mole	Pre-exponential Factor, mole/m <sup>2</sup> -kPa <sup>n</sup> -h	Maximum STY, g/kg <sub>cat</sub> -h		Rate at 873K, mol/m <sup>2</sup> -h
	CH <sub>4</sub>	O <sub>2</sub>				HCHO	CH <sub>3</sub> OH	
FePO <sub>4</sub>	0.66±0.07	0.45±0.05	--	164±9	10,300	59 <sup>†</sup>	0	1.2x10 <sup>-4</sup>
FePO <sub>4</sub> /SiO <sub>2</sub>	0.61±0.07	0.28±0.03	--	144±4	2465	285 <sup>‡</sup>	11	1.9x10 <sup>-4</sup>
	0.48±0.05	0.21±0.03	0.23±0.04	155±3	16,920	487 <sup>§</sup>	25	1.7x10 <sup>-4</sup>

<sup>†</sup>T=873 K, GHSV=30,000 h<sup>-1</sup>, P<sub>CH<sub>4</sub></sub>=37 kPa, P<sub>O<sub>2</sub></sub>=6 kPa, W<sub>cat</sub>=0.25 g.

<sup>‡</sup>T=873 K, GHSV=60,000 h<sup>-1</sup>, P<sub>CH<sub>4</sub></sub>=49 kPa, P<sub>O<sub>2</sub></sub>=49 kPa, W<sub>cat</sub>=0.1 g.

<sup>§</sup>T=873 K, GHSV=60,000 h<sup>-1</sup>, P<sub>CH<sub>4</sub></sub>=49 kPa, P<sub>O<sub>2</sub></sub>=49 kPa, W<sub>cat</sub>=0.1 g.

Source: Alptekin 1998

#### **2.3.2.2.2 The Effect of Catalyst Loading and Support:**

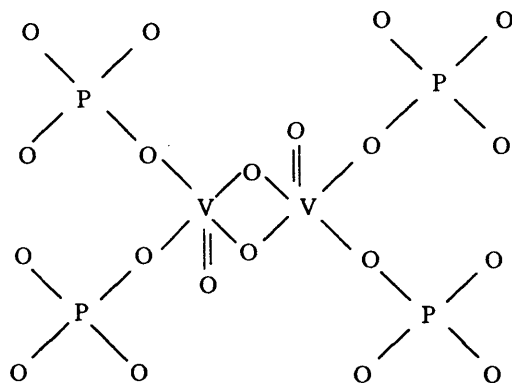
The selective oxidation of methane at atmospheric pressure was studied over a series of silica-supported  $\text{FePO}_4$  catalysts, with iron phosphate content ranging from 2 to 16 wt. %, Alptekin et al. (1998). The catalytic activity exhibited a clear dependence on the iron phosphate content. The highest yields to desired products are obtained at low iron phosphate loading levels and yield is unaffected by loading above 8 wt. %  $\text{FePO}_4$  on silica. The highest selectivity and space-time yield to formaldehyde and methanol were observed for the 2 wt. % catalyst.

$\text{FePO}_4$  catalysts supported on  $\text{Al}_2\text{O}_3$ ,  $\text{ZrO}_2$ ,  $\text{TiO}_2$  and  $\text{SiO}_2$  and with iron loading from 2 to 16 wt.% were tested in methane partial oxidation at atmospheric pressure, McCormick et al. (1998). Catalyst supported on silica produced the highest yield to oxygenated products. Characterization results, described below, indicate that the presence of easily reducible iron, in high coordination and isolated by phosphate groups is unique feature of the silica-supported iron phosphate catalyst at low iron loading.

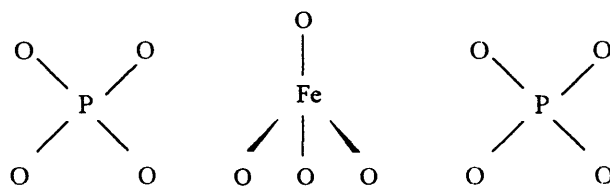
#### **2.3.2.2.3 Catalyst Characterization:**

The published structural data indicate that bulk  $\text{FePO}_4$  contains iron in tetrahedral coordination, where  $\text{FeO}_4$  is isolated by phosphate ( $\text{PO}_4$ ) groups. Figure 2.1 presents the structure for the different catalyst studied by our group. Much of the iron in the silica supported  $\text{FePO}_4$  is in crystalline form (bulk  $\text{FePO}_4$  structure), but a large fraction of the iron is in a different chemical environment, Alptekin et al. (1998). This unknown iron

a. VPO Catalyst:



b. Bulk FePO<sub>4</sub> Catalyst:



c. Silica Supported FePO<sub>4</sub> Catalyst:

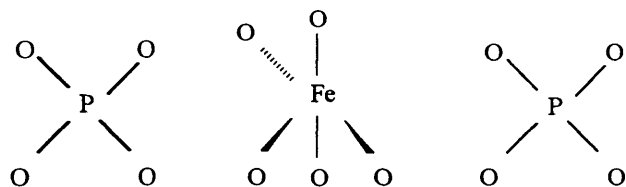


Figure 2.1 Catalysts Structure

structure is proposed to contain five-coordinate Fe, and the fraction of this species increases with decreasing iron content. Mossbauer and XPS studies indicate that the silica support increases the electron density on the iron and effectively lowers its oxidation state compared to other supports. The presence of five-fold coordinated iron, with high electron density (low oxidation state), and the isolation of this active site by phosphate groups may enhance chemisorption of reactive oxygen species potentially responsible for the methane activation, Alptekin et al. (1998). The achievement of high yields is related to the stability of the desired products on the support. Silica was found to have the lowest activity for conversion of methanol and formaldehyde.

### **2.3 Silica as a Catalyst:**

In methane partial oxidation, it was discovered that silica itself exhibits a significant selectivity to formaldehyde. Parmaliana et al. (1991, 1993 and 1994), studied different types of silica. It was found that precipitated silica gives the highest formaldehyde yield. The reason for the difference in activity among the silica catalysts is maybe due to the difference in surface area, level of contaminants and the number of defect sites, Kobayashi (1994). Parmaliana et al. (1994) proposed that in silica-supported catalysts, silica is the actual catalyst, and that metal oxides dispersed over the silica act as a promoter. In fact,  $V_2O_5$  enhanced HCHO formation while  $MoO_3$  depressed it.

The low loading (<5% catalyst/support) used in most methane partial oxidation studies suggests that the catalytic properties are controlled by the most abundant surface,

silica. Kobayashi et al. (1994), examined silica promoted with 3d transition metal ions, and Fe-SiO<sub>2</sub> was found to enhance HCHO production. They believe that Fe provides active re-dox centers that are responsible for the oxygen activation on silica.

## **2.4 Carbon monoxide, Formaldehyde and Methanol Oxidation:**

Methanol oxidation is an important process for formaldehyde production by oxidative dehydrogenation. Similarly, total oxidation of formaldehyde and carbon monoxide are important processes for environment and health reasons.

### **2.4.1 Carbon Monoxide Oxidation:**

Carbon monoxide is a hazardous gas that is produced as a by-product of many petrochemical processes and fuel combustion. Total catalytic oxidation of CO to CO<sub>2</sub> is one of the important steps occurring in vehicle catalytic converters.

The kinetics of carbon monoxide oxidation on vanadia were studied by Goldwasser and Trim (1979). Using initial rates, they reported first order kinetics in CO and zero order in O<sub>2</sub>. The reaction was not inhibited by CO<sub>2</sub> even when its concentration was twice that of CO. Generally, the mechanism for the catalytic oxidation of CO is suggested to be a Mars and Van Kreveln re-dox mechanism.

Matsuchima et al. (1979) studied CO oxidation over iridium. It was shown that there is a competition between CO and O<sub>2</sub> for the active sites. After a certain CO pressure, the rate-limiting step changes from CO oxidation to O<sub>2</sub> adsorption. They

discovered that the reaction was first order in CO and zero in O<sub>2</sub> at low CO pressures, while the oxidation was inhibited by CO (negative order in CO) above the critical CO pressure. Above that pressure the reaction was first order in O<sub>2</sub> and negative order in CO.

#### **2.4.2 Formaldehyde Oxidation:**

Total oxidation of formaldehyde is an environmentally important process to reduce formaldehyde emissions. Cheng (1996) examined the stability of formaldehyde over several metal oxides and supports in the temperature range of 473-623 K. Silica was found to be inactive for formaldehyde oxidation, while titania and alumina exhibited the highest activity of the materials tested. Cheng observed a 0.7 order in formaldehyde and 0.15 order in oxygen over bulk MoO<sub>3</sub>.

Spencer and Pereira (1989) assumed that formaldehyde and carbon monoxide oxidation proceed via first order reactions over V<sub>2</sub>O<sub>5</sub>/SiO<sub>2</sub>. Their power law based model was in good agreement with their experimental data and reported rates by Goldwasser (1979). Alptekin (1998) studied HCHO oxidation over VPO catalyst in the temperature range 473 to 623 K. He observed a first order and zero order behavior for HCHO and O<sub>2</sub>, respectively.

#### **2.4.3 Methanol Oxidation:**

Methanol is mainly oxidized over mixed iron-molybdenum based catalysts to produce formaldehyde in a commercial process. Industrially, a fluid bed reactor filled with ferric-

molybdate catalyst is operated at total methanol conversion to produce HCHO at 90% selectivity, Boreskov (1996). Klissurski et al. (1993) have also reported close to 100% conversion of methanol to formaldehyde over iron phosphate catalyst in the 570-650 K temperature range.

Alptekin (1998) reported first order and zero order kinetics for methanol and oxygen, respectively over VPO. Results of different kinetic studies are collected for the CO, HCHO and CH<sub>3</sub>OH oxidations in Table 2.2.

## **2.5 Methane Oxidation Transient Studies:**

Pulse studies of methane partial oxidation were carried out mainly to investigate the role of lattice oxygen in metal oxide based catalysts. Parmaliana et al. (1994), examined the role of molecular oxygen by performing tests in the presence and absence of gaseous oxygen. They ruled out the participation of lattice oxygen in the main reaction pathways. Moreover, they suggested that the reaction proceed via a concerted mechanism rather than a two-step (Mars and Van Krevelen) redox mechanism.

On the other hand, Wang and Otsuka (1995) think that lattice oxygen is responsible for the oxidation of methane to formaldehyde at relatively high temperatures (>673 K) over iron phosphate catalysts. When they examined the catalytic oxidation of methane with an H<sub>2</sub>-O<sub>2</sub> gas mixture they discovered that methanol was formed only when H<sub>2</sub> and O<sub>2</sub> were co-fed.

Table 2.2 Results Reported for the Methanol, Dimethyl Ether, Formaldehyde and Carbon Monoxide Oxidation/Hydration Reactions.

Catalyst	Activation Energy (kJ/mole)	Reaction Order		Reference
		HC <sup>a</sup>	O <sub>2</sub>	
<u>CH<sub>3</sub>OH Oxidation</u>				
(VO) <sub>2</sub> P <sub>2</sub> O <sub>7</sub>	76	1.12	0.06	Alptekin, 1998
MoO <sub>3</sub>	86	0.5-1.0	0.1	Farneth, 1985
MoO <sub>3</sub>	89	0.58	0.18	Macheils, 1982
Fe <sub>2</sub> (MoO <sub>4</sub> ) <sub>3</sub> /MoO <sub>3</sub>	82	1 <sup>b</sup>	0	Edwards, 1977
Fe <sub>2</sub> (MoO <sub>4</sub> ) <sub>3</sub> /MoO <sub>3</sub>	67-79	--	--	Bibin, 1969
Fe <sub>2</sub> (MoO <sub>4</sub> ) <sub>3</sub> /MoO <sub>3</sub>	54	--	--	Jiru, 1966
Fe <sub>2</sub> (MoO <sub>4</sub> ) <sub>3</sub> /MoO <sub>3</sub>	45	--	--	Habersberger, 1972
Fe <sub>2</sub> (MoO <sub>4</sub> ) <sub>3</sub> /MoO <sub>3</sub>	74	--	--	Evmenenko, 1969
V <sub>2</sub> O <sub>5</sub>	84-95	1 <sup>b</sup>	0	Gasser, 1988
Various Molybdates	69-76	0.4-0.7	0-0.15	Macheils, 1982
Ferric Molybdate	136-141	1 <sup>b</sup>	0	Spencer, 1989
<u>CH<sub>3</sub>OH Dehydration</u>				
Alumina hydroxide	63	--	--	Hashimoto, 1996
Montmorillonite Intercalated Al	21	--	--	Hashimoto, 1996
<u>HCHO Oxidation</u>				
(VO) <sub>2</sub> P <sub>2</sub> O <sub>7</sub>	72	0.95	0.06	Alptekin, 1998
MoO <sub>3</sub>	--	0.7	0.15	Farneth, 1985
Fe <sub>2</sub> (MoO <sub>4</sub> ) <sub>3</sub> /MoO <sub>3</sub>	79	1 <sup>b</sup>	0	Cheng, 1996
V <sub>2</sub> O <sub>5</sub> /SiO <sub>2</sub>	--	1 <sup>b</sup>	0	Spencer, 1989
<u>CO Oxidation</u>				
(VO) <sub>2</sub> P <sub>2</sub> O <sub>7</sub>	86	1 <sup>b</sup>	0	Alptekin, 1998
V <sub>2</sub> O <sub>5</sub> /SiO <sub>2</sub>	90	1 <sup>b</sup>	0	Spencer, 1989
V <sub>2</sub> O <sub>5</sub> /SiO <sub>2</sub>	--	1 <sup>b</sup>	0	Goldwasser, 1979

<sup>a</sup>Global order for hydrocarbon.

<sup>b</sup>Orders assumed, not measured.

Source: Alptekin 1998

They proposed two mechanisms, one in the presence of hydrogen in which methanol is produced then converted to formaldehyde and the other in the absence of hydrogen and in this case methane is converted to formaldehyde directly. It is thought that hydrogen reduce  $\text{Fe}^{+3}$  on the  $\text{FePO}_4$  surface to  $\text{Fe}^{+2}$ , producing protons on the catalyst surface. Oxygen then is coordinated on that reduced site followed by reductive activation of the oxygen by hydrogen. One oxygen atom then reacts with the protons producing water and the second oxygen atom forms a highly reactive oxygen species that can activate methane to produce methanol.

## **2.6 Characterization of the catalyst surface:**

Surface studies of methane oxidation catalysts are generally directed at measuring the number of active sites (or site density) and at observation of surface reaction intermediates.

### **2.6.1 Oxygen Chemisorption:**

The total site density cannot be evaluated theoretically, hence a technique like  $\text{O}_2$  chemisorption is used to measure the active site density experimentally. Nag et al. (1984) proposed a new chemisorption technique to measure the active surface area for supported and unsupported vanadium oxide catalysts. In this technique, the catalyst surface is reduced at high temperatures ( $500\text{ }^\circ\text{C}$ ) under hydrogen for six hours, then oxygen uptake at low temperature (room temperature) is measured. Assuming that every reduced site

will consume one oxygen atom and knowing the catalyst surface area, one can find the active site density.

Before the experiments, the temperature at which surface reduction occurs without reducing the bulk catalyst is evaluated using a temperature programmed reduction experiment. Then  $O_2$  chemisorption is achieved by dosing small amounts of oxygen at low temperatures over the pre-reduced catalyst. The ratio of oxygen uptake at this temperature found from product analysis to the surface area gives the site density in moles/m<sup>2</sup>, Oyama et al. (1989).

Another method for measuring  $O_2$  active site density that does not involve finding the reduction temperature was proposed by Faraldos et al. (1997). In this work, the authors search for optimum conditions for measuring the site density. They found that the catalyst should be reduced and re-oxidized at high temperatures. Reduction temperature was suggested to be above 800 K and re-oxidation temperature should be around 600 K to assure that only surface density is measured.

### **2.6.2 Infrared Spectroscopy:**

In-situ IR studies are used to probe the structure of molecules bonding with the surface. In IR, a beam of infrared light is directed at a solid surface, and a detector measures the fraction of photons that absorb as a function of frequency. Then the observed IR spectrum is compared to ones from a series of reference compounds to learn about the bounding of molecules to surfaces. The catalyst can be exposed to various gas

environments at elevated temperature to try and simulate actual reaction conditions. These experiments give some very useful information about the bonding of adsorbed complexes.

One goal of IR experiments related to methane partial oxidation is the detection of surface methoxide species which are proposed as an important intermediate in both methane and methanol oxidation. Busca (1989) studied the conversion of methanol to formaldehyde over  $\text{MoO}_3$  and  $\text{V}_2\text{O}_5$  catalysts and proposed that methoxide ions were intermediates during the partial oxidation. Also Pak and Lunsford (1997) used IR spectroscopy to detect methoxide species during the reaction of methyl radicals. Bands at 2930, 2830, 1445, 1430, 1150 and 1065 were assigned to surface methoxide over  $\text{V}_2\text{O}_5/\text{SiO}_2$ .

Although methanol is only observed in negligible amounts in methane partial oxidation, it is thought that methane activation proceeds through methoxy compounds. Methanol chemisorption can be used to generate these methoxide species. Therefore, in-situ infrared spectra for methanol adsorption and partial oxidation have been collected over silica and many metal oxides on silica. Jongsomjit (1998) collected IR spectra for methanol chemisorption over  $\text{SiO}_2$  and  $\text{V}_2\text{O}_5/\text{SiO}_2$ . In the spectra,  $\text{CO}_2$  exhibits a strong band at  $2400\text{ cm}^{-1}$ , indicating that methanol is reacting under the experiment conditions. The C-H bands in the  $2700\text{-}3200\text{ cm}^{-1}$  region were assigned to sorbed methanol and methoxide groups. Water bands were observed at  $2200$  and  $1800\text{ cm}^{-1}$ .

Clarke et al. (1994) suggested that all methanol bands seen over silica are types of physisorbed methanol. The  $3370\text{ cm}^{-1}$  band was attributed to O-H vibrations of  $\text{CH}_3\text{OH}$  and bands at  $3003, 2956$  and  $2848\text{ cm}^{-1}$  are characteristic for C-H vibrations in weakly adsorbed methanol. Comparing these results with Jongsomjit's work, one can roughly assign bands at  $2860, 2922$  and  $2960\text{ cm}^{-1}$  to the C-H vibrations from methanol and methoxide species. Bands below  $1800\text{ cm}^{-1}$  are assigned to C-H bands and C-O stretching modes.

In Clarke et al. (1994),  $\text{CH}_3\text{O}$  and  $\text{HCOO}$  species were observed over reduced and oxidized  $\text{Cu/SiO}_2$ . Chung et al. (1985) also suggested the presence of this type of species over  $\text{MoO}_3/\text{SiO}_2$  for methanol chemisorption. Busca et al. (1987) assign bands at  $2894, 2830$  and  $1501$  to  $\text{CH}_2$  species when formaldehyde chemisorption was carried out over silica at  $180\text{ K}$ .

IR spectra for carbon monoxide chemisorption over cobalt oxides at  $150$  and  $300\text{ K}$  was reported by Busca et al. (1990). At  $150\text{ K}$  one band was observed at  $2190\text{ cm}^{-1}$  and at room temperature two main bands were apparent at  $2180$  and  $2070\text{ cm}^{-1}$ . These bands were assigned to three different mono carbonyl species. The frequency of gaseous CO is at  $2143\text{ cm}^{-1}$ . Gaseous  $\text{CO}_2$  was also formed at the room temperature when CO was kept in contact with the catalyst at CO pressure equal to  $100\text{ torr}$ .

## **2.7 Modeling Methane Partial Oxidation:**

Methane partial oxidation modeling studies fall into two categories, either macro-kinetic or micro-kinetic analysis. By macro-kinetic modeling is meant the study of the reaction global kinetics without incorporating the catalyst surface intermediates in the rate equation. Usually in this method the rate of disappearance of methane is expressed in terms of the inlet gas pressures and some reaction rate constants.

By micro-kinetic analysis is meant kinetic models that incorporate the elementary surface reactions involved in the overall catalytic reaction. This includes the elementary reactions that occur on the catalyst surface and their relation with each other, and with the surface during the catalytic cycle, Dumesic et al., (1993).

### **2.7.1 Macro-Kinetic Analysis of Methane Oxidation:**

Global kinetic studies of methane partial oxidation are limited to the activity-selectivity patterns over  $\text{SiO}_2$ ,  $\text{MoO}_3/\text{SiO}_2$ ,  $\text{V}_2\text{O}_5/\text{SiO}_2$  and  $\text{FePO}_4/\text{SiO}_2$ . Spencer and Pereira (1989) studied methane partial oxidation by molecular oxygen over  $\text{MoO}_3/\text{SiO}_2$  and  $\text{V}_2\text{O}_5/\text{SiO}_2$  under atmospheric pressure and in the temperature range 773 to 873 K. They developed a first-order kinetic model that uses the rate constants as parameters. In their modeling, they assumed that hydrocarbons follow first order kinetics and oxygen is zero order. They proposed a sequential reaction network for methane oxidation over  $\text{V}_2\text{O}_5/\text{SiO}_2$  while they added a direct route from methane to carbon dioxide for

MoO<sub>3</sub>/SiO<sub>2</sub>. The mechanism was lumped to the essential steps and the global rate constants were used.

Arena et al. (1999) investigated methane partial oxidation to formaldehyde over silica at 650 °C. They suggested a concerted mechanism that is similar to the two-step (Mars and Van Krevelen) redox mechanism. They examined the effect of the inlet gas phase composition (P<sub>CH<sub>4</sub></sub>/P<sub>O<sub>2</sub></sub> ratio) on the catalytic activity. This technique was used previously by Mars and Van Krevlen when studying the redox reactions. They propose that both CH<sub>4</sub> and O<sub>2</sub> molecules dissociate competitively on two adjacent sites.

### 2.7.2 Micro-kinetic Analysis of Methane Oxidation:

The goal of micro-kinetic modeling is to relate in a quantitative manner theoretical concepts, appropriate correlations, and available experimental data relevant to the catalytic process. The formulation of elementary chemical reaction steps that capture the essential surface chemistry involved in the catalytic reactions is the fundamental starting point in micro-kinetic studies.

The second point is estimation of the rate of the elementary reactions and the surface coverage. Rate constants for the elementary reactions are used as the micro-kinetic modeling parameters and they follow the usual Arrhenius behavior:

$$k = A e^{-E/RT} \quad (2.12)$$

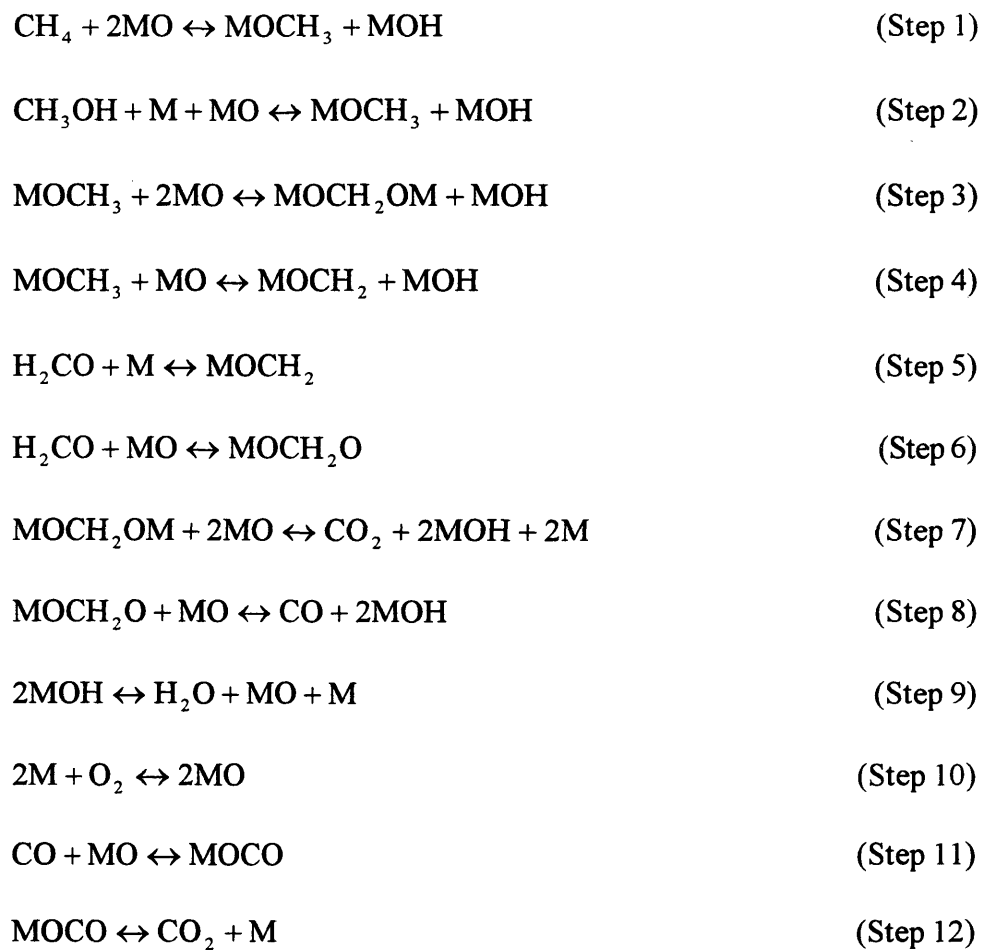
where A is the pre-exponential factor and E is the activation energy. The pre-exponential factor can be evaluated using the transition state theory, whereas the activation energy

can be found from the heat of adsorption of the reactants and products, either experimentally or by appropriate correlation. The surface coverage problem may be solved using simple models like Langmuir-isotherm unless specific information is available to quantify the nature of the non-Langmuirian behavior. Micro-kinetic simulation can be carried out at different levels of detail, depending on the availability of surface kinetic, thermodynamic, spectroscopic and structural information, Dumesic et al. (1993).

Although the idea of micro-kinetics has been known for along time, mathematical difficulties, shortage of experimental data, and insufficient theoretical concepts have prevented application until recently. To our knowledge, the only work done on methane selective oxidation was published by Amiridis et al., (1991). The objective of that study was to simulate methane partial oxidation over silica-supported  $\text{MoO}_3$  and  $\text{V}_2\text{O}_5$ . The authors suggested a mechanism for methane partial oxidation over supported metal oxides, the mechanism is shown in Figure 2.2. It should be mentioned that reactions 1, 2 and 5 are non-elementary steps, and this was justified as simplifying the reaction network. Due to shortage of experimental data and theoretical concepts, most of the kinetic coefficients were taken from related and analogous catalytic systems. Parameters used in the Evans-Polanyi expression<sup>1</sup> and the chemical bonding parameters were obtained by an optimization process that minimized the deviations of the model predictions from the experimental data. Although the work has a lot of assumptions and

---

<sup>1</sup> A correlation used to estimate the activation energy.



Source: Dumesic et al. 1993

Figure 2.2 Methane Partial Oxidation over Silica-Supported MoO<sub>3</sub> and V<sub>2</sub>O<sub>5</sub>.

weaknesses, it gives the framework for future studies. The model failed to describe CO and CO<sub>2</sub> formation although it predicted HCHO and CH<sub>3</sub>OH amounts. Micro-kinetic models of methane oxidative coupling and methane catalytic combustion have also been published, Dumesic et al. (1993).

## **2.8 Economics and Engineering**

Natural gas world reserves are over 100E12 m<sup>3</sup>, Sanger and Smith (1991). Usually natural gas is transported by pipeline at high pressures ( $P > 8$  MPa) and by ships as a liquid at very low temperatures ( $T < -162$  °C), Mimoun (1987). Because of its low energy content per unit volume, natural gas transportation from the wellhead to the consumer is difficult. Actually its transportation accounts for 30% of the selling price. Table 2.3 gives the costs of transporting different fuels over distances of 1000 and 10000 km. Using natural gas as vehicle fuel also suffers from its low energy density because vehicle range is limited. Methane is used in many industrial processes; the different chemicals produced from methane conversion are shown in Figure 2.3.

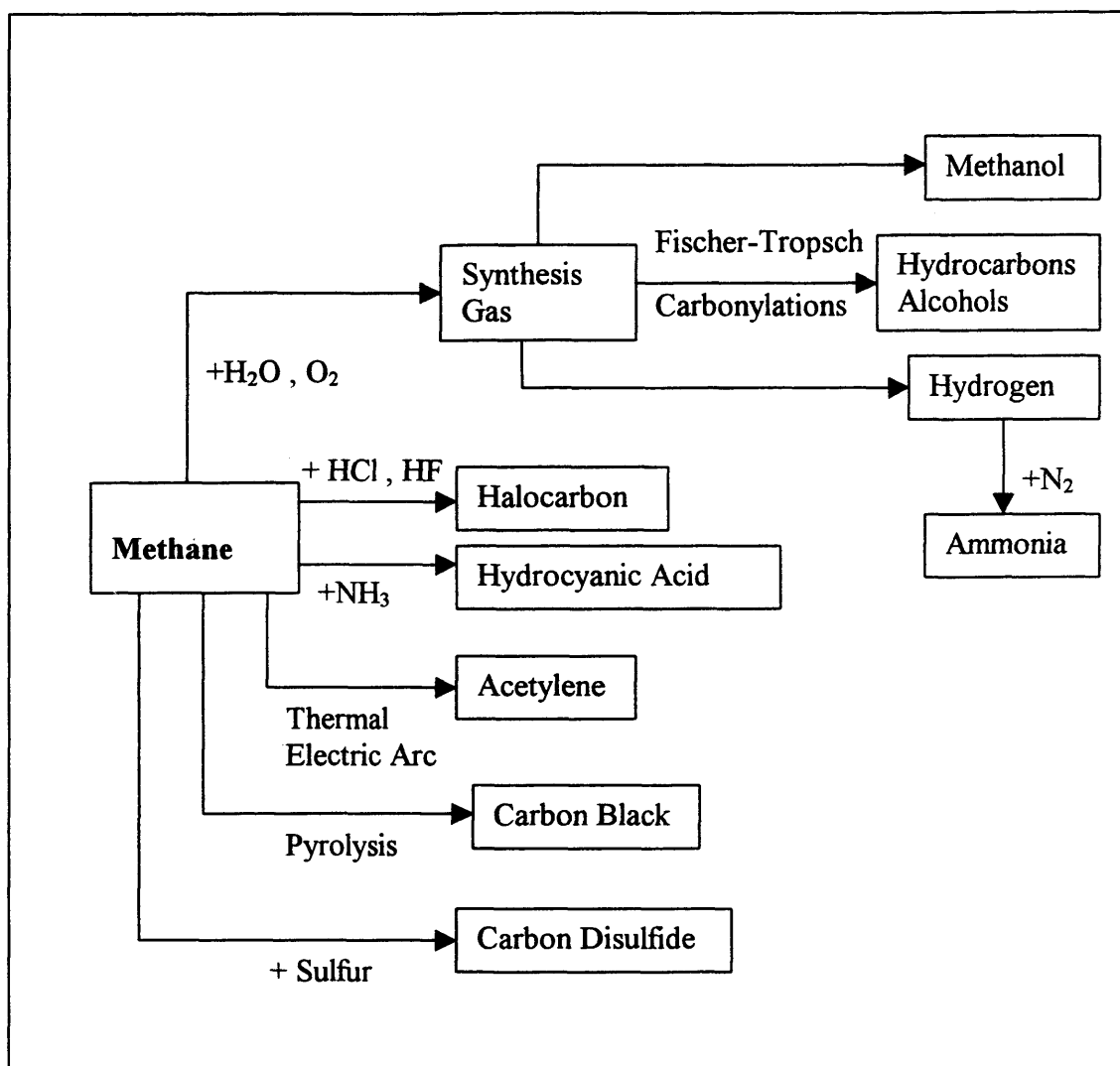
The direct oxidation to formaldehyde and methanol could potentially substitute for the conventional industrial process, with a great reduction in capital and maintenance expenses. Economically, the direct oxidation of methane will be superior to the synthesis gas processes if reasonable conversions ( $> 20\%$ ) and selectivity approaching 100% are achieved, along with mild operating conditions: low temperature and around atmospheric pressure, Fox et al. (1990). This might also lead to greater utilization of natural gas

reserves, of which only 7% is used for commercial production of chemicals, Poirer et al. (1991) and in particular allow utilization of reserves that are remote or small in scale.

Table 2.3 Cost of Transporting Fuel as a Function of Distance

Fuel	Cost \$./GJ	
	1 000 km	10 000 km
Oil	12.6	126
Methanol	21	126
LNG	84	735
Natural Gas		
Land-based pipeline	126	1260
Submarine pipeline	210	2100

Source : Parkyns et al. 1993



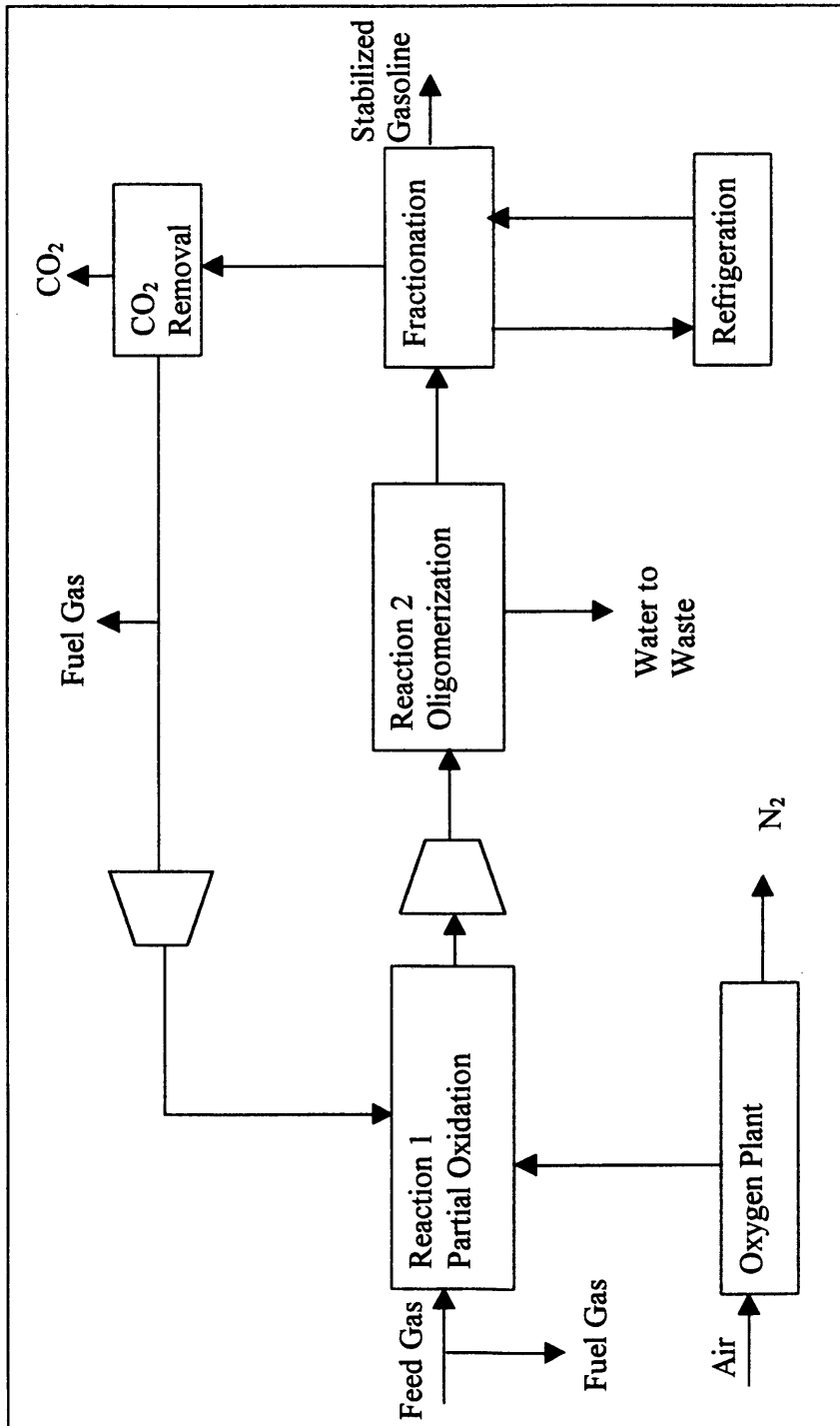
Source : St-Just et al. 1990

Figure 2.3 Methane Industrial Processes

Fox et al. (1990) made an economic evaluation comparing among three types of direct methane conversion processes (oxidative coupling, oxyhydrochlorination and partial oxidation). All cases considered involve oligomerization as a second step to produce gasoline. The work of Hunter et al. (1984) was used in the evaluation. In this work, methane partial oxidation was accomplished with 99.5% oxygen and the reaction was at elevated pressure (60 atm) and a temperature range of 672-772 K. Methane conversion of 5.5% and 80% selectivity were used in the process design and in the cost estimation. The process flow diagram is shown in Figure 2.4. An oxygen plant is used to produce high purity oxygen and an oligomerization unit is used to produce gasoline and by-product water. Light products are recovered in the refrigeration system and recycled. Since carbon dioxide is the major by-product its removal from the recycle stream is also required.

For a production rate of 14500 bbl/day, the capital cost of a gas to liquid process, by direct methane conversion was \$1012.8 million. The operating cost was calculated to be \$75 million/year. Compared to the other two-step conversion processes, one-step methane oxidation at 5.5% conversion is 20% higher in capital cost and almost the same in operating cost.

A sensitivity analysis showed that an increase in conversion from 5.5% to 10% would result in 15% reduction in capital cost. Also achieving close to 100% selectivity will eliminate the CO<sub>2</sub> by product and improve the product H/C ratio. This will reduce



Source: Fox et al. 1990

Figure 2.4 Case Study for Methane Partial Oxidation

the total plant cost to \$500 million. Reducing the high pressure used will eventually reduce both the capital and the operating costs.

Since the reforming process to produce synthesis gas is not part of the one step methane oxidation process, transforming methane to liquid fuels is potentially less expensive. If high selectivity at reasonable conversion is achieved, a capital cost of \$300-\$350 million may be feasible for the direct methane oxidation process producing 14,500 bbl/day of products.

## CHAPTER 3

### EXPERIMENTAL SECTION

#### 3.1 Introduction

Additional experimental data are needed to more fully understand the reaction mechanism and kinetics of methane partial oxidation. Ideally a mechanism consisting of elementary surface reactions and adsorption/desorption steps should be developed. However, a less fundamental network where certain steps are lumped can also be used successfully. To achieve this goal a continuous/pulse reactor, oxygen chemisorption, and in-situ infrared (IR) experiments were used. In the continuous reactor studies, the global macro-kinetics for methane oxidation can be evaluated, moreover other subsequent reactions like carbon monoxide, formaldehyde and methanol oxidation can be investigated. Pulse experiments were used to investigate the role of gaseous oxygen, the oxidation rates and whether oxygen in the bulk catalyst has any role in the mechanism.

In situ infrared (IR) experiments for methanol and carbon monoxide can be used to examine the structure of species sorbed on the catalyst surface. These experiments may provide evidence for the different types of adsorbed species present on the catalyst surface.

Another goal of this work is to identify the active sites of this catalyst and to measure the density of these sites. Recent studies have proposed that active sites where methane activation occurs are highly reactive chemisorbed oxygen species. To this end, oxygen chemisorption experiments were used to titrate these sites.

A more specific objective is to understand the methane activation step on silica and silica-supported iron phosphate. Rate limiting and significant reactions for selectivity will be studied and outlined in this study.

## **3.2 Experimental Setup and Procedure:**

### **3.2.1. Catalyst Preparation:**

#### **3.2.1.1 Precipitated Silica:**

The silica support is a precipitated, acid washed material obtained from Cerac Chemical with a BET surface area of 398 m<sup>2</sup>/g. The silica was washed with 7% nitric acid solution at room temperature then rinsed with deionized water to remove any residual sodium ions. After that, it was dried at 383 K in air and activated when used at 923 K for 24 hours.

#### **3.2.1.2 Silica-Supported Iron Phosphate:**

Ferric nitrate Fe(NO<sub>3</sub>)<sub>3</sub> and orthophosphoric acid H<sub>3</sub>PO<sub>4</sub> solutions are used to impregnate the precipitated silica as a support. First, the iron nitrate solution is added to

the dried silica and the resulting material is then dried in the oven. The product is then impregnated with the orthophosphoric acid solution to provide a P/Fe ratio of one. Impregnation was followed by drying at 363 K and calcination in air for 24 hrs at 973 K. The iron phosphate loading used in this study was 2 wt%. This method of preparation is presented in Alptekin (1998).

### **3.2.2. Catalyst Testing**

#### **3.2.2.1. Continuous/Pulse Reactor Studies:**

These experiments are designed to understand the global reaction scheme of methane selective oxidation over iron phosphate catalysts on a fundamental basis. The flow reactor experiments will be used to examine the catalytic oxidation of carbon monoxide, formaldehyde and methanol over both the precipitated silica and the silica supported iron phosphate. Investigations of the oxidation of the possible reaction intermediates will provide a better understanding of the overall reaction scheme of methane oxidation over the catalyst. These experiments are also important in studying the stability of the desired products on the silica-supported iron phosphate.

Pulse reactor experiments will be used mainly to investigate the role of gaseous oxygen and the participation of lattice oxygen in the reaction pathways. Catalyst surface oxidation and reduction will be carried out with the pulse reactor. In these experiments

the effect of lattice oxygen depletion from an oxidized catalyst are examined and the performance of the catalyst is studied.

A conventional flow apparatus operating in both continuous and pulse mode will be used in the catalyst testing. Figure 3.1 represents a schematic diagram of the reactor system. The composition and flow rate of the gas streams ( $\text{CH}_4$  (99.9%, Alpha Gas);  $\text{O}_2$  (99.99%, Alpha Gas); He (Grade 5.0, General Air); CO (10%, Scott gas);  $\text{H}_2$  (99.9%, Scott gas)) are controlled by Brooks 5850E electronic mass flow controllers. Methanol and formaldehyde will be introduced to the system by passing  $\text{O}_2/\text{He}$  mixture through a series of sealed flasks immersed in a thermostated oil bath. In this case, the desired concentrations are achieved by controlling the mixture flow rate and by varying the oil bath temperature.

Flow reaction studies were performed in a fixed-bed microreactor, shown in Figure 3.2. The reactor is a quartz tube, 30 cm long and 1.0 cm ID at the catalyst bed portion, mounted vertically in a tubular furnace. The catalyst samples is loaded into the reactor and covered with a layer of quartz beads to obtain a uniform gas distribution and a preheating zone. The exit diameter is decreased to 5 mm ID right after the quartz frit so the reaction products leave the heated zone more rapidly. Pulse reaction tests were carried out in a thin quartz reactor shown in Figure 3.3. The reactor is 30 cm long and 5 mm ID. A smaller diameter reactor was used to reduce the dead volume in the tube since we are pulsing small amounts of reactant to the catalyst. Two K-type (chromel-alumel)

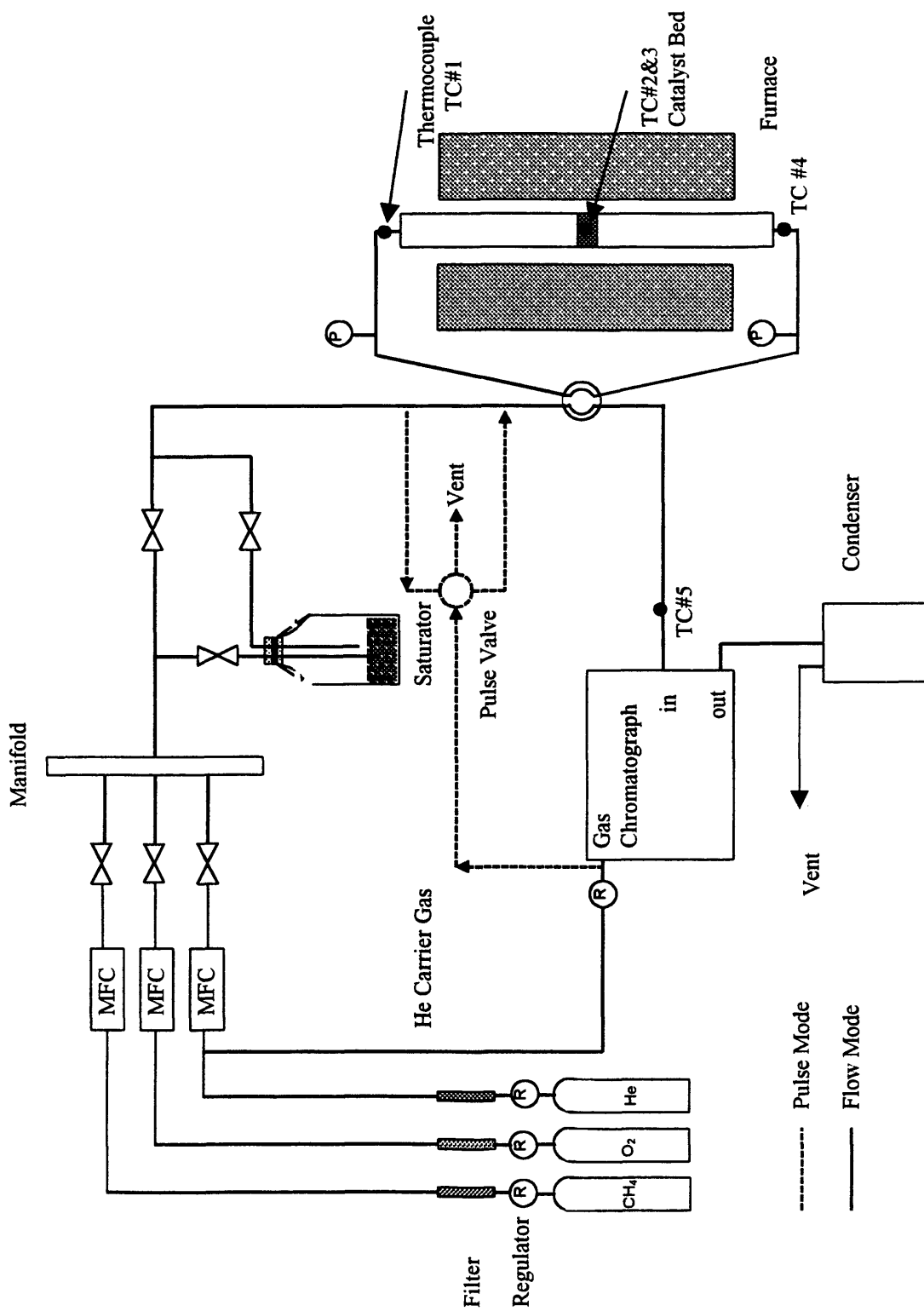
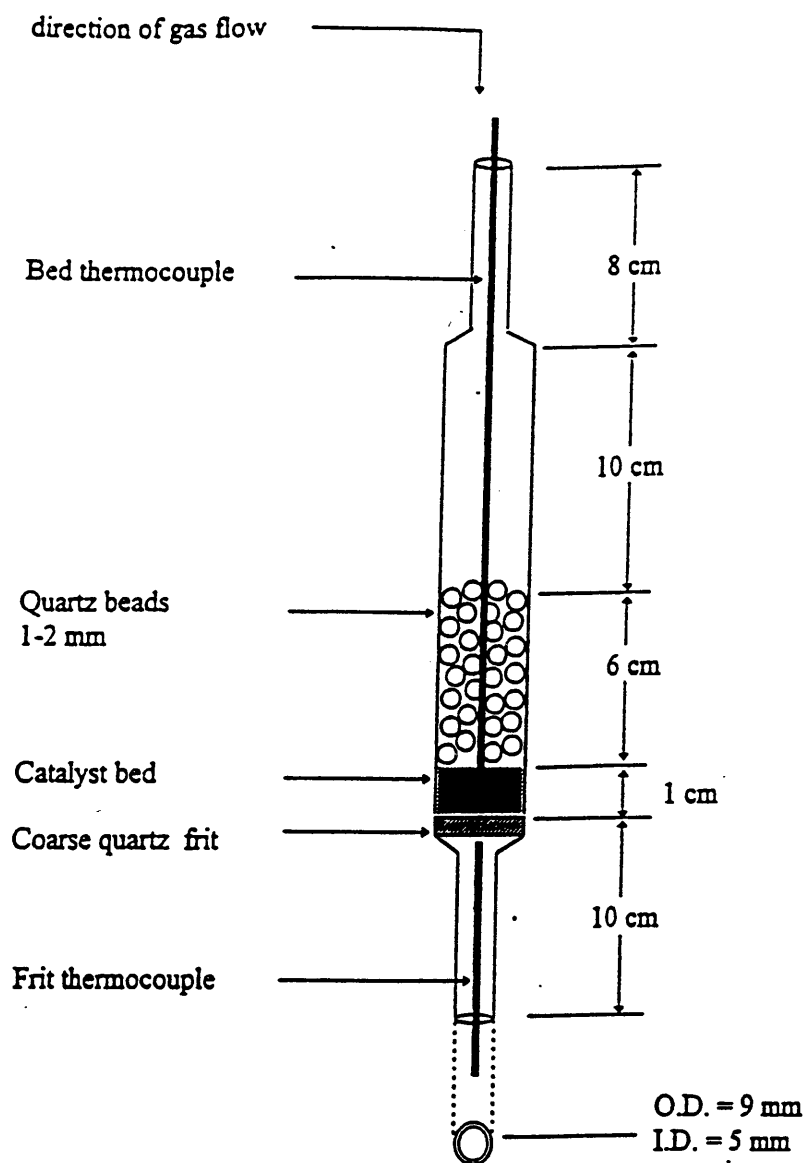


Figure 3.1 Reactor System



Source: Harrick Science Corporation, 88 Broadway, NY.

Figure 3.4 Reaction Chamber for In-situ IR experiments.

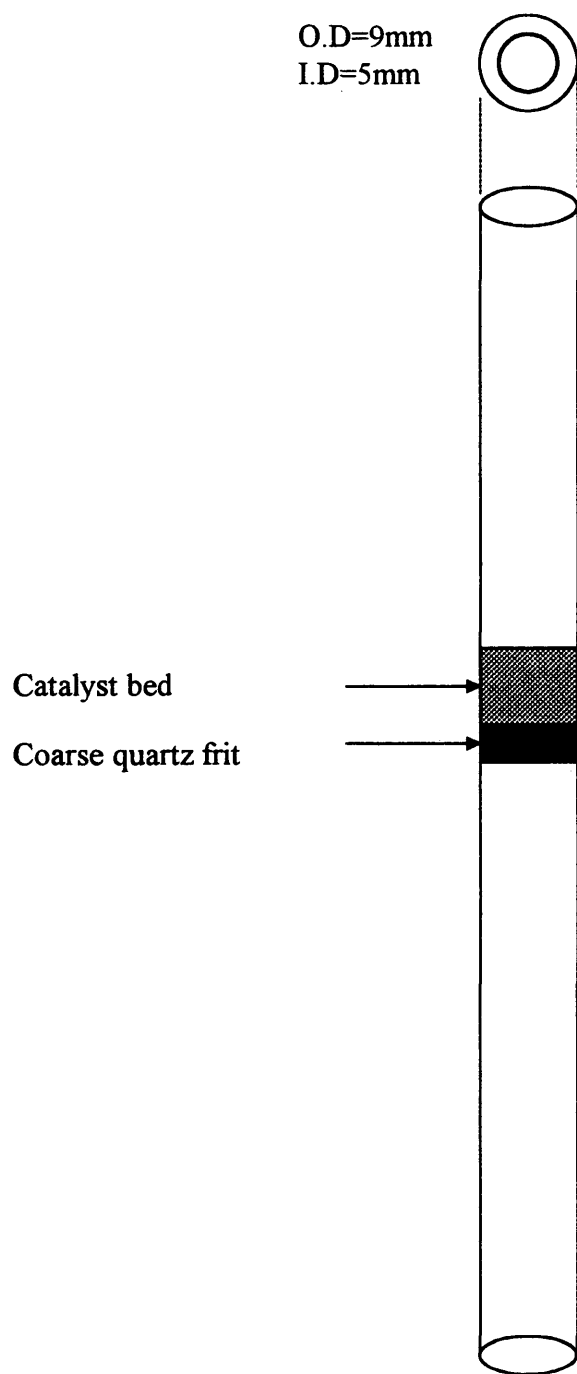


Figure 3.3 Pulse Reactor

thermocouples, one placed in contact with the catalyst bed and the other right under the frit, are used to monitor the temperature.

The catalyst is heated in situ up to reaction temperature (723-923 K) in a helium flow (20 ml/min). To stay above the upper flammability limit, methane is introduced into the reactor first and methane conversion is kept below 10% for all experiments reported.

Conversion and selectivity are defined as:

$$\text{Conversion} = \frac{\text{moles (HCHO + CO + CO}_2\text{) formed}}{\text{moles CH}_4\text{ fed}} \quad (3.1)$$

$$\text{Selectivity} = \frac{\text{moles HCHO formed}}{\text{moles (HCHO + CO + CO}_2\text{) formed}} \quad (3.2)$$

The overall carbon balance closures obtained are within 5 %.

The product stream is analyzed by an on-line Hewlett-Packard 5890 Gas Chromatograph (GC) equipped with a thermal conductivity detector (TCD). Specifications of the GC are given in Alptekin (1998a).

In pulse experiments, an unknown peak was detected on the GC. To further examine the outlet gas of a pulse test the products stream was connected to a mass spectrometer. A VG Quadrupoles mass spectrometer was used to continuously analyze the reactor outlet gas.

To insure that the measured rate data were not confounded by internal and external mass or heat transfer limitations, experimental and analytical tests were carried out by Alptekin, (1998). In these tests, it was shown that the methane oxidation reaction

is kinetically controlled and not limited by internal and external mass or heat transfer processes under the reaction conditions used in this study. Since this work is done under the same conditions, there was no need to check them again.

#### **3.2.2.2. Oxygen Chemisorption:**

O<sub>2</sub> chemisorption experiments are used to measure the oxygen atom surface site density. Before the experiments, the catalyst was reduced in hydrogen for two hours at 823 K. At this high temperature surface reduction occurs without reducing the bulk catalyst, Faraldos et al. (1997). Then O<sub>2</sub> chemisorption is achieved by dosing small amounts of oxygen over the pre-reduced catalyst. The pulse system is used in this experiment and the GC-TCD is used to record the peaks. The ratio of oxygen uptake to the surface area gives the site density in moles/m<sup>2</sup>, Oyama et al. (1989).

Catalyst samples of 0.25 gm were dried in helium (30 cm<sup>3</sup>/min) and then reduced in hydrogen at 823 K under 30 cm<sup>3</sup>/min for two hours. The catalyst is then cooled to room temperature in 30 cm<sup>3</sup>/min He. Oxygen chemisorption was performed by dosing 0.05 cm<sup>3</sup> pulses of oxygen. A GC-TCD was used to determine the amount of consumed oxygen.

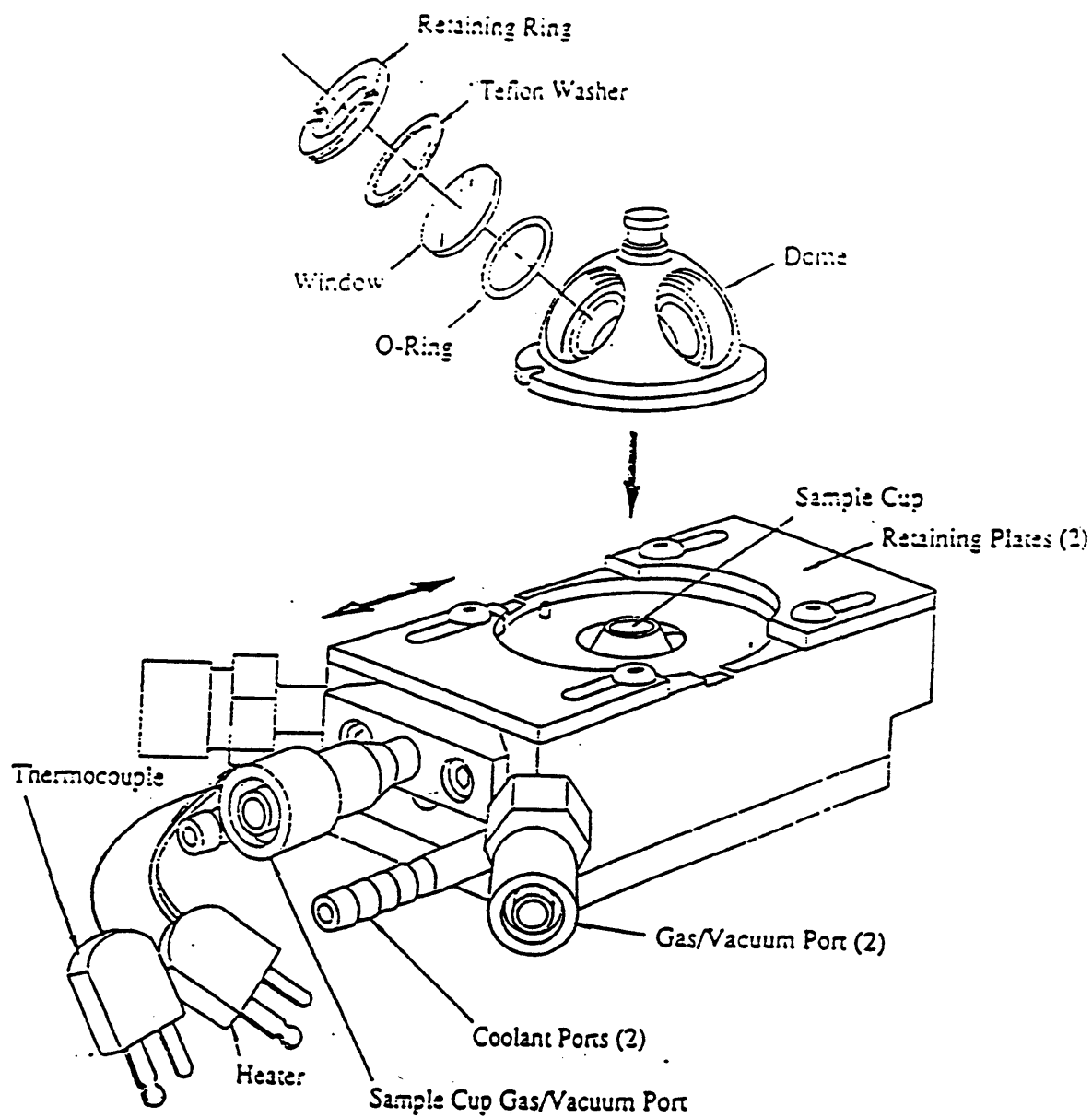
#### **3.2.2.3. Fourier Transform Infrared Spectroscopy (FTIR):**

IR studies for methanol and carbon monoxide provide evidence for the different types of molecules present on the catalyst surface. Many studies suggest that the first step

in methane activation occurs via methoxy groups. Probing the catalyst surface while the reaction is in progress may help in suggesting an acceptable mechanism.

In IR, a beam of infrared light is directed at a solid sample, and a detector measures the fraction of photons that absorb as a function of frequency. Then the observed IR spectrum is compared to ones from a series of reference compounds to learn about the bonding of molecules to the surface. In many studies, these experiments give some very useful information about the bonding of adsorbed complexes, however only minimal useful information was obtained in this work.

In-situ infrared spectra were acquired for methanol and carbon monoxide chemisorbed on both the precipitated silica and the iron phosphate catalyst. Spectra were acquired using a BioRad FTS-40 infrared spectrometer. The device is equipped with a Harrick diffuse reflectance attachment and a liquid nitrogen cooled MCT detector. In these experiments the catalyst (50 mg) is placed in a sample cell covered by a dome with KBr windows allowing exposure of the sample to the controlled gas environments. Temperature of the cell is controlled by an electric heater. IR tests were carried out at 298, 473 and 673 K. At each temperature the IR spectrum was collected before and after the methanol adsorption. Argon is used in collecting a spectrum before the adsorption of reactant gases and this spectrum is used as a reference. It is also used after the adsorption experiment to remove the methanol from the system. Spectra acquired following the argon purge indicate if there is anything chemisorbed on the catalyst surface. The reaction chamber used for in-situ IR experiments is presented in Figure 3.4.



Source: Harrick Science Corporation, 88 Broadway, NY.

Figure 3.4 Reaction Chamber for In-situ IR experiments.

## CHAPTER 4

### METHANE PARTIAL OXIDATION OVER SILICA

Because of its high porosity and surface area, silica is used as a support in many catalytic processes. It also can withstand severe process conditions (high temperatures and pressures). At the present time, it is believed that silica is the best support for methane partial oxidation. Moreover, many researchers think that precipitated silica is the active catalyst, Parmaliana et al. (1991, 1994, 1997). Therefore, an extensive study of precipitated silica was made in this work. On the other hand, this work can be used as a reference for studying the silica-supported iron phosphate. Since there are no quantitative results comparing methane partial oxidation over both catalysts, qualitatively the difference in the catalyst activity is attributed to the presence of the iron phosphate.

#### 4.1 Flow Reactor Studies:

The objective of these experiments is to examine the reaction of possible intermediates and to gain some kinetic insight on what is happening in these steps. In addition, experimental data are collected for comparison to model and parameter evaluation.

The gas phase reactions are negligible under the given experimental conditions. A series of experiments was performed in the absence of a catalyst and no oxygenated

products were seen. Hence, the results reported in this section are due to heterogeneous reactions.

#### 4.1.1 Carbon Monoxide Oxidation:

Carbon monoxide oxidation is the simplest reaction in the methane partial oxidation series of reactions. Carbon dioxide is the only reaction product. The oxidation experiments were conducted over precipitated silica catalyst in the temperature range of 673-833 K, gas hourly space velocity (GHSV) of  $40000 \text{ h}^{-1}$ , carbon monoxide pressure of 2.5-10 kPa at constant oxygen pressure of 2.5 kPa, and in oxygen range of 2-9 kPa at constant carbon monoxide pressure of 9 kPa. Carbon monoxide to oxygen ratio varied from 1 to 4. The effect of reactant partial pressure is shown in Figure 4.1. Power-law kinetics ( $-r_{\text{CO}} = k P_{\text{CO}}^x P_{\text{O}_2}^y$ ) gives an order of  $0.8 \pm 0.1$  in oxygen concentration and  $-0.27 \pm 0.08$  in carbon monoxide concentration over silica. The negative order in CO indicates a competition between CO and O<sub>2</sub> for surface sites, or that as carbon monoxide pressure increases the number of oxidized surface sites able to convert CO to CO<sub>2</sub> goes down. The approximately first order kinetics in oxygen partial pressure may indicate slow surface re-oxidation. The activation energy for the reaction over silica is  $56 \pm 8$  kJ/mol (see Arrhenius plot in Figure 4.2). The main result in this section is the self inhibiting effect of CO for oxidation on silica.

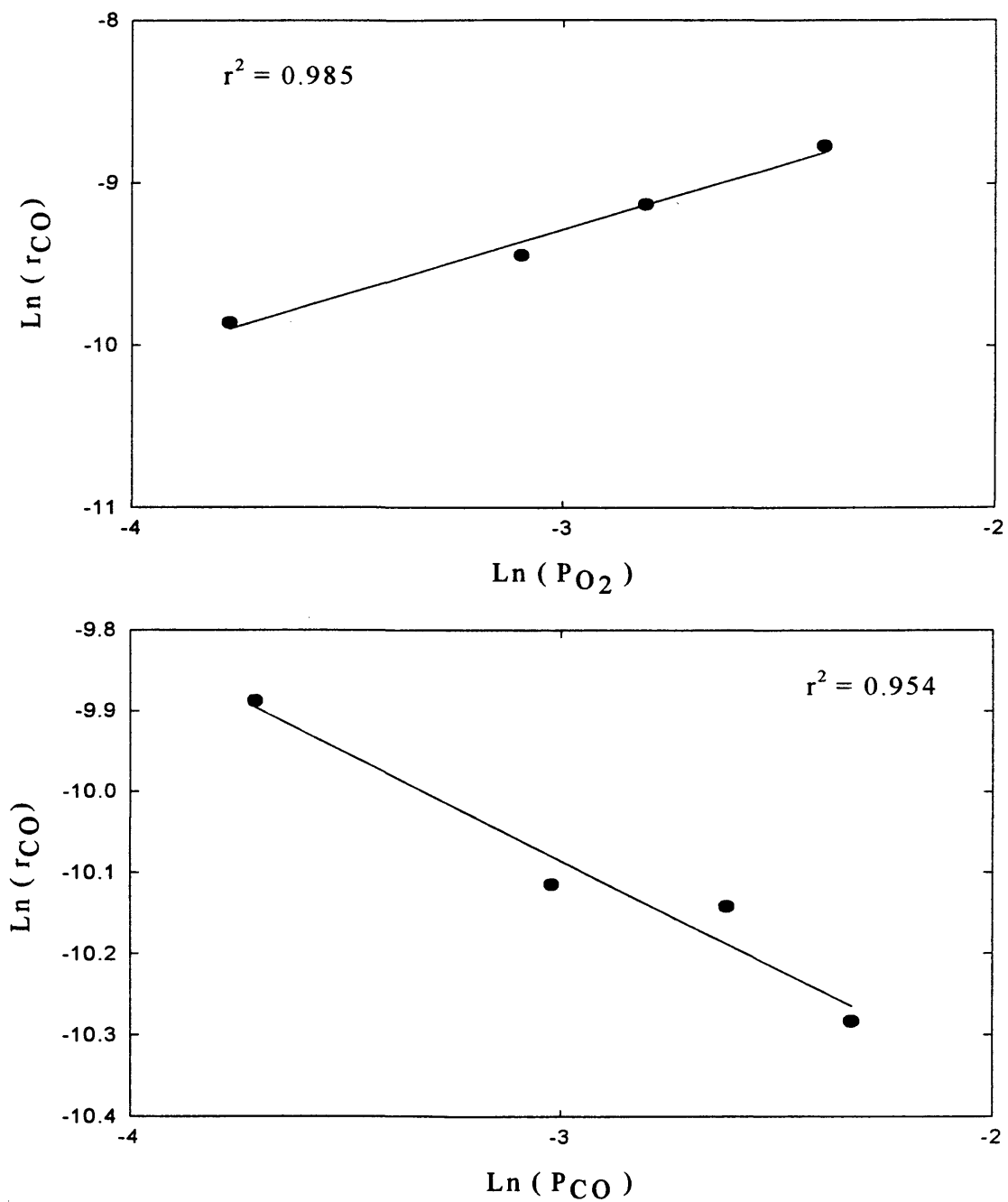


Figure 4.1 Effect of reactants partial pressure on carbon monoxide oxidation rate over silica. GHSV= 40000 h<sup>-1</sup>, P<sub>O<sub>2</sub></sub>=2-9 kPa@P<sub>CO</sub>=9 kPa, P<sub>CO</sub>=2.5-10 kPa @ P<sub>O<sub>2</sub></sub>=2.5 kPa, , and T=673 K.

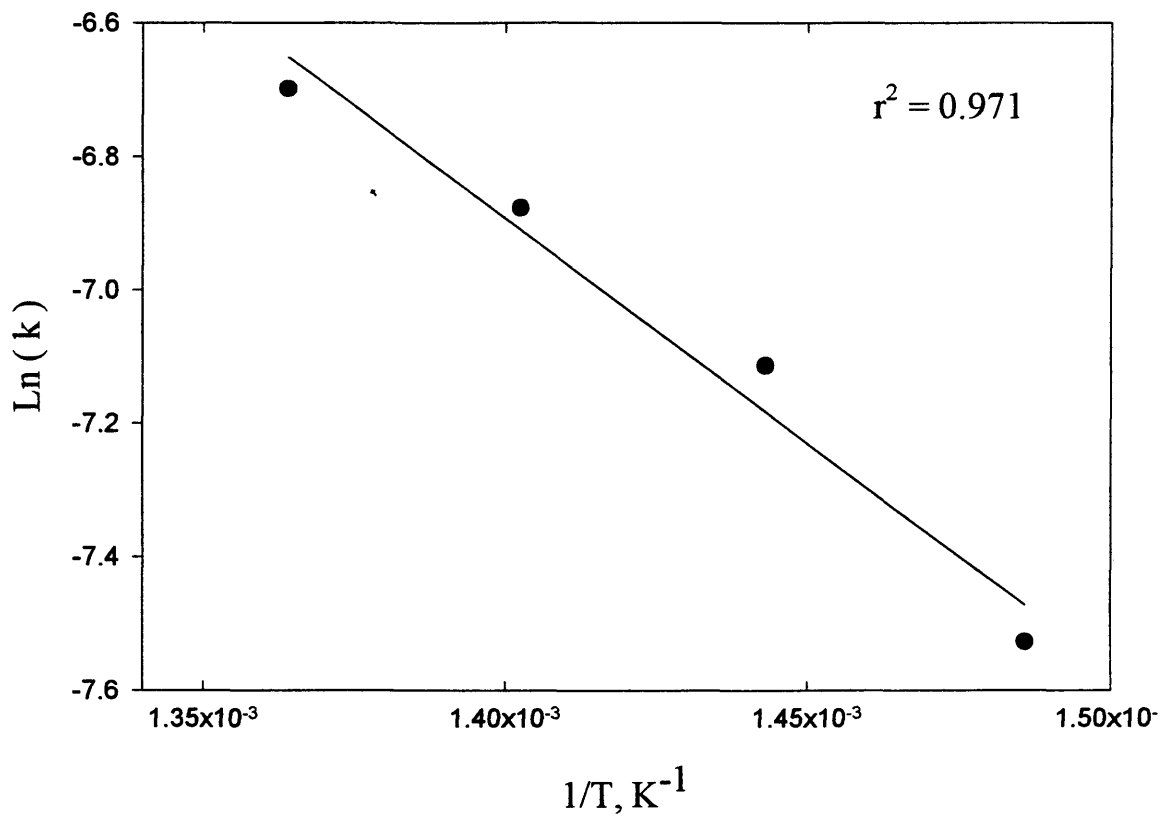


Figure 4.2 Arrhenius plot for carbon monoxide oxidation over silica.  $P_{\text{CO}} = P_{\text{O}_2} = 9 \text{ kPa}$  and  $T=673\text{-}733 \text{ K}$ .

#### 4.1.2 Formaldehyde Oxidation:

Formaldehyde oxidation experiments were conducted under the following conditions, temperature range of 623-673K, GHSV=5000-45000 h<sup>-1</sup>, formaldehyde partial pressure of 2.5-15kPa at constant oxygen pressure of 50 kPa, and oxygen partial pressure of 23-76 kPa at constant formaldehyde pressure of 4 kPa. Formaldehyde to oxygen ratio was in the range of 0.05-0.3. The effect of the reactant partial pressure is shown in Figure 4.3. The reaction order is  $0.69 \pm 0.05$  in oxygen and  $0.8 \pm 0.09$  in formaldehyde concentration. The positive order in oxygen pressure shows the importance of gaseous (or chemisorbed) oxygen in the oxidation reaction as compared to lattice oxygen. Arrhenius plot is shown in Figure 4.4 for this reaction. The activation energy for the oxidation over silica is  $111 \pm 4$  kJ/mol. Carbon monoxide and carbon dioxide are the only reaction products. Product selectivity as a function of formaldehyde conversion is given in Figure 4.5. As the formaldehyde conversion approaches 2%, CO selectivity is increasing slowly. No experimental data are available between the 2% and zero conversion. If carbon monoxide selectivity increases exponentially with decreasing conversion, then it is the principle product in formaldehyde oxidation and is converted sequentially to CO<sub>2</sub>. That can be presented as follows:



If, on the other hand, CO selectivity increased in the same slow rate when approaching zero conversion then CO<sub>2</sub> is also produced in parallel path directly from formaldehyde oxidation.

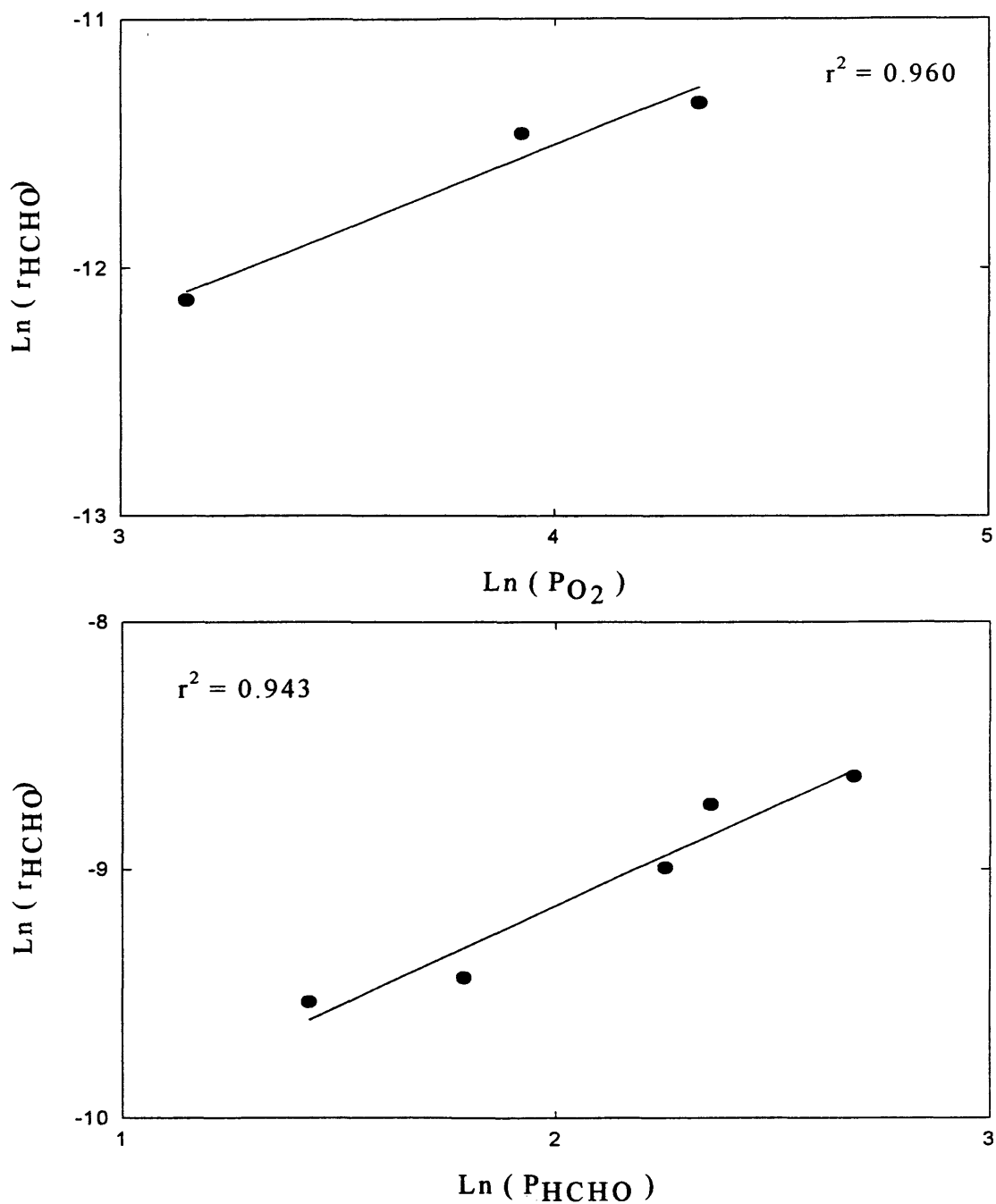


Figure 4.3 Effect of reactants partial pressure on formaldehyde oxidation rate over silica. GHSV= 25000 h<sup>-1</sup>, P<sub>O<sub>2</sub></sub> = 23-76 kPa @ P<sub>HCHO</sub>= 4 kPa, P<sub>HCHO</sub> = 4-15 kPa @ P<sub>O<sub>2</sub></sub> = 50 kPa and T= 648 K.

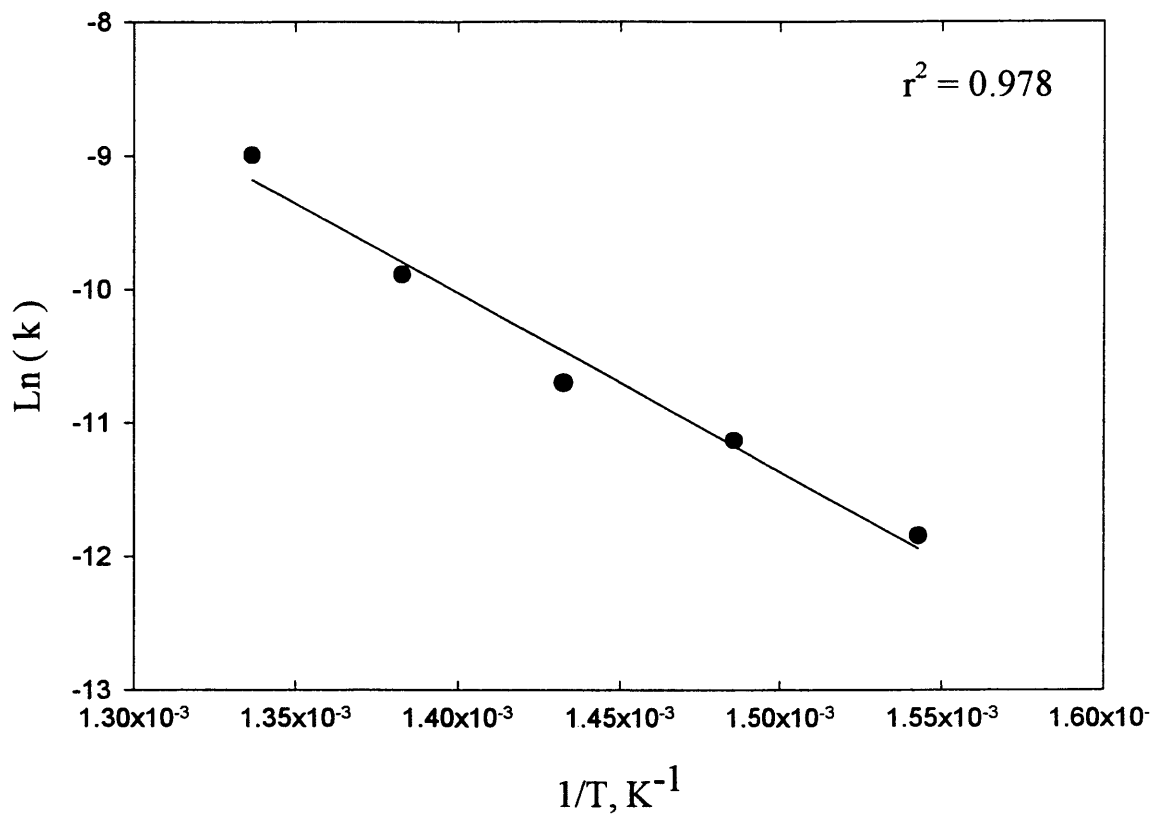


Figure 4.4 Arrhenius plot for formaldehyde oxidation over silica.  $P_{\text{O}_2} = 50 \text{ kPa}$ ,  $P_{\text{HCHO}} = 4.5 \text{ kPa}$ , and  $T = 648\text{--}723 \text{ K}$ .

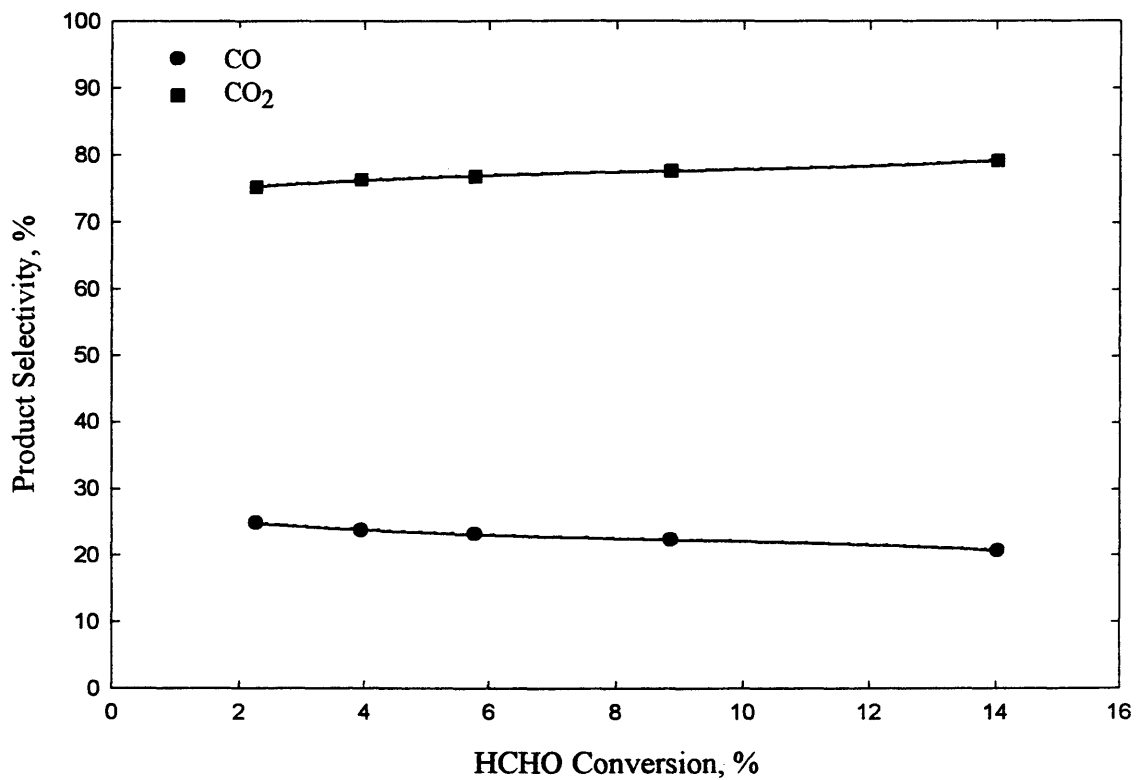


Figure 4.5 Product selectivity (%) as a function of formaldehyde conversion (%) for silica. GHSV= 5000-45000 h<sup>-1</sup>, P<sub>O<sub>2</sub></sub> = 50 kPa, P<sub>HCHO</sub> = 4.5 kPa, and T= 623-673 K.



Both cases are possible, especially considering that a direct path from methane to  $\text{CO}_2$  is reported.

#### 4.1.3 Methanol Oxidation:

The methanol experiments were studied in the temperature range of 648-748K, GHSV= 5000-45000  $\text{h}^{-1}$ , methanol pressure range of 33-42 kPa, oxygen partial pressure of 18-63 kPa, and methanol to oxygen ratio of 0.2-1.4. The effect of methanol and oxygen partial pressure is given in Figure 4.6. The reaction orders are  $0.4 \pm 0.03$  and  $0.43 \pm 0.05$  in oxygen and methanol, respectively, with activation energy of  $133 \pm 6$  kJ/mol. The Arrhenius plot for methanol oxidation is shown in Figure 4.7. Compared to formaldehyde oxidation, the low reaction orders and the similar activation energies may indicate that methanol oxidation is less complicated. Formaldehyde, carbon monoxide and carbon dioxide are the only products of methanol oxidation. Product selectivity as a function of methanol conversion is presented in Figure 4.8. Formaldehyde is the only product at the zero conversion, then CO is produced from HCHO oxidation and converted to  $\text{CO}_2$  after that. The sequential reaction is :



It should be noticed that formaldehyde is relatively stable over silica. Up to methanol conversion of 3%, HCHO is almost the only product. In that conversion range, CO and  $\text{CO}_2$  selectivity are always less than 15%.

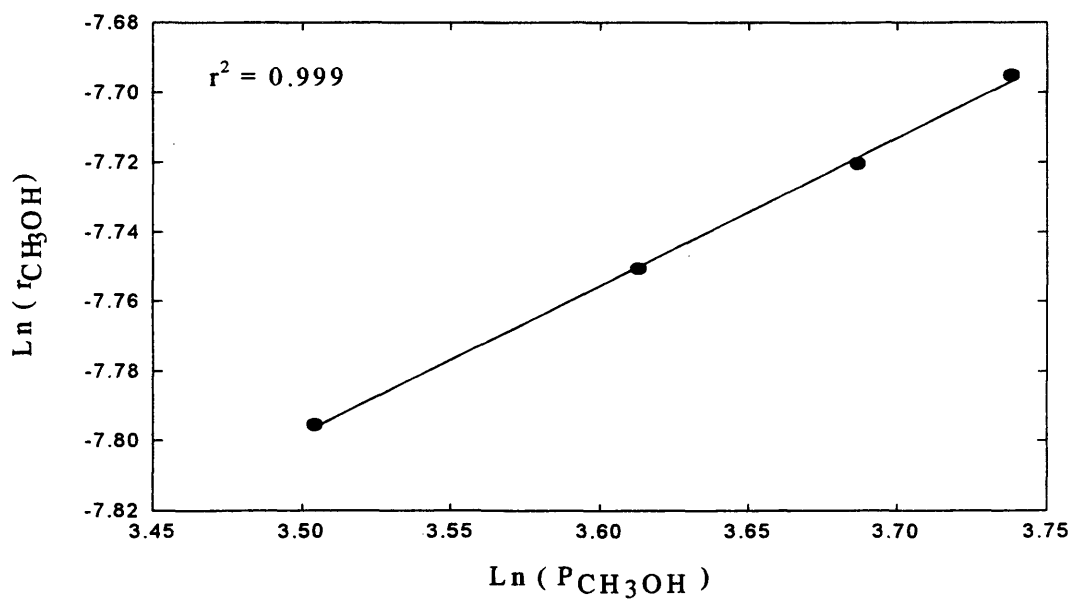
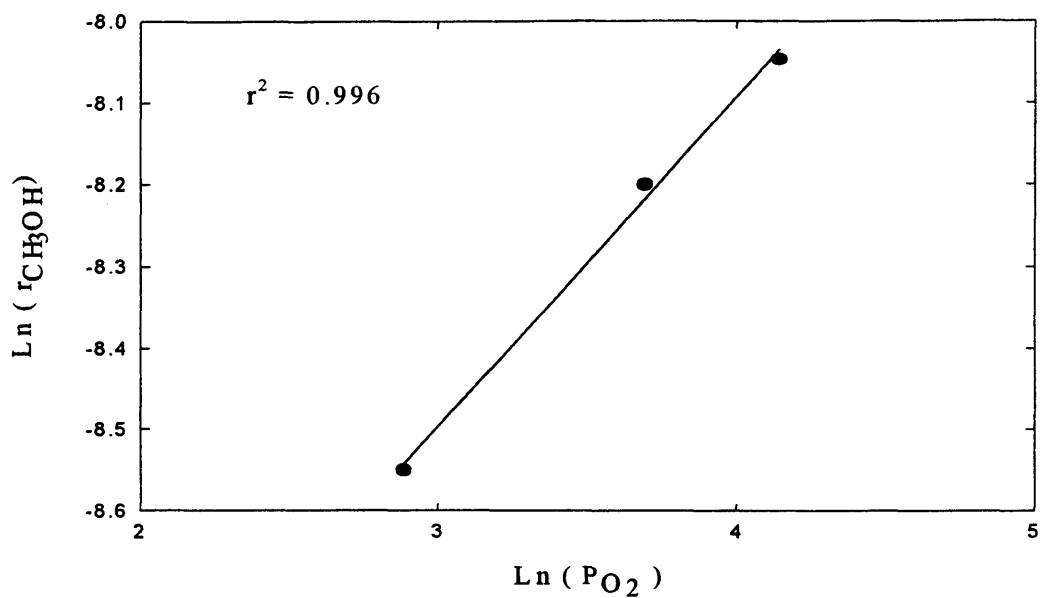


Figure 4.6 Effect of reactants partial pressure on methanol oxidation rate over silica. GHSV= 35000  $\text{h}^{-1}$ ,  $P_{\text{O}_2} = 18\text{-}63$  kPa @  $P_{\text{CH}_3\text{OH}} = 24$  kPa,  $P_{\text{CH}_3\text{OH}} = 33\text{-}42$  kPa @  $P_{\text{O}_2} = 33$  kPa and  $T = 723$  K.

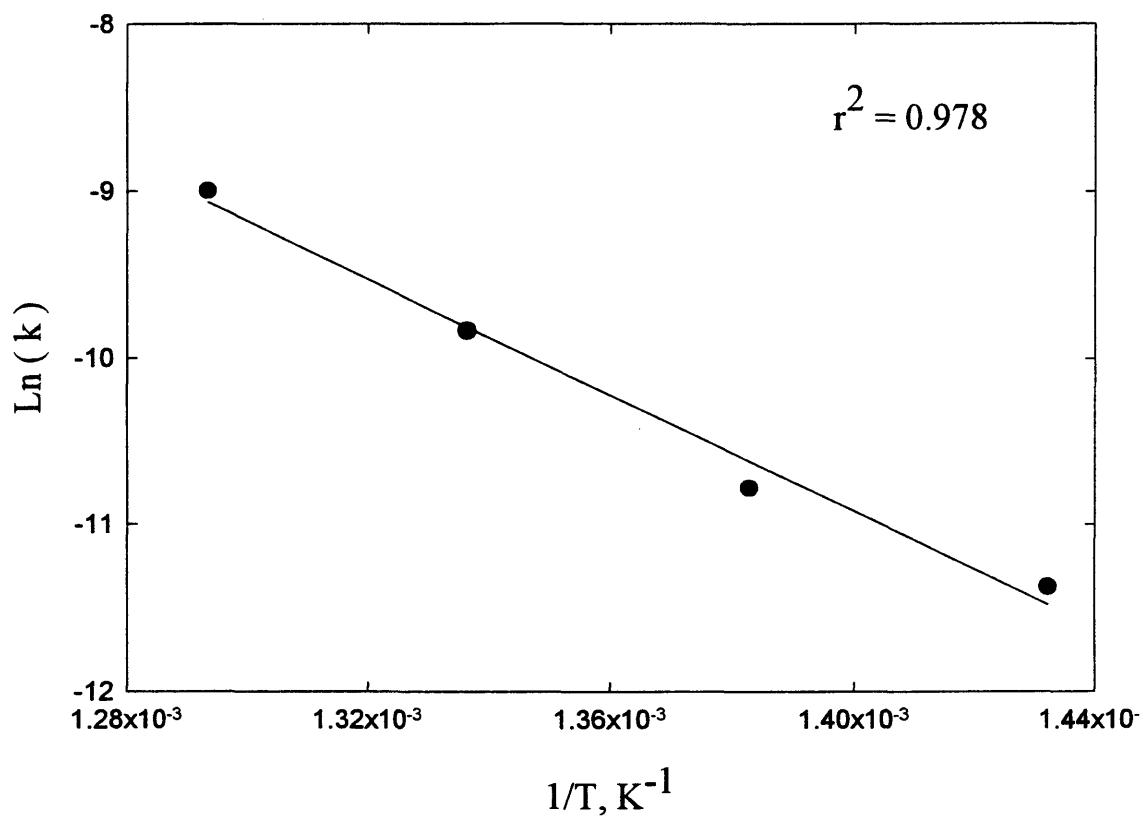


Figure 4.7 Arrhenius plot for methanol oxidation over silica.  $P_{\text{O}_2} = 50$  kPa,  $P_{\text{CH}_3\text{OH}} = 6$  kPa, and  $T = 673$ - $773$  K.

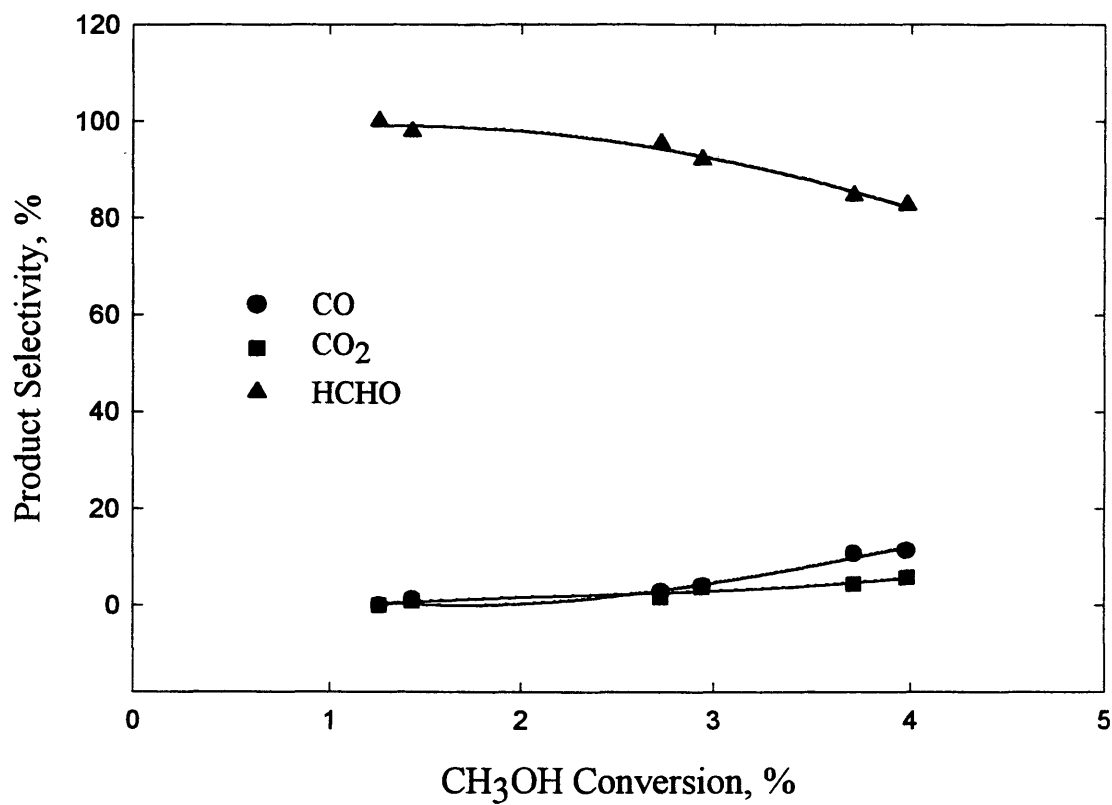


Figure 4.8 Product selectivity (%) as a function of methanol conversion (%) for silica. GHSV= 5000-45000 h<sup>-1</sup>, P<sub>O<sub>2</sub></sub> = 50 kPa, P<sub>CH<sub>3</sub>OH</sub> = 6 kPa, and T= 673-773 K.

#### 4.1.4 Methane Oxidation:

These experiments were conducted in the temperature range of 823-898 K, GHSV= 30000 h<sup>-1</sup>, methane partial pressure of 9-50 kPa and oxygen partial pressure of 9-40 kPa. Methane to oxygen ratio varied from 1 to 4. Note that the temperature required for methane partial oxidation is much higher than used for carbon monoxide, formaldehyde and methanol oxidation. The effect of reactant partial pressure on the observed rate is shown in Figure 4.9. The reaction order for methane is  $0.9 \pm 0.07$ . The plot of reaction rate versus oxygen partial pressure is not linear, suggesting that a simple power-law model cannot accurately describe the kinetics of this reaction. Oxygen reaction order appears to be changing with temperature from 1 at 848 K to 2 at 873 K; this is shown in Figure 4.10. Figure 4.11 show that the activation energy for this reaction is  $142 \pm 4$  kJ/mol over silica. Figure 4.12 shows product selectivity as a function of methane conversion. At conversions approaching zero, CO<sub>2</sub> selectivity is high ( 30% ) suggesting a direct path from CH<sub>4</sub> to CO<sub>2</sub>. CO selectivity is almost zero at this conversion meaning it is mainly produced from formaldehyde oxidation. That can be presented as:



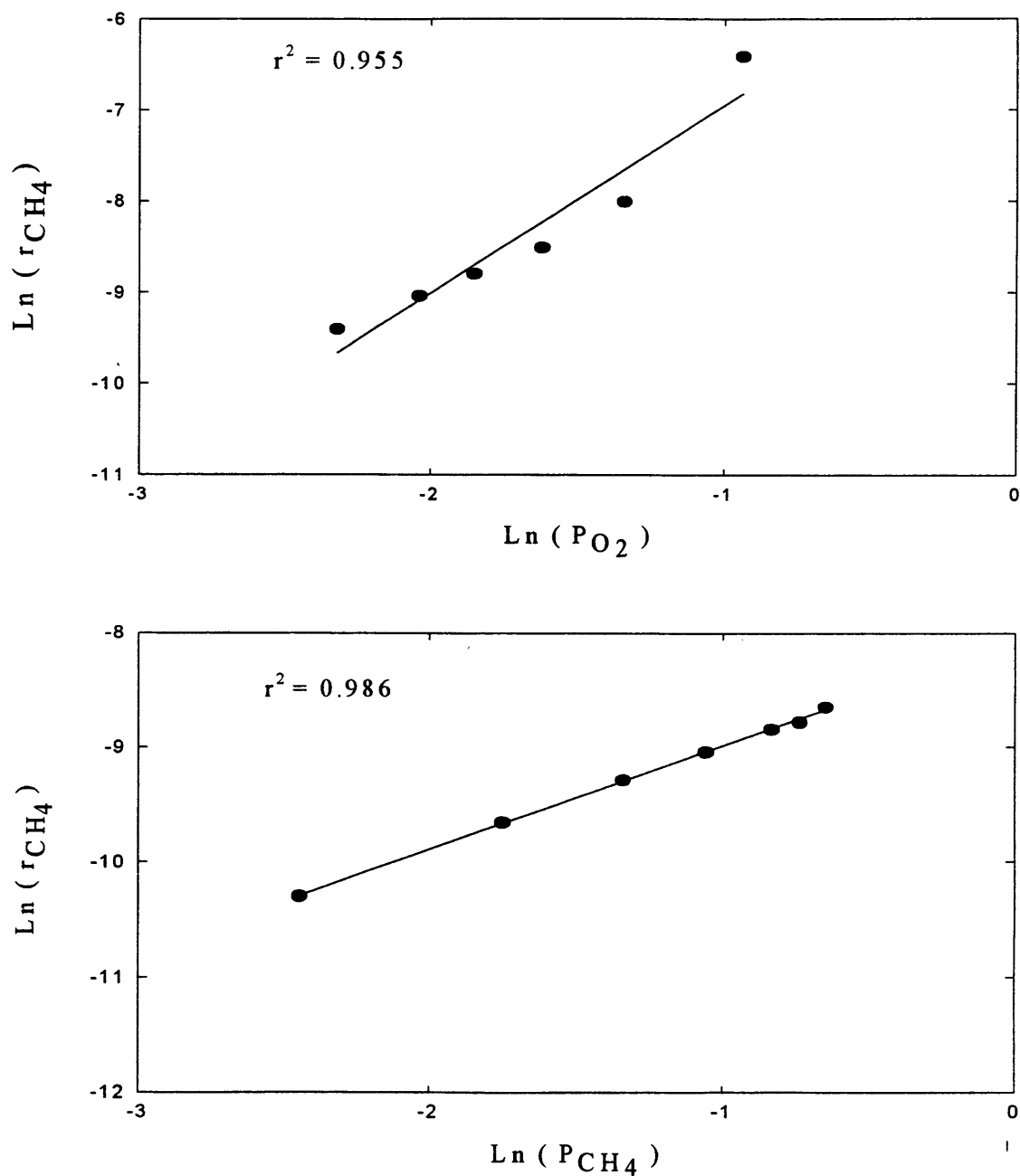


Figure 4.9 Effect of reactants partial pressure on methane oxidation rate over silica. GHSV= 30000 h<sup>-1</sup>, P<sub>O<sub>2</sub></sub> = 9-40 kPa @ P<sub>CH<sub>4</sub></sub> = 40 kPa, P<sub>CH<sub>4</sub></sub> = 9-50 kPa @ P<sub>O<sub>2</sub></sub> = 9 kPa and T= 873 K.

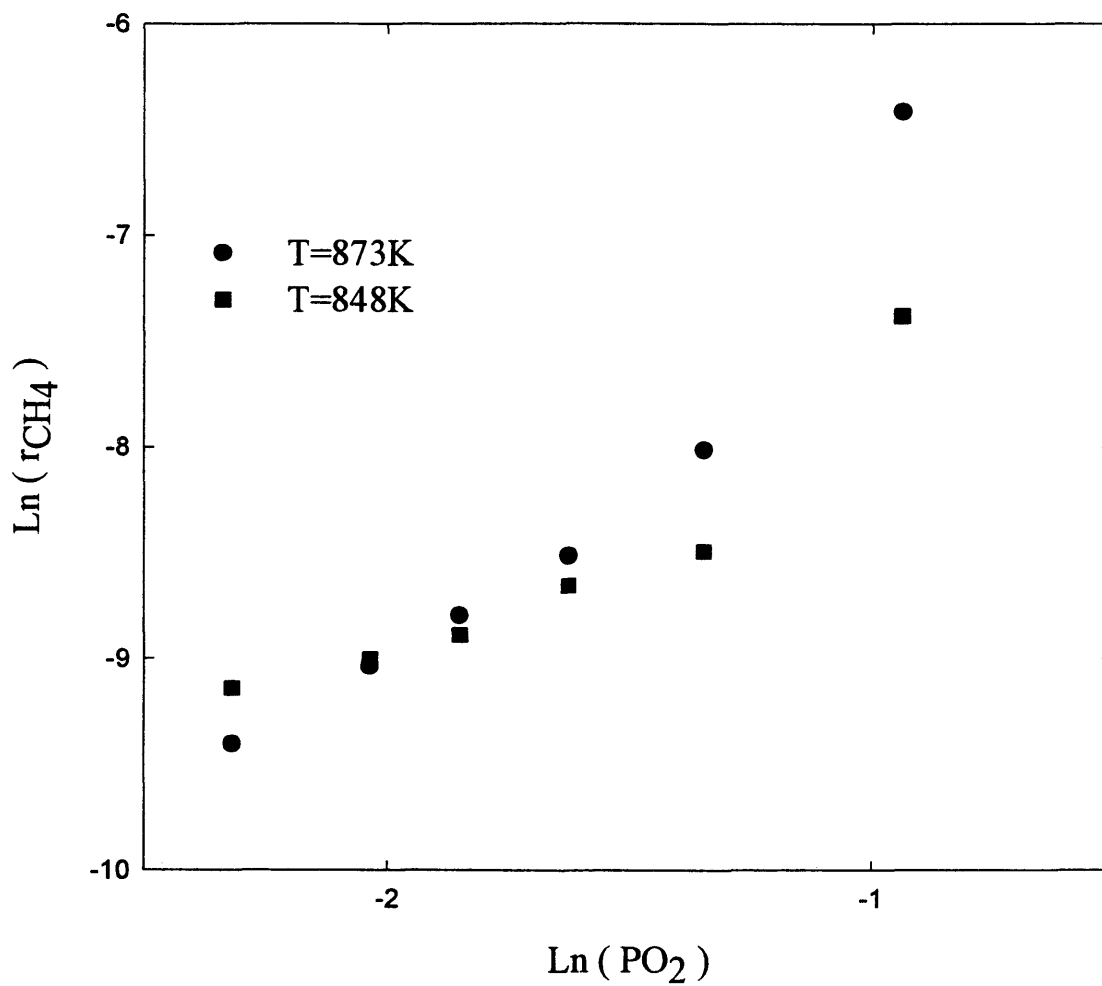


Figure 4.10 The effect of oxygen partial pressure on methane partial oxidation rate over silica. GHSV=30000  $\text{h}^{-1}$ ,  $P_{\text{O}_2}$ =9-40 kPa @ $P_{\text{CH}_4}$ =40 kPa.

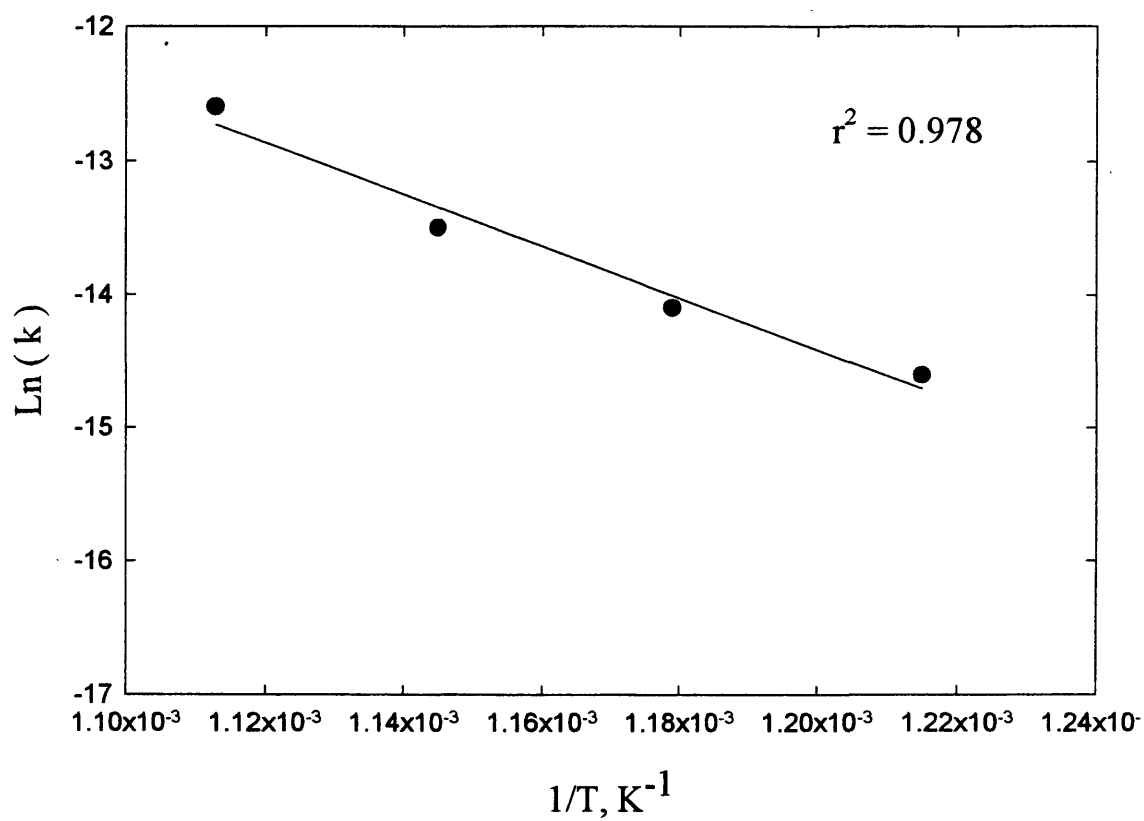


Figure 4.11 Arrhenius plot for methane oxidation over silica.  $P_{\text{O}_2} = 20$  kPa,  $P_{\text{CH}_4} = 40$  kPa, and  $T = 823$ - $898$  K.

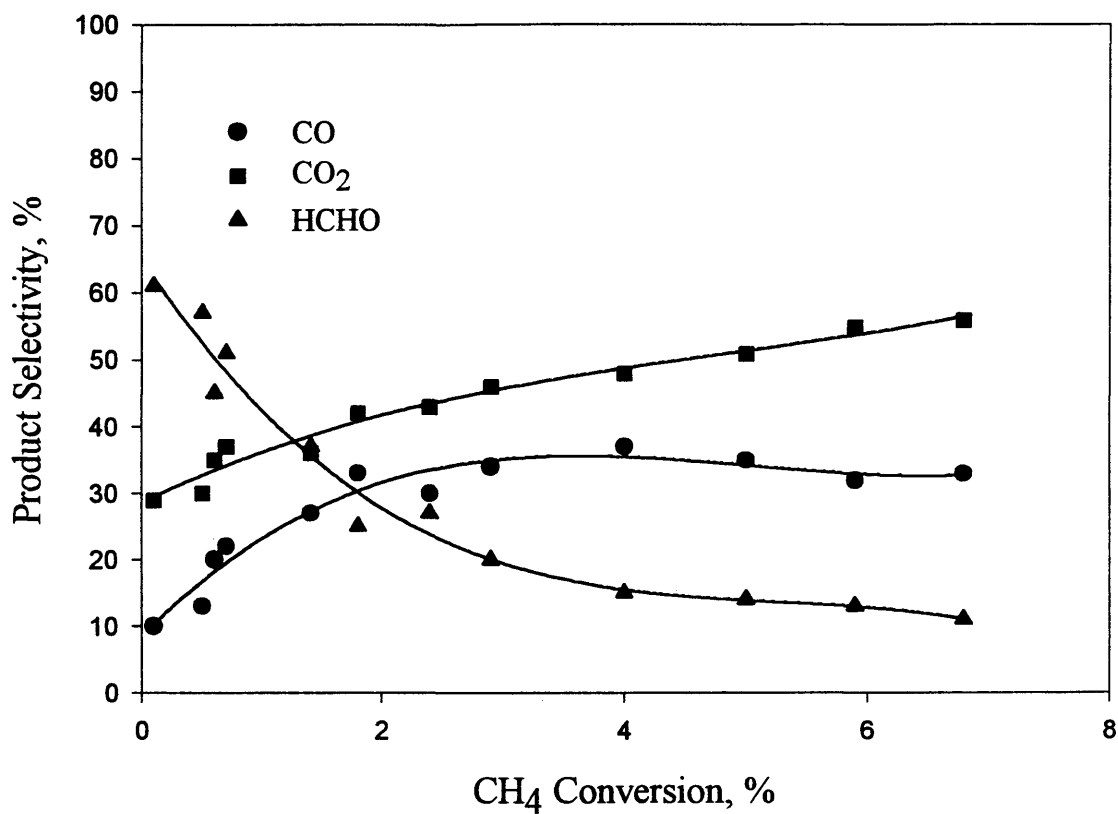


Figure 4.12 Product selectivity (%) as a function of methane conversion (%) for silica. GHSV= 30000 h<sup>-1</sup>, P<sub>O<sub>2</sub></sub> = 20 kPa, P<sub>CH<sub>4</sub></sub> = 40 kPa, and T= 823-898 K.

## 4.2 Pulse Reactor Studies:

Pulse studies were divided into three parts. The first experiment is to investigate the role of molecular and lattice oxygen in the methane partial oxidation. The second experiment was to study the different types of catalyst surface pretreatment. The last were designed to examine an unknown peak that was produced in the pulse tests when analyzing the product stream by GC. In this case the same experiments were repeated using a mass spectrometer.

### 4.2.1 The Role of Gaseous and Lattice Oxygen:

Methane partial oxidation on silica in the presence and in the absence of molecular oxygen was studied in the temperature range 823-923 K by a pulse reactor connected to a GC. If the methane reaction rate is the same in the presence and absence of gaseous oxygen, then it is reacting with lattice oxygen. But if it react only in the presence of molecular oxygen, then surface or chemisorbed oxygen is necessary for methane oxidation. To avoid a change in the catalytic surface state in the pulse experiments from its state under steady state conditions, the reaction mixture ( $\text{CH}_4/\text{O}_2/\text{He}$ ) was pulsed before and after the reducing pulse ( $\text{CH}_4$ ). The result of these experiments is presented in Table 4.1. We can see that only when gas mixtures containing oxygen are sent over the catalyst do we have significant conversion. Perhaps at the highest temperature lattice oxygen has a limited role in methane oxidation, and the participation of lattice oxygen can therefore be neglected.

Table 4.1 Methane partial oxidation in the presence and absence of gas-phase oxygen in pulsed reaction experiment.

Catalyst	T <sub>r</sub> (°C)	Reagents	CH <sub>4</sub> Conv. %	Selectivity		
				HCHO	CO	CO <sub>2</sub>
SiO <sub>2</sub>	550	CH <sub>4</sub> +O <sub>2</sub>	0.37	9.0	0.0	91.0
		CH <sub>4</sub>	0.00	0.0	0.0	
	600	CH <sub>4</sub> +O <sub>2</sub>	0.65	9.2	0.0	90.8
		CH <sub>4</sub>	0.00	0.0	0.0	
	650	CH <sub>4</sub> +O <sub>2</sub>	1.10	8.9	7.4	83.7
		CH <sub>4</sub>	0.15	0.0	0.0	100.0

#### **4.2.2 The Effect of Different Pretreatment on the Catalyst Surface:**

The second part of this study investigated pretreatment of the catalyst surface. Pretreatments include oxidizing and reducing the surface and reacting with the reactant mixture. The results in Table 4.2 show that only when the reaction mixture is used do we get products, independent of pretreatment. The presence of gaseous oxygen is required to get significant conversion. Comparing runs 1 and 6, pre-treating the catalyst with the reactant gas mixture gives higher conversions but oxidizing the surface gives better formaldehyde selectivity. This shows the importance of the adsorbed oxygen species in producing the oxygenated products.

#### **4.2.3 Investigating Unknown Peak:**

When using the GC to analyze the outlet gas from the pulse experiments, we noticed the presence of an unknown peak. To further study that phenomenon, a VG Quadrupole mass spectrometer was used. The results of the mass spectrometer runs are shown in Figures 4.13. Each peak in this graph shows the products of a  $\text{CH}_4/\text{O}_2$  pulse. Over silica, formic acid was detected. Methanol was not observed in the GC analysis for continuous and pulse experiments, but was known to be present based on prior work of Alptekin (1998). Formic acid has been observed in methanol IR experiments as  $\text{CH}_2$  bonded to two surface oxygen, Busca (1989). Amiridis et al. (1991) assumed that this species is weakly adsorbed formaldehyde on an oxidized site over metal oxides. On

Table 4.2 Pulse study results for methane partial oxidation over silica at 873 K.

Run	Pretreatment (3 Pulses)	Pulse	CH <sub>4</sub> Conv.%	Selectivity			Rate mol/(g <sub>cat</sub> ·min) g/(kg <sub>cat</sub> ·hr)	STY
				HCHO	CO	CO <sub>2</sub>		
1	CH <sub>4</sub> /O <sub>2</sub> /He	CH <sub>4</sub> /O <sub>2</sub> /He	0.65	9.2	0.0	90.8	5.8E-05	10.5
2	CH <sub>4</sub> /O <sub>2</sub> /He	CH <sub>4</sub> /He	0.00	0.0	0.0	0.0	0.0	0.0
3	CH <sub>4</sub> /O <sub>2</sub> /He	O <sub>2</sub> /He	0.00	0.0	0.0	0.0	0.0	0.0
4	CH <sub>4</sub> /He	CH <sub>4</sub> /O <sub>2</sub> /He	0.11	0.0	0.0	100.0	1.0E-05	0.0
5	CH <sub>4</sub> /He	O <sub>2</sub> /He	0.00	0.0	0.0	0.0	0.0	0.0
6	O <sub>2</sub> /He	CH <sub>4</sub> /O <sub>2</sub> /He	0.30	18.9	0.0	81.1	2.7E-05	9.9
7	O <sub>2</sub> /He	CH <sub>4</sub> /He	0.00	0.0	0.0	0.0	0.0	0.0

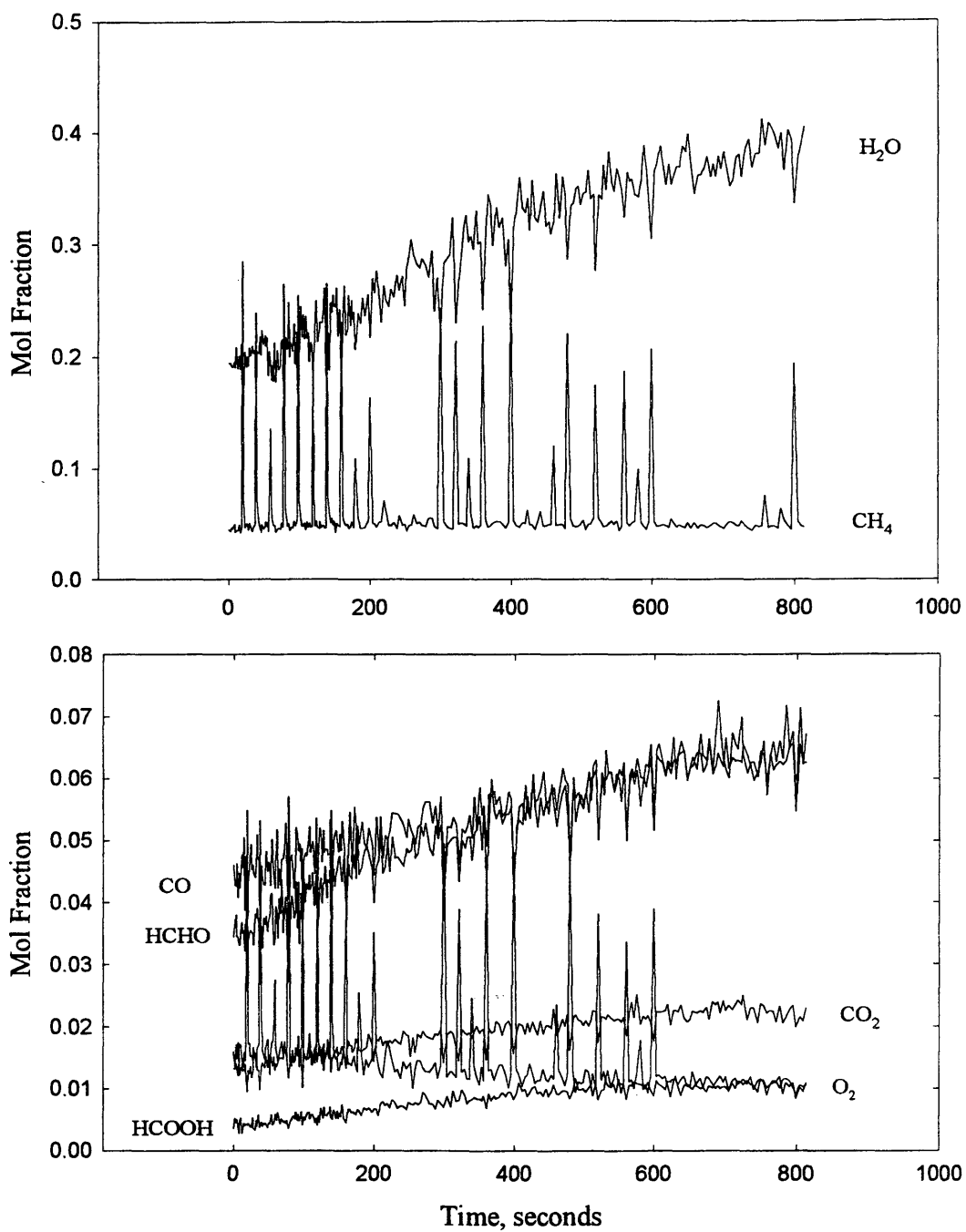


Figure 4.13 Mass spectral gas analysis of the effluent from pulse experiment over  $\text{SiO}_2$  at  $T=873$  K,  $P_{\text{O}_2}=20$  kPa and  $P_{\text{CH}_4}=40$  kPa.

silica, this is the first time it has been detected. Note that the formic acid was not seen in the product from the first few pulses but after that it increased dramatically. In the beginning, formic acid was confused with dimethyl ether (DME) since they have the same mass. However, DME is detected at a different retention time in the gas chromatogram, Alptiken (1998), indicating that the peak is formic acid. In that respect we can say that methane is converted to formic acid then to carbon monoxide and water, and in turn CO is converted to CO<sub>2</sub>.

Pulse product concentrations increase with the number of methane pulses. This may be explained by the slow desorption of these products. CO<sub>2</sub> and HCOOH are produced at the same rate, which means that the formic acid is the main source for carbon dioxide production.

#### **4.3 Oxygen Chemisorption:**

Oxygen chemisorption is the simplest technique for measuring the active surface area of metal oxide based catalysts. In this method, the catalyst is reduced in hydrogen then oxygen is chemisorbed to measure the number of reduced sites. Although silica does not have redox abilities (silicon does not cycle through two oxidation states), this technique was used and oxygen was chemisorbed on the silica surface, meaning that the bare precipitated silica itself has active sites that react with oxygen. Presumably these are defect sites but little is known about silica chemistry at the atomic level.

The surface area for silica is 398 m<sup>2</sup>/gm. This area was evaluated using the BET method, Alptekin (1998). Oxygen uptake over silica yields an oxygen atom site density of  $4.2 \times 10^{15}$  atoms/m<sup>2</sup>. This atom site density is close to the site density reported by Arena et al. (1999) for silica, but is considered high for catalyst without redox ability. During the continuous study, precipitated silica was a good catalyst for methane and other oxidation reactions mainly because of its ability to adsorb an active oxygen species on some type of active site. These active sites may be defects consisting of silicon atoms that are bonded to only three oxygen atoms. Due to the high activity of silica and the need for adjacent sites for methane and oxygen activation and dissociation, it is suggested that these active sites are present in island or line defects.

#### **4.4 In-situ IR Experiment:**

Carbon monoxide and methanol IR spectra were acquired for precipitated silica. Little was understood from the CO spectra, because bands are very weak. It is clear that carbon monoxide is only weakly adsorbed on silica. IR results for CO oxidation and chemisorption are presented in Appendix A. Methanol on the other hand adsorbs strongly on silica and more information is drawn from this study.

Methoxide species are believed to be an important intermediate in methane partial oxidation, Pac and Lunsford (1997) and Jongsomjit (1998). To investigate this assumption, in-situ IR for methanol chemisorption was performed. The experiments were done at room temperature, 473 and 673 K. In this temperature range, the methoxy groups

are reasonably stable, Jongsomjit (1998). The IR spectrum for methanol oxidation over silica at 673 K is shown in Figure 4.14. Bands in the range 1600-1700 and 3200-3700 are assigned to hydroxyl groups. Strong CO<sub>2</sub> bands are observed on silica at 2400 cm<sup>-1</sup>. Note that before and after methanol introduction the CO<sub>2</sub> bands were not seen, ruling out the possibility that CO<sub>2</sub> is coming from air. This indicates that methanol is reacting under the experimental conditions.

Methanol adsorption over silica was studied at three different temperatures; the results of these experiments are shown in Figures 4.15, 4.16 and 4.17. Since all graphs give the same results, only the one at T=473 K will be discussed. The spectrum indicates the presence of C-H vibrations in the range 2800-3000 cm<sup>-1</sup>, these are assigned to methanol and methoxy groups. CO<sub>2</sub> bands are also seen in the adsorption experiments, this means that methanol is reacting with lattice oxygen over silica or that there is a small oxygen impurity in the argon or dissolved in the methanol. Note that the CO<sub>2</sub> band did not appear before or after the methanol chemisorption and the band increases in intensity as the temperature increases.

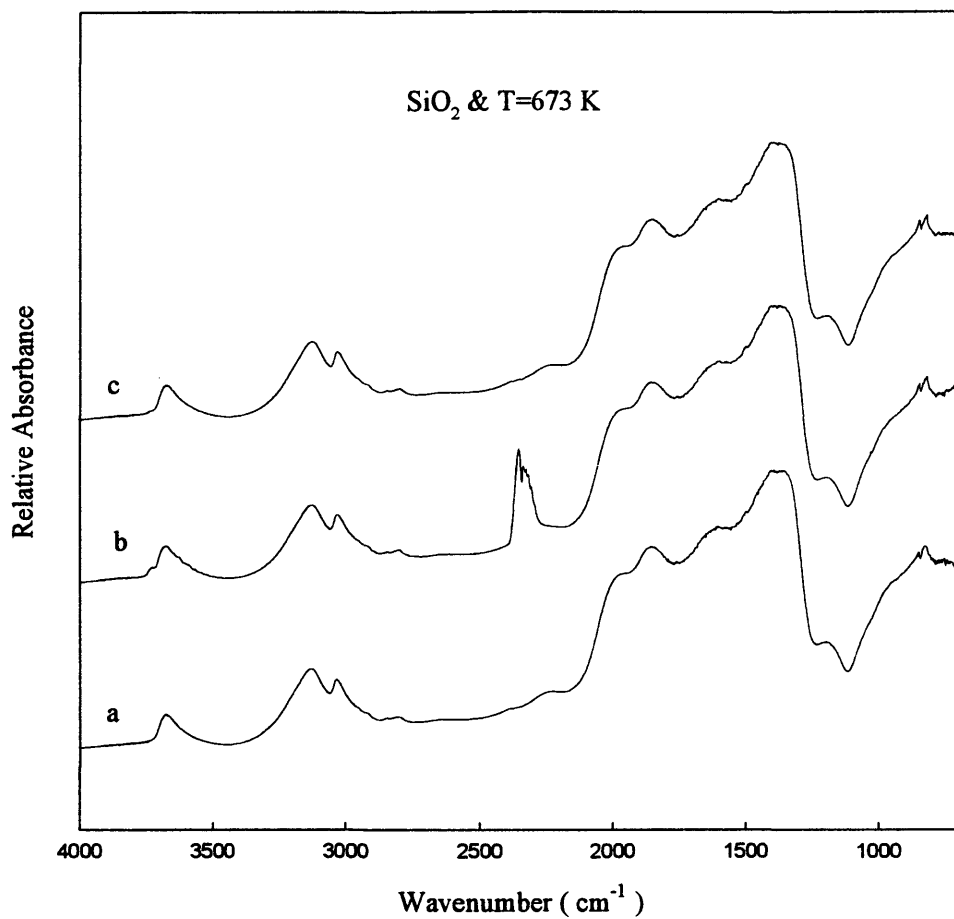


Figure 4.14 IR spectra of methanol oxidation over silica catalyst at T=673 K:  
a. Before oxidation, Ar was introduced for 1 hr.  
b. During reaction, CH<sub>3</sub>OH + O<sub>2</sub> was introduced for 1 hr.  
c. After oxidation, Ar was introduced for 1 hr.

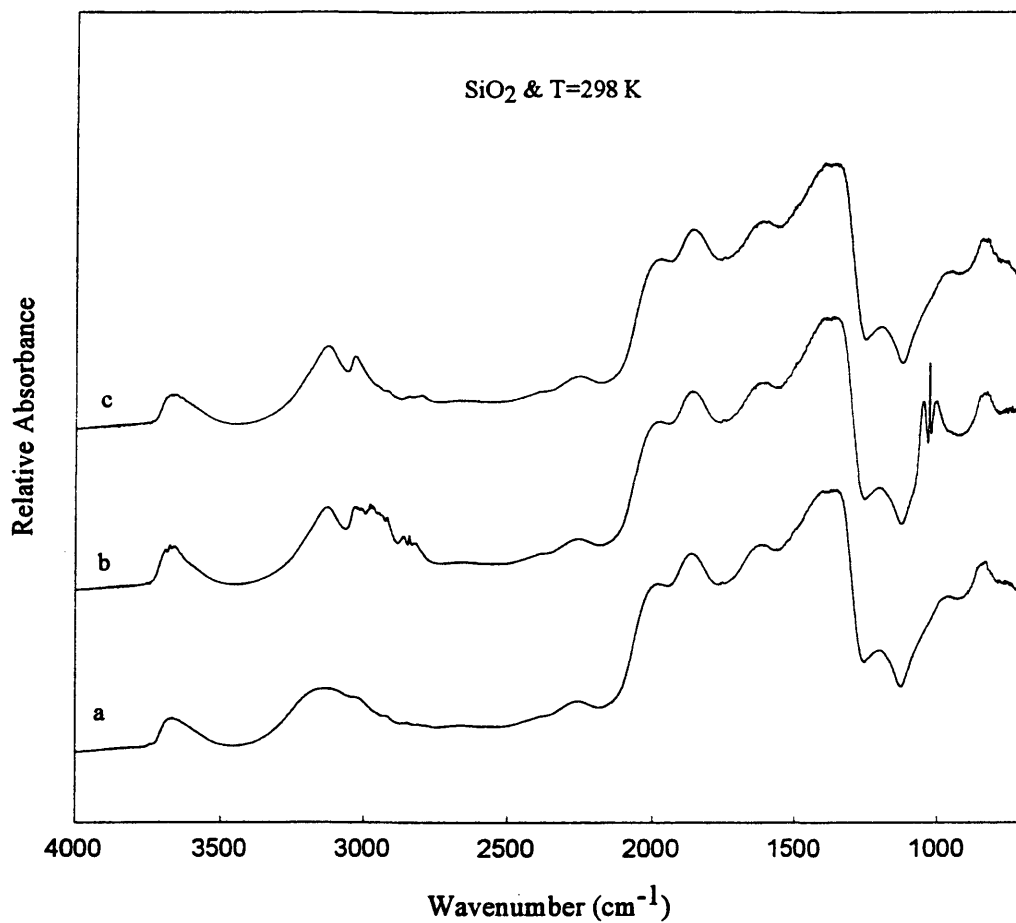


Figure 4.17 IR spectra of methanol adsorption over silica catalyst at T=673 K:  
a. Before adsorption, Ar was introduced for 1 hr.  
b. During adsorption, CH<sub>3</sub>OH was introduced for 1 hr.  
c. After adsorption, Ar was introduced for 1 hr.

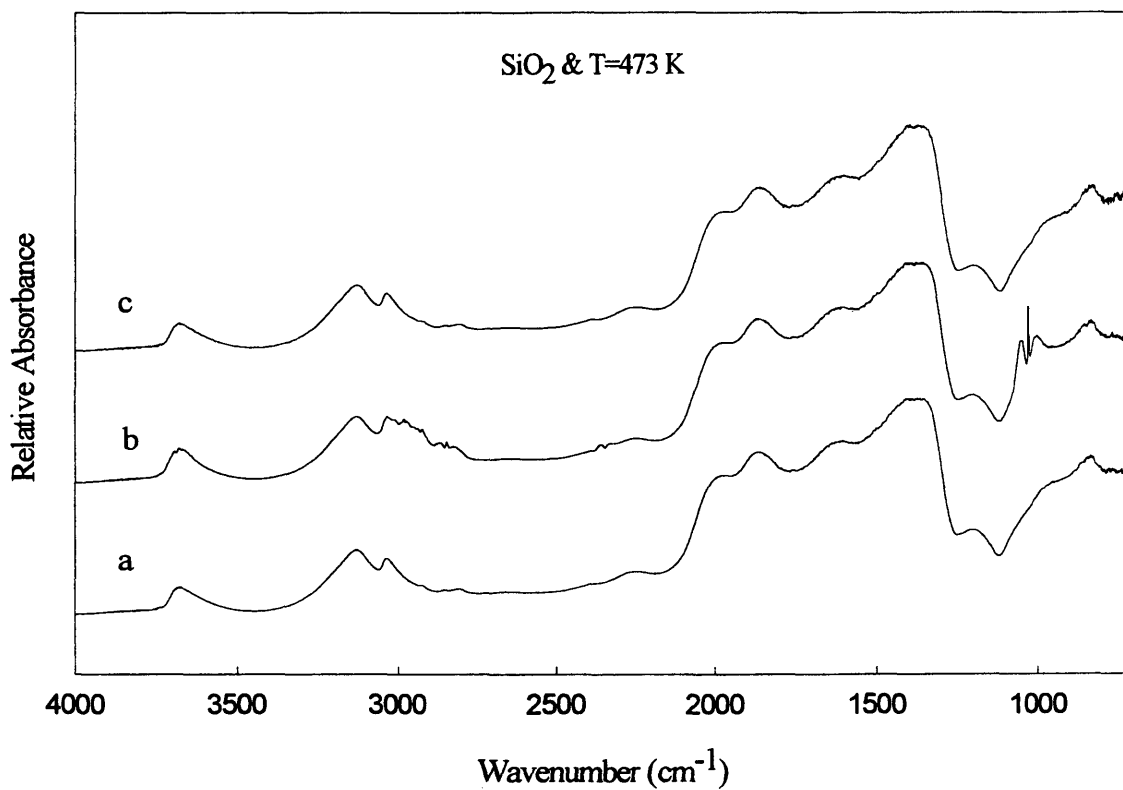


Figure 4.16 IR spectra of methanol adsorption over silica catalyst at  $T=473$  K:  
a. Before adsorption, Ar was introduced for 1 hr.  
b. During adsorption,  $\text{CH}_3\text{OH}$  was introduced for 1 hr.  
c. After adsorption, Ar was introduced for 1 hr.

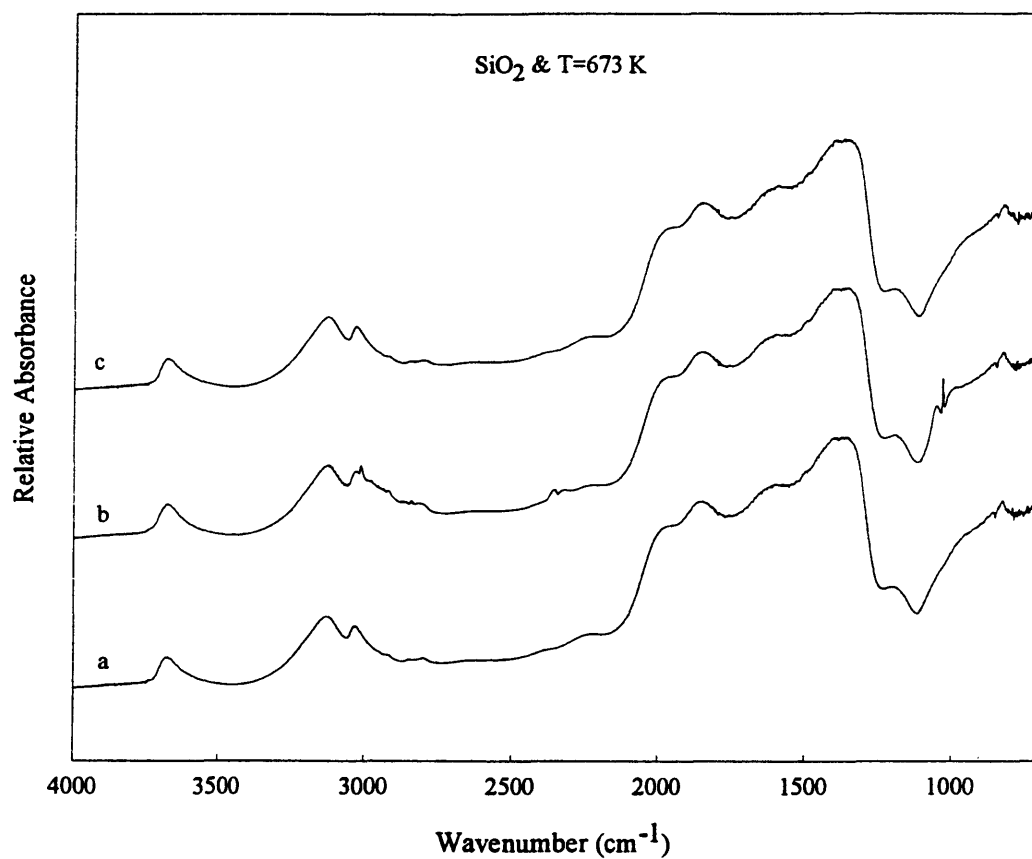


Figure 4.17 IR spectra of methanol adsorption over silica catalyst at  $T=673$  K:  
a. Before adsorption, Ar was introduced for 1 hr.  
b. During adsorption,  $\text{CH}_3\text{OH}$  was introduced for 1 hr.  
c. After adsorption, Ar was introduced for 1 hr.

## CHAPTER 5

### METHANE PARTIAL OXIDATION OVER IRON PHOSPHATE/SILICA

The majority of the research in the methane partial oxidation field has been focused on metal oxides catalysts, primarily  $V_2O_5/SiO_2$  and  $MoO_3/SiO_2$  systems. Silicon oxide appears to be the most effective support for transition metal oxides. Iron phosphate based catalysts are used commercially in the oxidative dehydrogenation of saturated carboxylic acids to unsaturated acids, Millet (1990,1995). Lately, Wang and Otsuka (1995) and Alptekin et al. (1998), reported relatively high yields of methanol and formaldehyde over  $FePO_4$  and  $FePO_4/SiO_2$  catalysts in methane partial oxidation.

An extensive study of silica-supported iron phosphate has been carried out under the best reaction conditions reported by Alptekin (1998). Most of our work in methane partial oxidation was done over silica-supported iron phosphate 2wt.% at  $P_{CH_4}/P_{O_2}$  ratio of 1:1 to 4:1, in the temperature range of 848 to 898 K, and at gas hourly space velocity =30,000  $h^{-1}$ .

#### 5.1 Flow Reactor Studies:

The partial oxidation of desired intermediates produced from methane oxidation have been investigated over the 2wt.% iron phosphate on silica catalyst at the same reaction conditions used for these oxidations over precipitated silica. Any differences in

the catalytic behavior are therefore due to the addition of the 2wt.% iron phosphate or due to the interaction between the iron phosphate and support.

### 5.1.1 Carbon Monoxide Oxidation:

The CO oxidation experiments were conducted in the temperature range of 673-833 K, GHSV of 40000 h<sup>-1</sup>, carbon monoxide pressure of 2.5-10 kPa at constant oxygen pressure of 2.5 kPa, and in oxygen range of 2-9 kPa at constant carbon monoxide pressure of 9 kPa. Carbon monoxide to oxygen ratio varied from 1 to 4. The effect of reactant partial pressure on the reaction rate is shown in Figure 5.1. Power-law kinetics gives an order of  $1.2 \pm 0.11$  and  $-0.1 \pm 0.06$  in oxygen and in carbon monoxide concentrations, respectively. These results are similar to those for silica, with minor differences in the reaction orders. The negative order in CO indicates a competition between CO and O<sub>2</sub> for surface sites, or that as carbon monoxide pressure increases the number of oxidized surface sites able to convert CO to CO<sub>2</sub> goes down. Satterfield (1980) states that a zero-order or negative-order reaction suggests strong adsorption of one or more reactants, (self inhibition). The increased reaction order kinetics in oxygen partial pressure to that over silica may confirm the slow surface re-oxidation. The activation energy for the reaction over iron phosphate/silica is  $32 \pm 3$  kJ/mol, this value almost half the activation energy over silica. The Arrhenius plot is given in Figure 5.2. Similar to the result over silica, the main result here is the inhibiting effect of CO (negative reaction order observed for carbon monoxide).

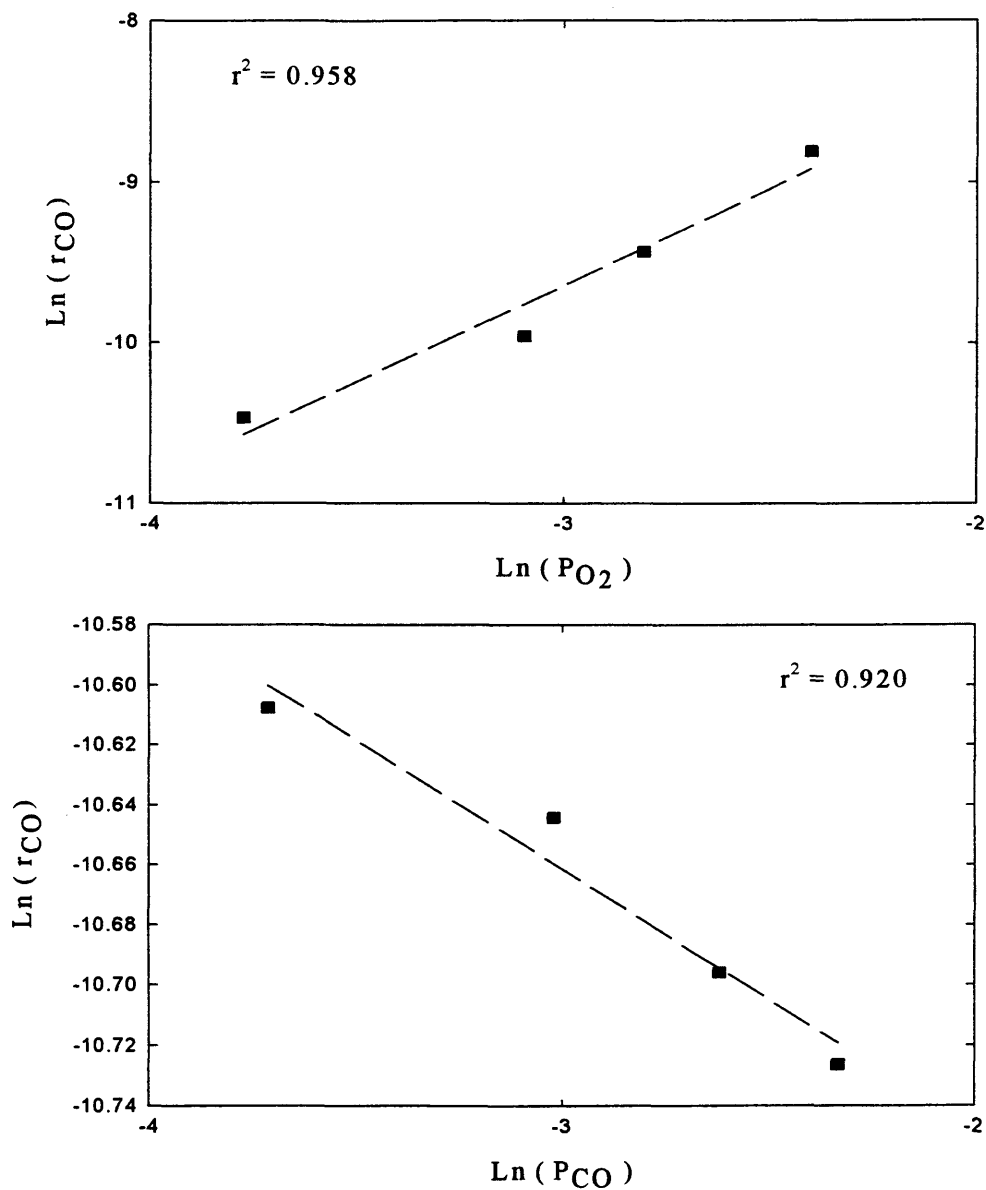


Figure 5.1 Effect of reactants partial pressure on carbon monoxide oxidation rate over supported iron phosphate catalyst. GHSV= 40000  $\text{h}^{-1}$ ,  $P_{\text{O}_2}$ =2-9 kPa @  $P_{\text{CO}}$ =9 kPa,  $P_{\text{CO}}$ =2.5-10 kPa @  $P_{\text{O}_2}$ =2.5 kPa, , and  $T$ =673 K.

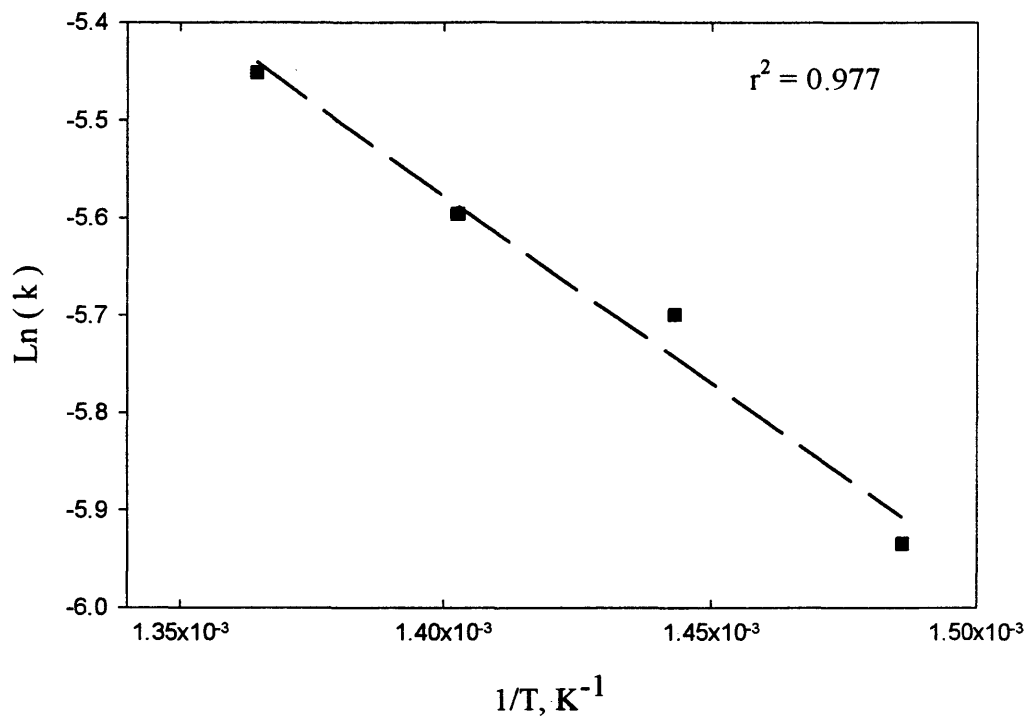


Figure 5.2 Arrhenius plot for carbon monoxide oxidation over supported iron phosphate catalyst.  $P_{\text{CO}} = P_{\text{O}_2} = 9 \text{ kPa}$  and  $T=673\text{-}733 \text{ K}$ .

### 5.1.2 Formaldehyde Oxidation:

Formaldehyde oxidation experiments were conducted under the following conditions: temperature range of 623-673 K, GHSV=5000-45000 h<sup>-1</sup>, formaldehyde partial pressure of 2.5-15 kPa at constant oxygen pressure of 50 kPa, oxygen partial pressure of 23-76 kPa at constant formaldehyde pressure of 4 kPa, and formaldehyde to oxygen ratio of 0.05-0.3. These are the same reaction conditions used in formaldehyde oxidation over silica. The effect of the reactant partial pressure is shown in Figure 5.3. The reaction order is  $0.64 \pm 0.06$  in oxygen and  $0.8 \pm 0.1$  in formaldehyde concentration. The positive order in oxygen pressure shows the importance of gaseous oxygen in the oxidation reaction, also the high reaction order in formaldehyde may imply a difficulty in formaldehyde adsorption. The Arrhenius plot is shown in Figure 5.4 for this reaction. The activation energy for this oxidation over silica-supported iron phosphate is  $100 \pm 7$  kJ/mol. Reaction orders and activation energy are the same for formaldehyde oxidation over both catalysts. Carbon monoxide and carbon dioxide are the only reaction products. Product selectivity as a function of formaldehyde conversion is given in Figure 5.5. This plot is the same as that found over the silica catalyst. Note that the CO<sub>2</sub> production is slightly higher over silica. Formaldehyde reaction chemistry is therefore dominated by the silica surface and little effected by addition of FePO<sub>4</sub>. The reaction network could be as follows:



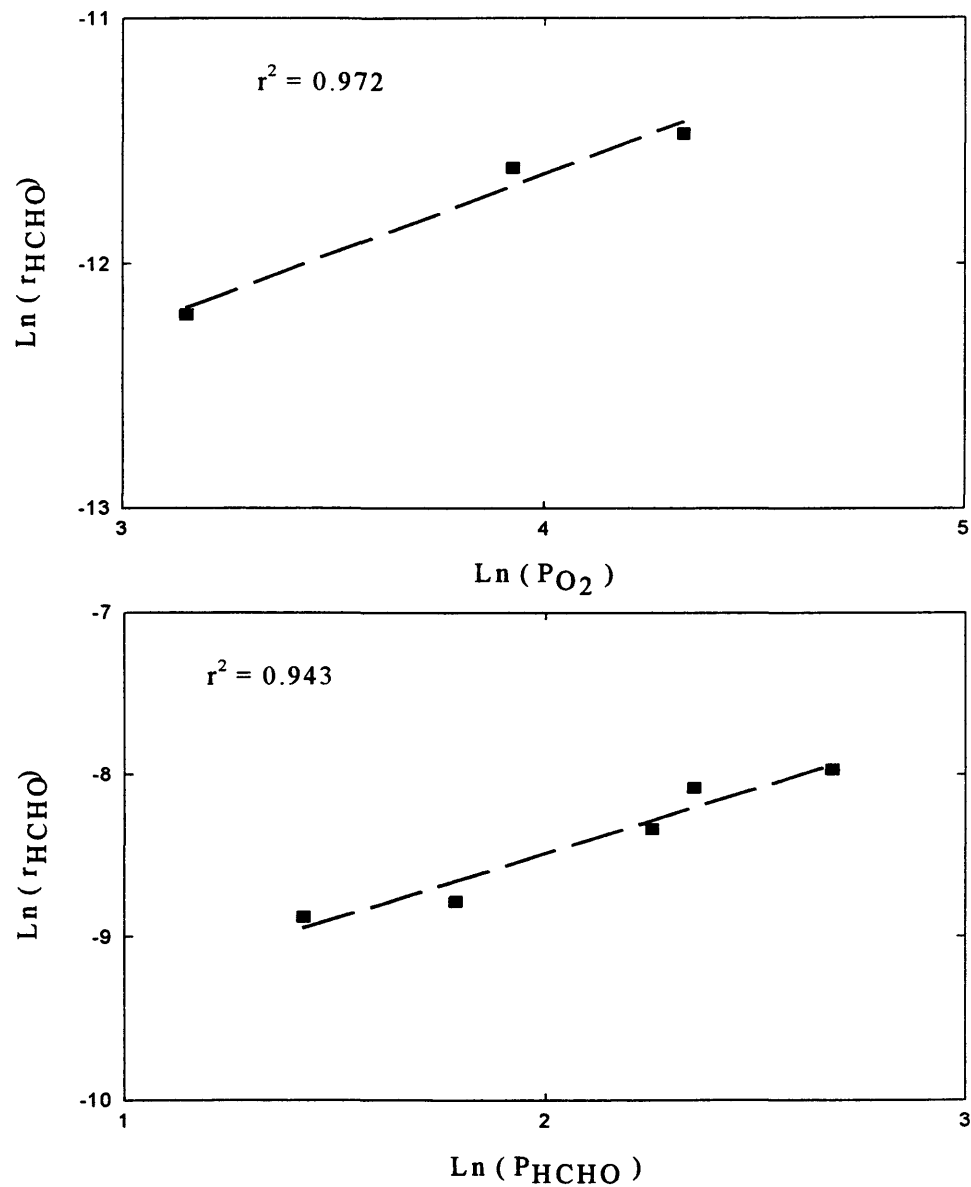


Figure 5.3 Effect of reactants partial pressure on formaldehyde oxidation rate over silica supported iron phosphate catalyst. GHSV= 25000 h<sup>-1</sup>, P<sub>O<sub>2</sub></sub> = 23-76 kPa @ P<sub>HCHO</sub>= 4 kPa, P<sub>HCHO</sub> = 4-15 kPa @ P<sub>O<sub>2</sub></sub> = 50 kPa and T= 648 K.

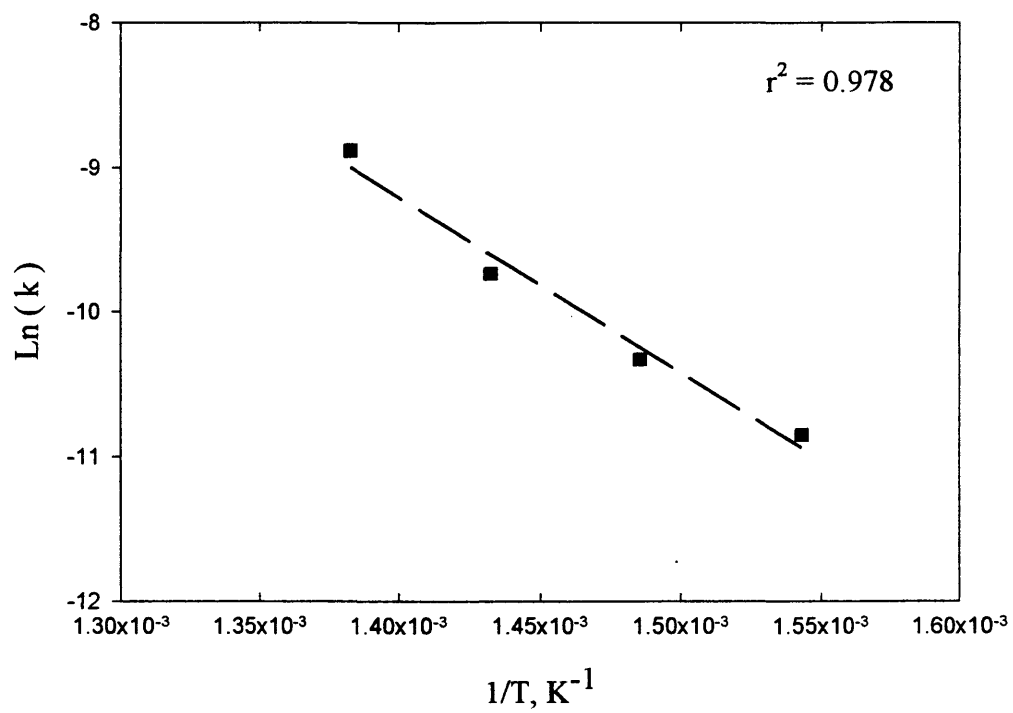


Figure 5.4 Arrhenius plot for formaldehyde oxidation over silica-supported iron phosphate catalyst.  $P_{\text{O}_2} = 50 \text{ kPa}$ ,  $P_{\text{HCHO}} = 4.5 \text{ kPa}$ , and  $T = 648\text{--}723 \text{ K}$ .

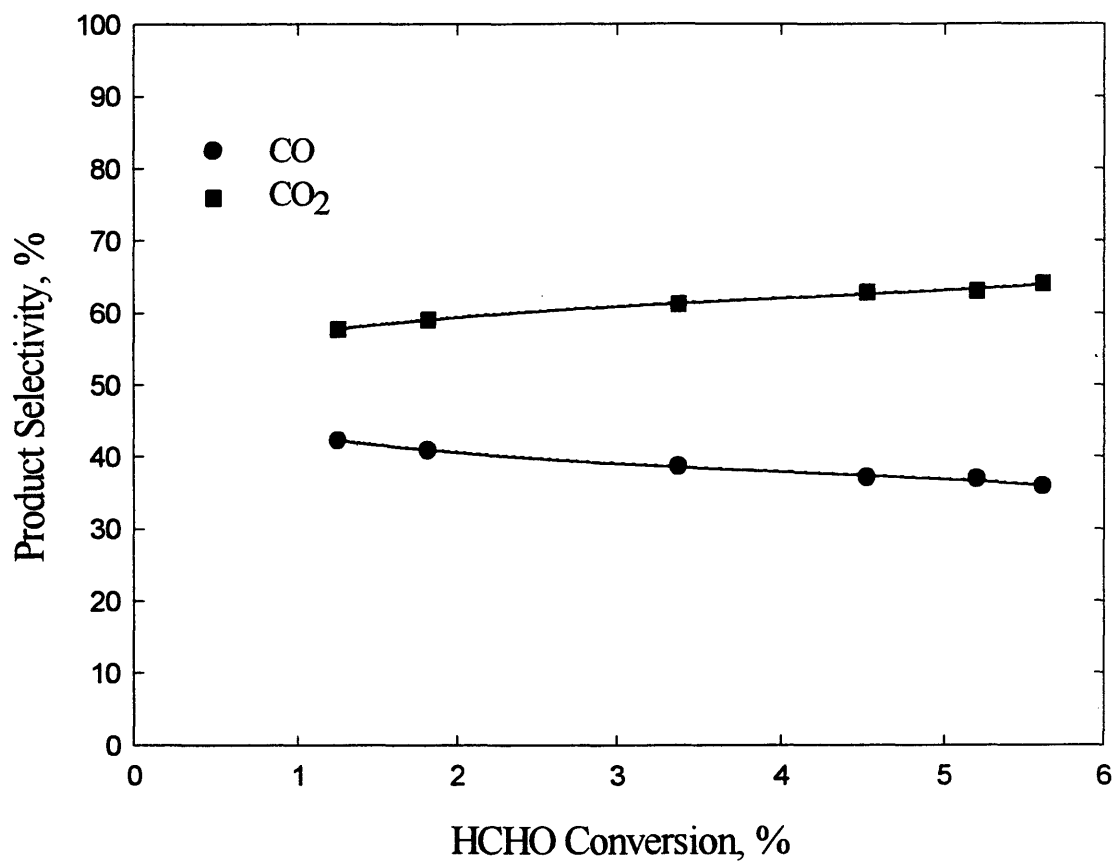
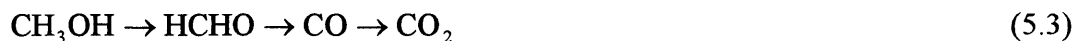


Figure 5.5 Product selectivity (%) as a function of formaldehyde conversion (%) for Silica-supported iron phosphate catalysts. GHSV= 5000-45000 h<sup>-1</sup>, P<sub>O<sub>2</sub></sub> = 50 kPa, P<sub>HCHO</sub> = 4.5 kPa, and T= 623-673 K.

### 5.1.3 Methanol Oxidation:

The methanol experiments were studied in the temperature range of 648-748 K, GHSV= 5000-45000 h<sup>-1</sup>, methanol pressure range of 33-42 kPa, oxygen partial pressure of 18-63 kPa, and methanol to oxygen ratio of 0.2-1.4. The effect of methanol and oxygen partial pressure is given in Figure 5.6. The reaction orders are 0.8±0.05 and 1.0±0.09 in oxygen and methanol, respectively, with activation energy of 88±4 kJ/mol. The Arrhenius plot for methanol oxidation is shown in Figure 5.7. Formaldehyde, carbon monoxide and carbon dioxide are the only products of methanol oxidation. Product selectivity as a function of methanol conversion is presented in Figure 5.8. Formaldehyde is the only product at the zero conversion, then CO is produced from HCHO oxidation and converted to CO<sub>2</sub> after that. The sequential reaction is :



The product distribution is identical to that over silica, which supports the silica surface domination. Iron phosphate/silica catalyst is better in stabilizing formaldehyde and methanol total conversion to HCHO is achieved at low conversion (<5%).

### 5.1.4 Methane Oxidation:

These experiments were conducted in the temperature range of 823-898 K, GHSV= 30000 h<sup>-1</sup>, methane partial pressure of 9-50 kPa, oxygen partial pressure of 9-40 kPa, and methane to oxygen ratio varied from 1 to 4.

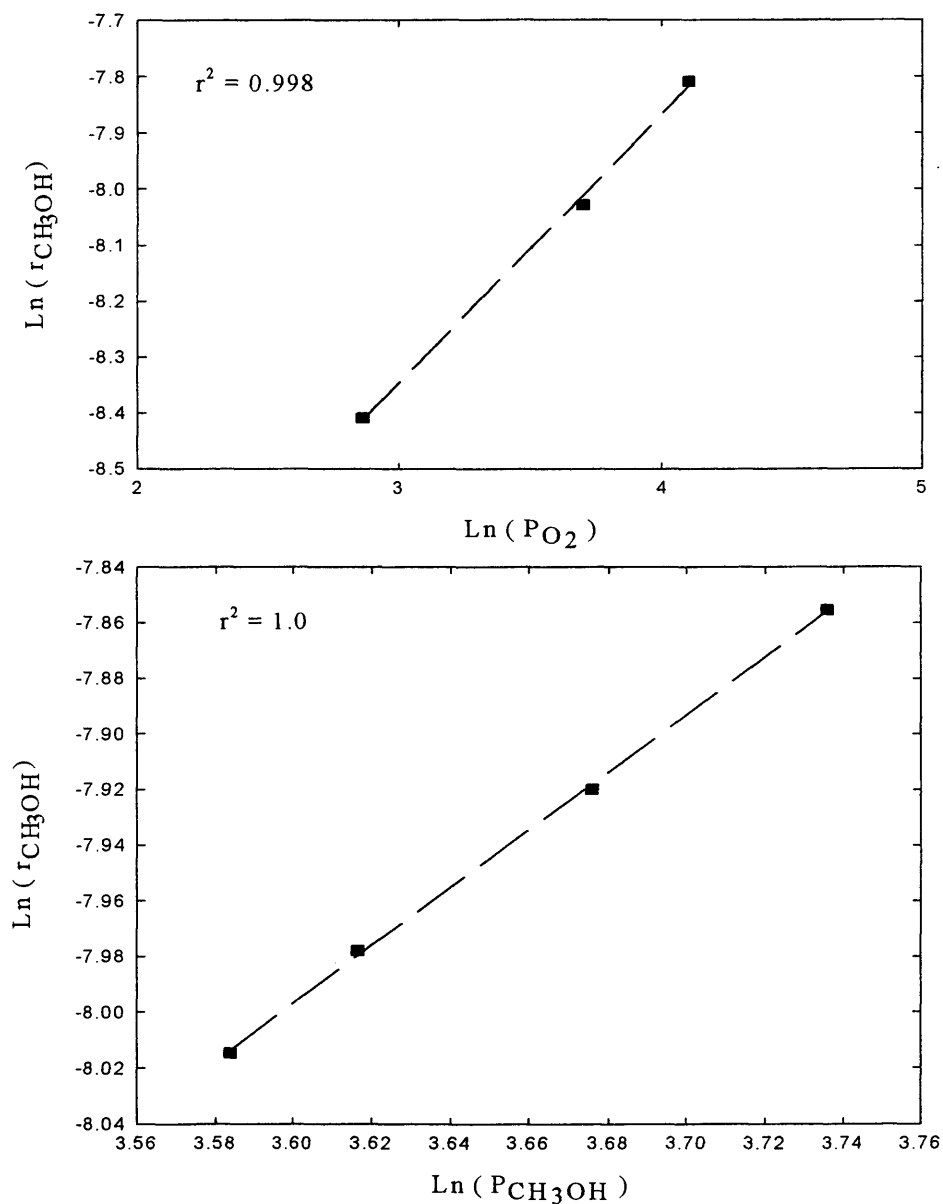


Figure 5.6 Effect of reactants partial pressure on methanol oxidation rate over silica supported iron phosphate catalysts. GHSV= 35000  $\text{h}^{-1}$ ,  $P_{\text{O}_2}$  = 18-63 kPa @  $P_{\text{CH}_3\text{OH}}$  = 24 kPa,  $P_{\text{CH}_3\text{OH}}$  = 33-42 kPa @  $P_{\text{O}_2}$  = 33 kPa and  $T$  = 723 K.

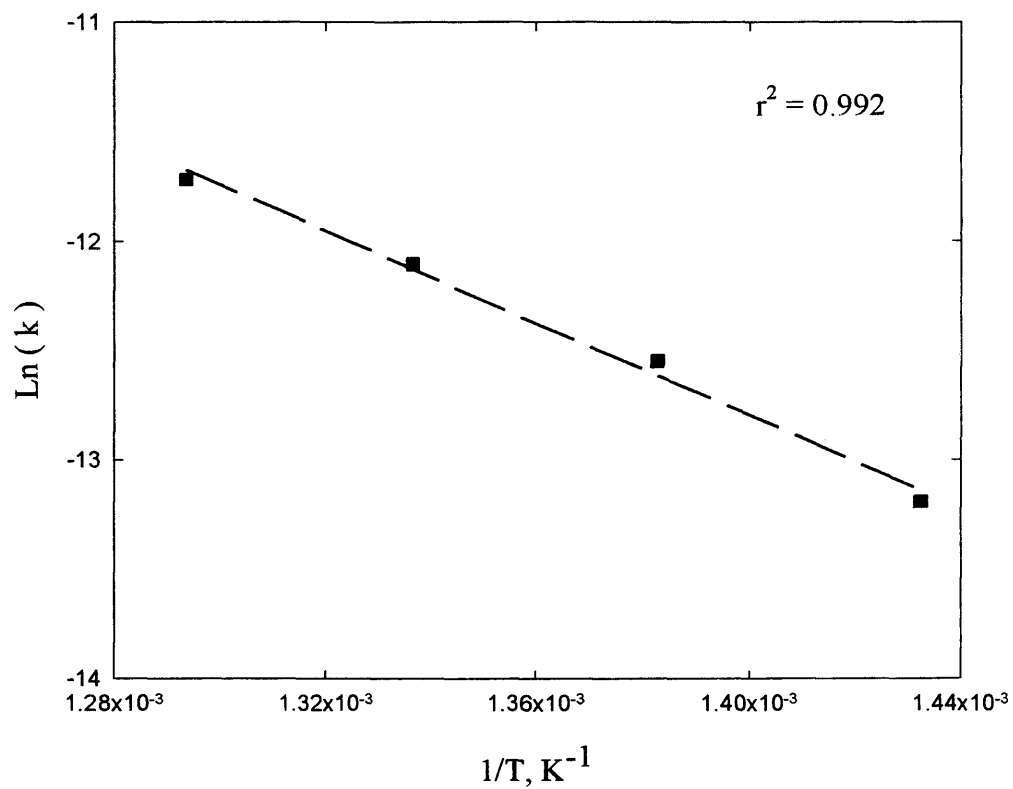


Figure 5.7 Arrhenius plot for methanol oxidation over silica-supported iron phosphate catalyst.  $P_{\text{O}_2} = 50 \text{ kPa}$ ,  $P_{\text{CH}_3\text{OH}} = 6 \text{ kPa}$ , and  $T = 673\text{-}773 \text{ K}$ .

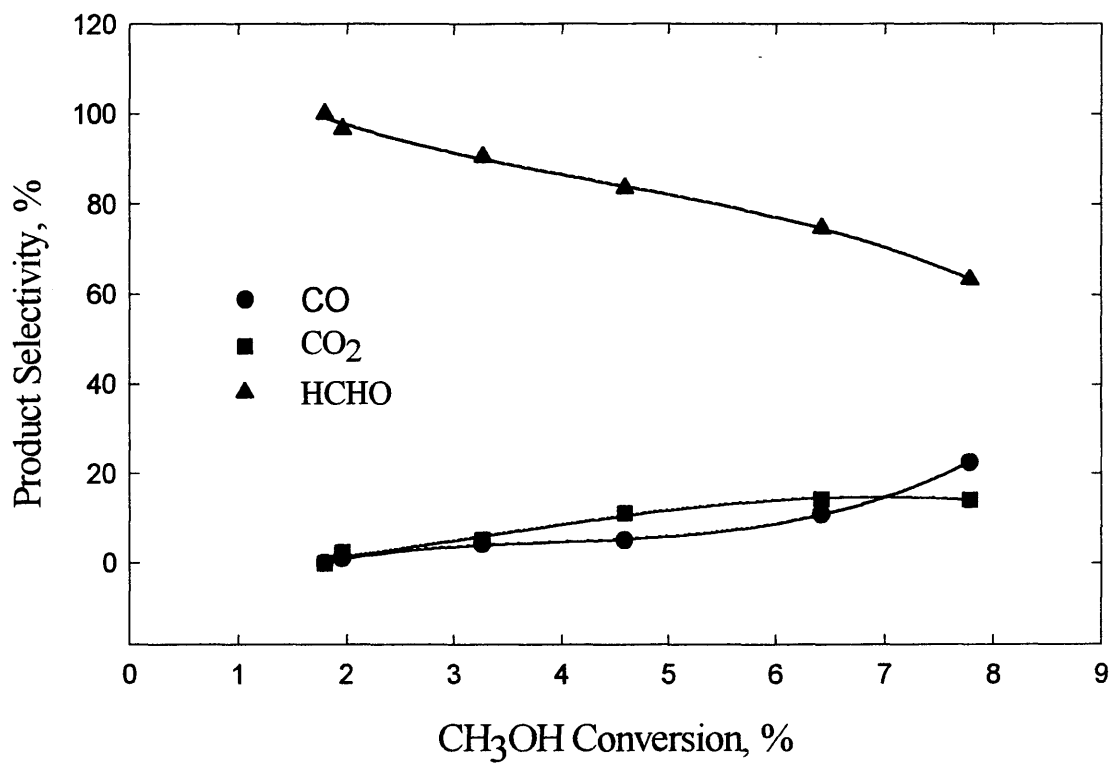


Figure 5.8 Product selectivity (%) as a function of methanol conversion (%) for silica supported iron phosphate catalyst. GHSV= 5000-45000 h<sup>-1</sup>, P<sub>O<sub>2</sub></sub> = 50 kPa, P<sub>CH<sub>3</sub>OH</sub> = 6 kPa, and T= 673-773 K.

Note that the temperature required for methane partial oxidation is much higher than used for carbon monoxide, formaldehyde and methanol oxidation. The effect of reactant partial pressure on the observed rate is shown in Figure 5.9. The reaction order for methane is  $0.66 \pm 0.11$ . It is clear that the rate dependence on oxygen partial pressure does not follow a power-law expression. Oxygen order is changing with temperature from 1 at 823 K to 2.5 at 898 K, this is shown in Figure 5.10. Figure 5.11 shows that the activation energy for this reaction is  $202 \pm 4$  kJ/mol over silica-supported iron phosphate. Figure 5.12 shows the product selectivity as a function of methane conversion. Methanol is not observed in these experiments, in spite of the fact that Alptekin (1998) observed low levels of methanol under similar conditions. At conversions approaching zero,  $\text{CO}_2$  selectivity is high ( 30% ) suggesting a direct path from  $\text{CH}_4$  to  $\text{CO}_2$ . CO selectivity is almost zero at this conversion meaning it is mainly produced from formaldehyde oxidation. That can be presented as:



Note the same reaction network is proposed for methane partial oxidation over silica. The only difference is that for silica-supported iron phosphate  $\text{CO}_2$  selectivity decreased.

## 5.2 Pulse Reactor Studies:

As over silica, pulse studies were divided into three parts. The first experiment is to investigate the role of molecular and lattice oxygen in the methane partial oxidation.

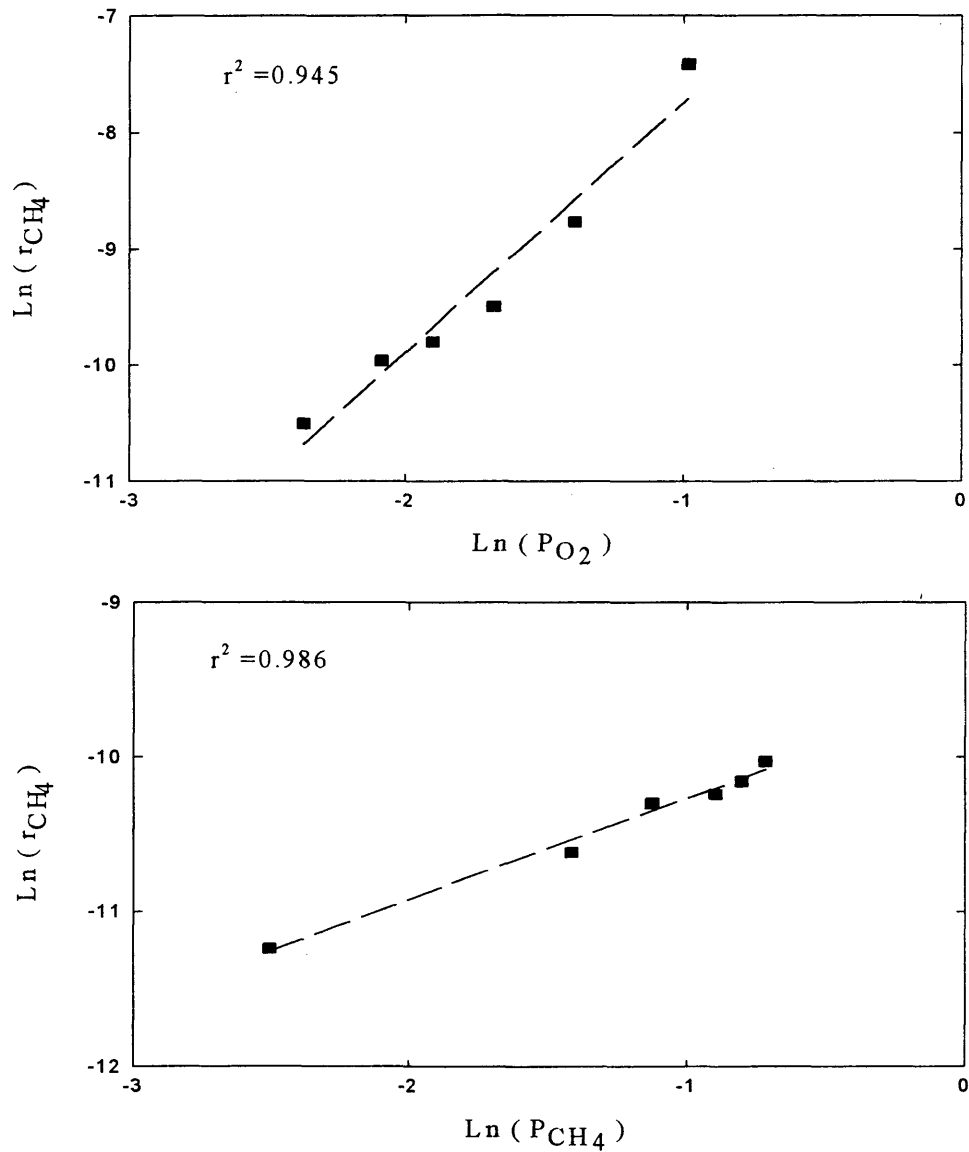


Figure 5.9 Effect of reactants partial pressure on methane oxidation rate over silica supported iron phosphate catalyst. GHSV= 30000  $\text{h}^{-1}$ ,  $P_{\text{O}_2}$  = 9-40 kPa @  $P_{\text{CH}_4}$  = 40 kPa,  $P_{\text{CH}_4}$  = 9-50 kPa @  $P_{\text{O}_2}$  = 9 kPa and  $T$  = 873 K.

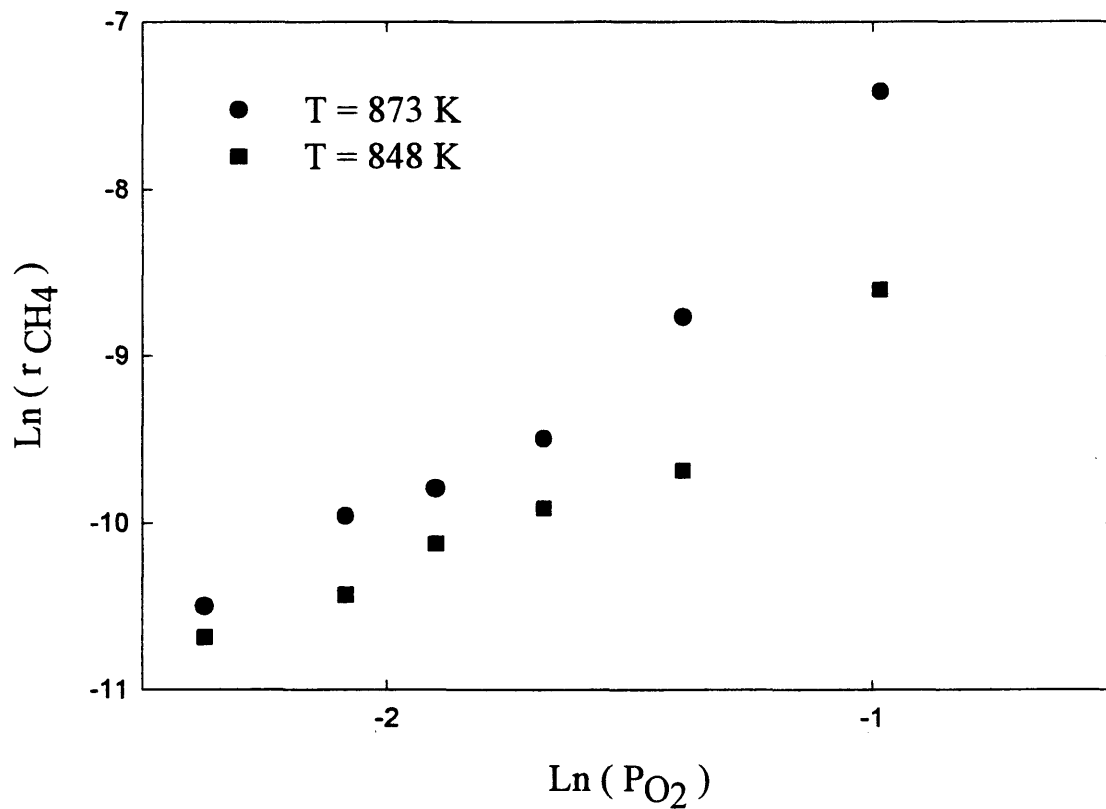


Figure 5.10 The effect of oxygen partial pressure on methane oxidation rate over silica supported catalysts. GHSV= 30000  $\text{h}^{-1}$ ,  $P_{\text{O}_2} = 9\text{-}40 \text{ kPa}$  @  $P_{\text{CH}_4} = 40 \text{ kPa}$ .

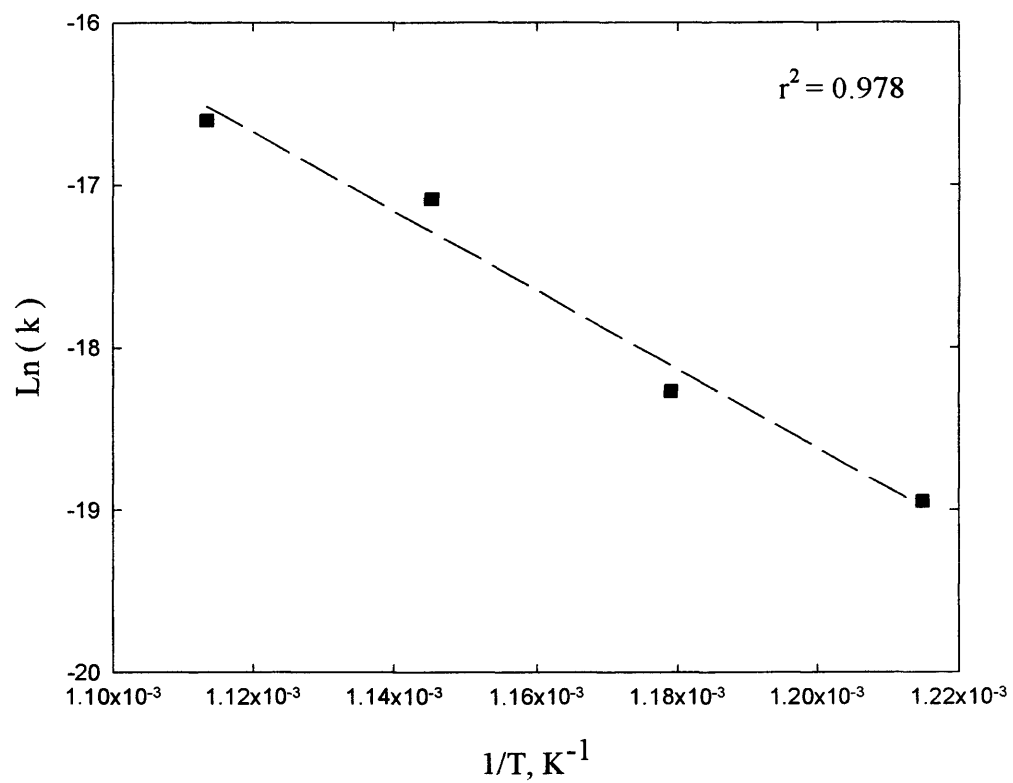


Figure 5.11 Arrhenius plot for methane oxidation over silica-supported iron phosphate catalyst.  $P_{\text{O}_2} = 40 \text{ kPa}$ ,  $P_{\text{CH}_4} = 40 \text{ kPa}$ , and  $T = 823\text{-}898 \text{ K}$ .

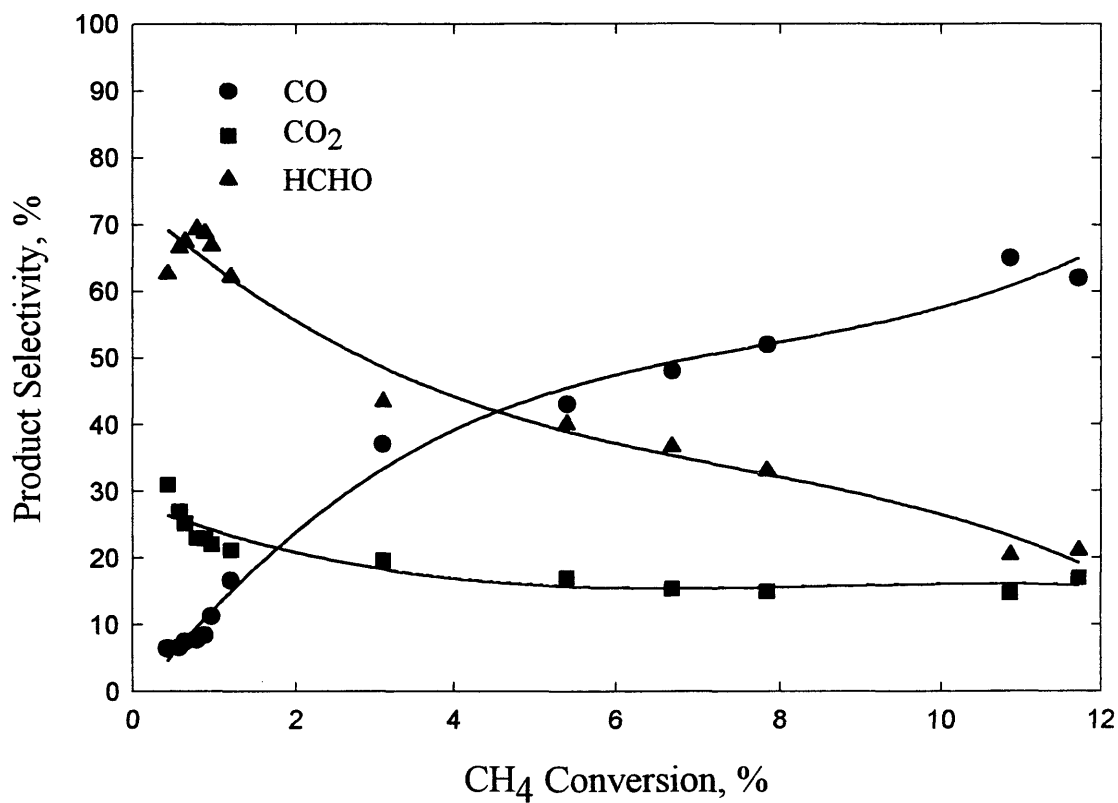


Figure 5.12 Product selectivity (%) as a function of methane conversion (%) for silica supported iron phosphate catalyst. GHSV= 30000 h<sup>-1</sup>, P<sub>O<sub>2</sub></sub> = 40 kPa, P<sub>CH<sub>4</sub></sub> = 40 kPa, and T= 823-898 K.

The second experiment was to study the different types of catalyst surface pretreatment. The last was designed to examine an unknown peak that was produced in the pulse tests over the silica-supported iron phosphate when analyzing the product stream by GC. In this case the same experiments were repeated using a mass spectrometer.

### **5.2.1 The Role of Gaseous and Lattice Oxygen:**

Methane partial oxidation on silica-supported iron phosphate in the presence and in the absence of molecular oxygen was studied in the temperature range 823-923 K by a pulse reactor connected to a GC. To avoid a change in the catalytic surface state in the pulse experiments from its state under steady state conditions, the reaction mixture ( $\text{CH}_4/\text{O}_2/\text{He}$ ) was pulsed before and after the reducing pulse ( $\text{CH}_4$ ). The result of these experiments is presented in Table 5.1. We can see that only when gas mixture is sent that significant conversion observed. Thus gas phase oxygen is required for methane oxidation over this catalyst. Only at high temperatures does lattice oxygen have a role in methane oxidation but it is limited, and the participation of lattice oxygen can therefore be neglected.

### **5.2.2 The Effect of Different Pretreatments on the Catalyst Surface:**

The second part of this study was to investigate the effect of pretreatment of the catalyst surface. The results in Table 5.2 show again that only when the reaction mixture

Table 5.1 Methane partial oxidation in the presence and absence of gas-phase oxygen in pulsed reaction experiment.

Catalyst	T <sub>r</sub> (°C)	Reagents	CH <sub>4</sub> Conv. %	Selectivity		
				HCHO	CO	CO <sub>2</sub>
2 wt.% FePO <sub>4</sub> /SiO <sub>2</sub>	550	CH <sub>4</sub> +O <sub>2</sub>	0.65	7.11	39.26	53.63
		CH <sub>4</sub>	0.00	0.00	0.00	
	600	CH <sub>4</sub> +O <sub>2</sub>	1.80	6.22	55.61	38.17
		CH <sub>4</sub>	0.00	0.00	0.00	
	650	CH <sub>4</sub> +O <sub>2</sub>	2.97	6.03	60.46	33.51
		CH <sub>4</sub>	0.39	6.51	58.14	35.35

is used do we get products. The presence of gaseous oxygen is required to get significant conversion. Comparing runs 1 and 6, pre-treating with this gas mixture gives higher conversions but oxidizing the surface gives better formaldehyde selectivity. This shows the importance of the adsorbed oxygen species in producing the oxygenated products, as apposed to lattice oxygen from reduction of iron phosphate. Higher conversion is recorded over iron phosphate/silica than silica; still overall results confirm that silica is the main active catalyst.

### **5.2.3 Investigating Unknown Peak:**

When using the GC to analyze the outlet gas from the pulse experiments, we noticed the presence of an unknown peak. To further study that phenomenon, a VG Quadrupole mass spectrometer was used. The results of the mass spectrometer are shown in Figures 5.13. Over both silica and iron phosphate/silica, formic acid was detected. Methanol was not observed in the GC analysis for continuous and pulse experiments, but was known to be present based on prior work of Alptekin (1998). Formic acid was the unknown peak. Note that the formic acid was not seen in the first few pulses but after that it increased dramatically. Apparently methane is converted to formic acid then converted to CO<sub>2</sub>. The amount of pulse products increases with methane pulse number. This may be explained by the slow desorption of these products. CO<sub>2</sub> and HCOOH are produced at the same rate, which means that the formic acid is an intermediate for carbon dioxide production.

Table 5.2 Pulse study results for methane partial oxidation over silica supported iron phosphate at 873 K.

Run	Pretreatment (3 Pulses)	Pulse	CH <sub>4</sub> Conv. %	HCHO	CO	CO <sub>2</sub>	Rate mol/(g <sub>cat</sub> .min)	STY g/(kg <sub>cat</sub> .hr)
1	CH <sub>4</sub> /O <sub>2</sub> /He	CH <sub>4</sub> /O <sub>2</sub> /He	1.80	6.2	55.6	38.2	2.0E-04	19.8
2	CH <sub>4</sub> /O <sub>2</sub> /He	CH <sub>4</sub> /He	0.00	0.0	0.0	0.0	0.0	0.0
3	CH <sub>4</sub> /O <sub>2</sub> /He	O <sub>2</sub> /He	0.00	0.0	0.0	0.0	0.0	0.0
4	CH <sub>4</sub> /He	CH <sub>4</sub> /O <sub>2</sub> /He	0.43	15.0	48.3	36.7	4.0E-05	11.4
5	CH <sub>4</sub> /He	O <sub>2</sub> /He	0.00	0.0	0.0	0.0	0.0	0.0
6	O <sub>2</sub> /He	CH <sub>4</sub> /O <sub>2</sub> /He	0.99	19.5	29.3	51.2	9.0E-05	34.2
7	O <sub>2</sub> /He	CH <sub>4</sub> /He	0.75	8.6	31.0	60.3	7.0E-05	11.5

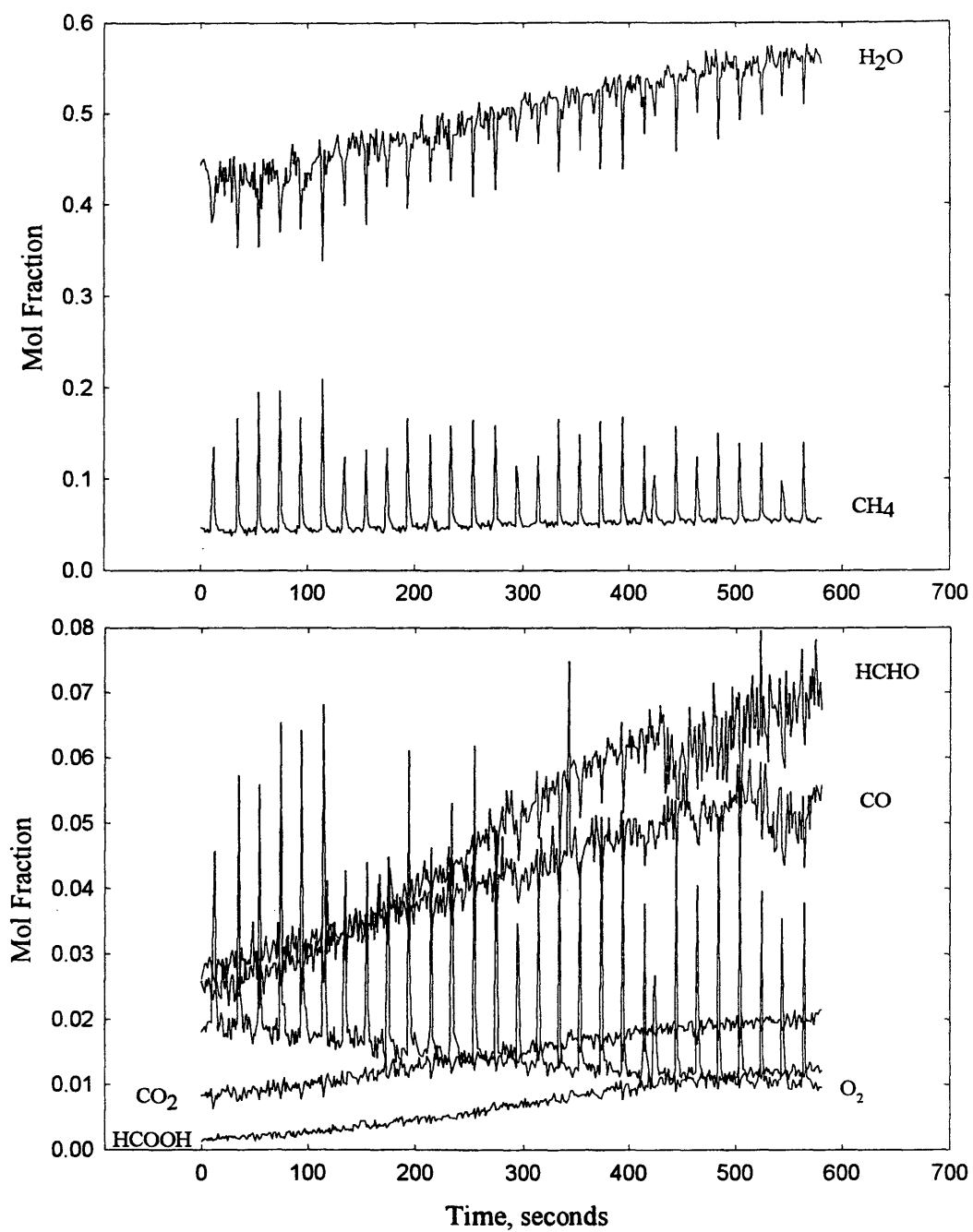


Figure 5.13 Mass spectral gas analysis of the effluent from pulse experiment over  $\text{FePO}_4/\text{SiO}_2$  at  $T=873$  K and  $P_{\text{O}_2}=P_{\text{CH}_4}=40$  kPa.

The similar pulse results also support the fact that silica is the active catalyst for methane partial oxidation.

### 5.3 Oxygen Chemisorption:

The surface area for 2 wt.% FePO<sub>4</sub>/SiO<sub>2</sub> is 288 m<sup>2</sup>/gm. This area was evaluated using the BET method, Alptekin (1998). Oxygen uptake over silica-supported iron phosphate has an oxygen atom site density of  $7.5 \times 10^{15}$  atoms/m<sup>2</sup>. The site density for silica is doubled with the addition of a 2 wt.% FePO<sub>4</sub>. Most likely iron phosphate did not introduce more defects but simply added reducible iron sites. Although adding iron phosphate doubled oxygen site density, methane conversion rate did not increase. On the contrary the conversion decreased at the expense of CO<sub>x</sub> production.

### 5.4 In-situ IR Experiment:

Carbon monoxide and methanol IR spectra were acquired for iron phosphate/silica. Little was learned from the CO spectra, but it is clear that carbon monoxide is weakly adsorbed on silica. IR results for CO oxidation and chemisorption are presented in Appendix A. Methanol adsorbs strongly on iron phosphate/silica and more information is drawn from this study.

Methoxide species are believed to be an important intermediate in methane partial oxidation. To investigate this assumption, in-situ IR for methanol chemisorption was performed. The experiments were done at room temperature, 473 and 673 K. In this

temperature range the methoxy groups are reasonably stable, Jongsomjit (1998). The IR spectrum for methanol oxidation over iron phosphate/silica is shown in Figure 5.14. Bands in the range 1600-1700 and 3200-3700 are assigned to hydroxyl groups. Strong CO<sub>2</sub> bands are observed on silica at 2400 cm<sup>-1</sup>.

Methanol adsorption on iron phosphate/silica was studied at three different temperatures, the results of these experiments are shown in figures 5.15, 5.16 and 5.17. Since all graphs give the same results, only the one at T=473 K will be discussed. The iron phosphate/silica catalyst spectrum indicates the presence of C-H vibrations in the range 2800-3000 cm<sup>-1</sup>, these are assigned for methanol and methoxy groups. CO<sub>2</sub> bands are also seen with the adsorption experiments, suggesting that methanol is being oxidized even though no gas oxygen is present. Methanol could be reacting with lattice oxygen, or with an oxygen impurity from the argon or dissolved in the methanol. Note that the CO<sub>2</sub> band did not appear before or after the methanol chemisorption and the band increases in intensity as the temperature increases. Only methanol and carbon dioxide bands were observed on the IR experiments. The same results were seen over silica.

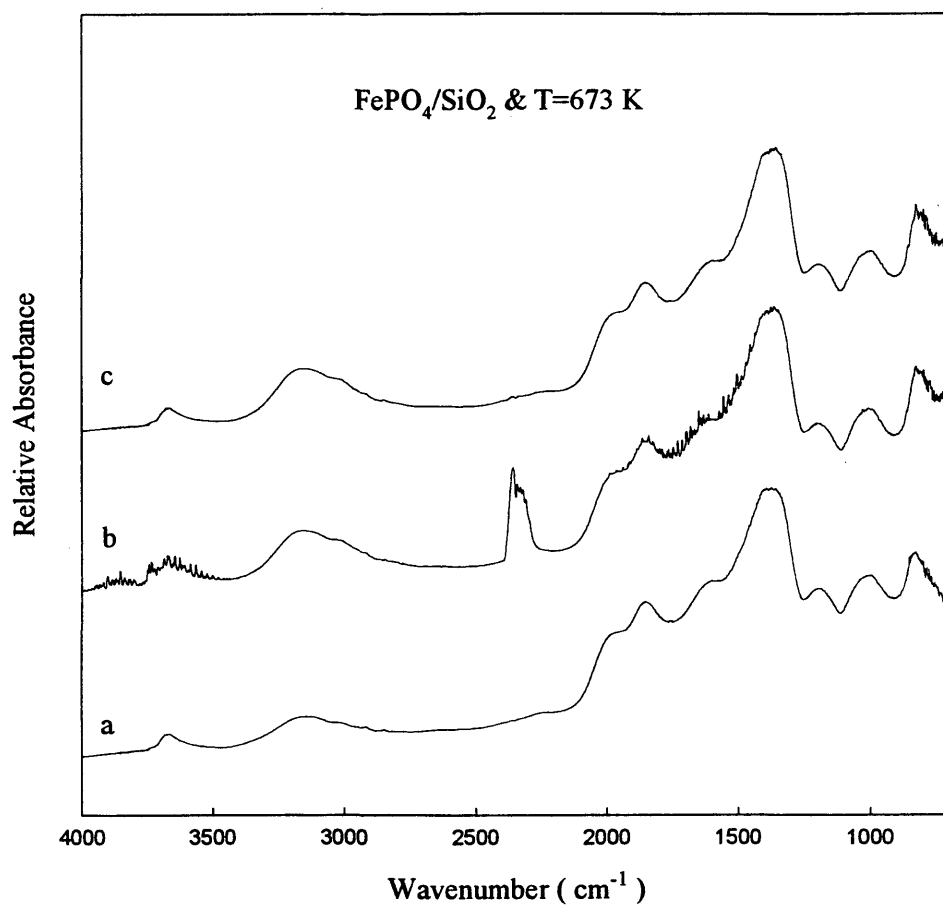


Figure 5.14 IR spectra of methanol oxidation over silica-supported catalyst at  $T=673\text{ K}$ :  
a. Before oxidation, Ar was introduced for 1 hr.  
b. During reaction,  $\text{CH}_3\text{OH} + \text{O}_2$  was introduced for 1 hr.  
c. After oxidation, Ar was introduced for 1 hr.

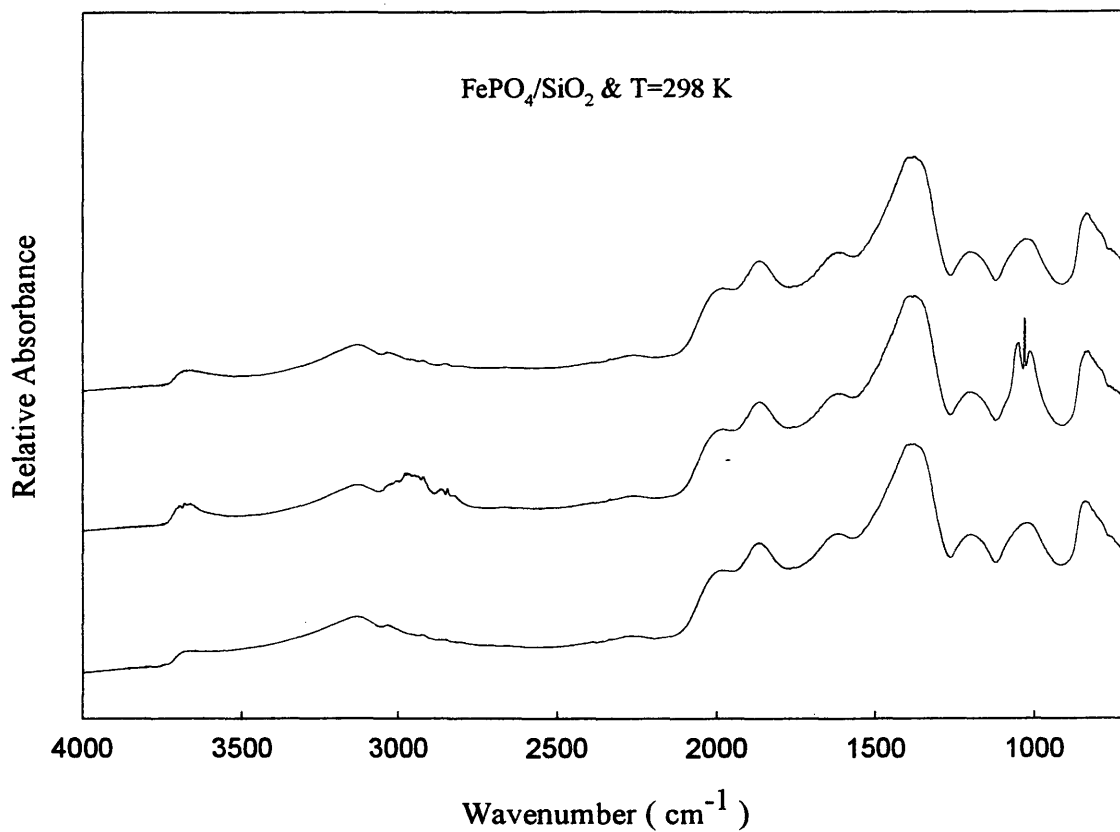


Figure 5.15 IR spectra of methanol adsorption over silica-supported iron phosphate catalyst at  $T=298\text{ K}$ :

- Before adsorption, Ar was introduced for 1 hr.
- During adsorption,  $\text{CH}_3\text{OH}$  was introduced for 1 hr.
- After adsorption, Ar was introduced for 1 hr.

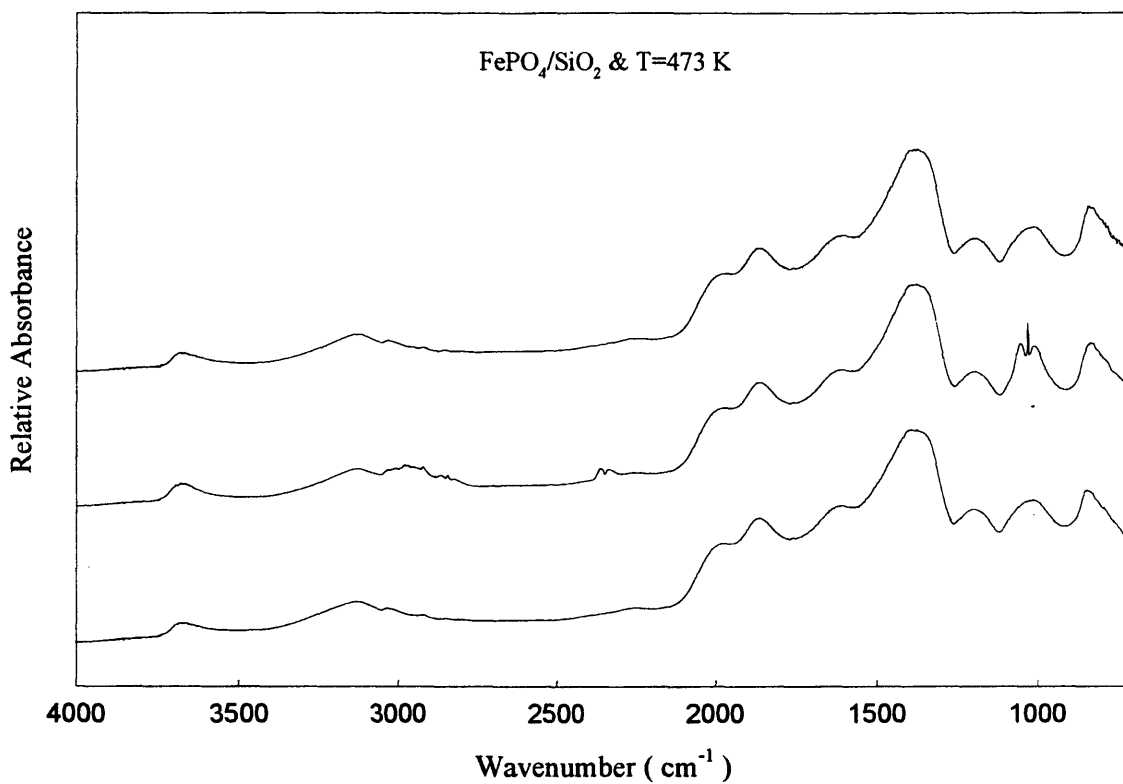


Figure 5.16 IR spectra of methanol adsorption over silica-supported iron phosphate catalyst at  $T=473\text{ K}$ :

- a. Before adsorption, Ar was introduced for 1 hr.
- b. During adsorption,  $\text{CH}_3\text{OH}$  was introduced for 1 hr.
- c. After adsorption, Ar was introduced for 1 hr.

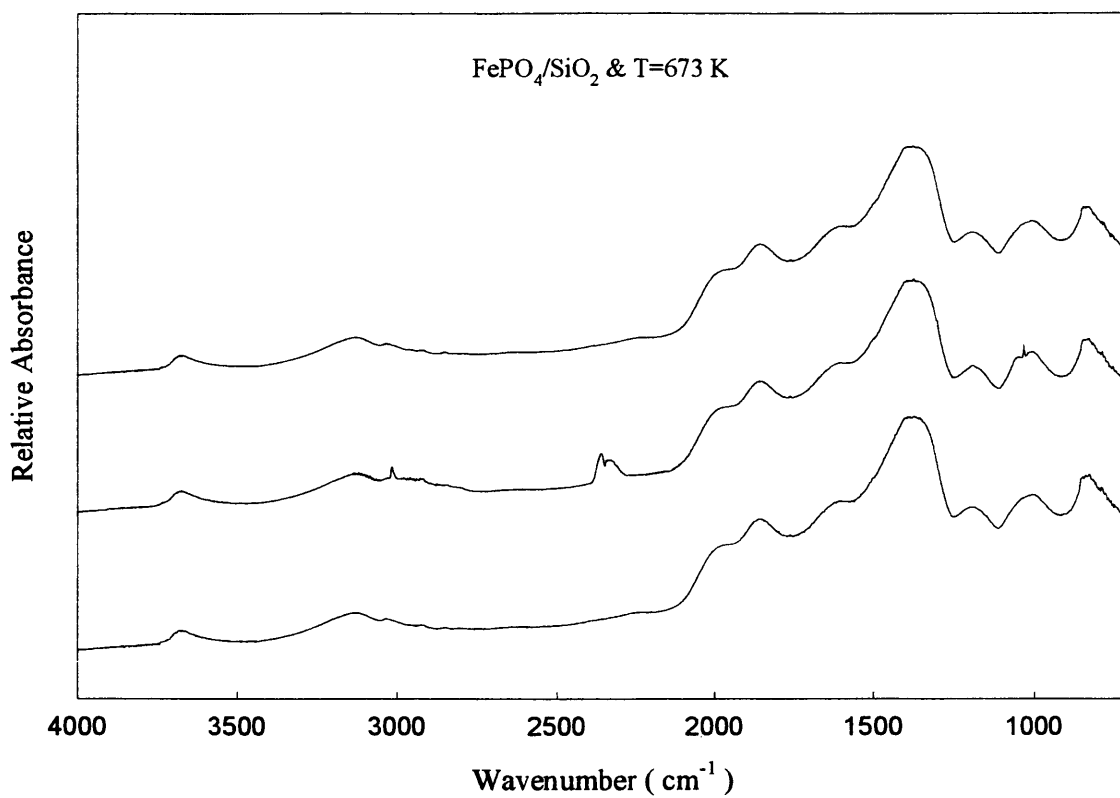


Figure 5.17 IR spectra of methanol adsorption over silica-supported iron phosphate catalyst at  $T=673\text{ K}$ :

- Before adsorption, Ar was introduced for 1 hr.
- During adsorption,  $\text{CH}_3\text{OH}$  was introduced for 1 hr.
- After adsorption, Ar was introduced for 1 hr.

## CHAPTER 6

### DISCUSSION AND COMPARISON

#### 6.1 Background and Objectives:

Alptekin (1998) studied the influence of iron phosphate loading over silica on catalyst activity and product selectivity. It was discovered that catalytic activity and formaldehyde selectivity depend on iron phosphate content, the highest yield toward formaldehyde was observed at low loading levels. At 2 wt.%  $\text{FePO}_4/\text{SiO}_2$ , formaldehyde and methanol yields were 622  $\text{g}/(\text{kg}_{\text{cat}}\cdot\text{h})$  and 25  $\text{g}/(\text{kg}_{\text{cat}}\cdot\text{hr})$ , respectively. It should be mentioned that when  $\text{MoO}_3$  and  $\text{V}_2\text{O}_5$  are added to silica, low loading also gives the highest formaldehyde yields, Spencer and Pereira (1989). For bare silica, formaldehyde space-time yield was 177  $\text{g}/(\text{kg}_{\text{cat}}\cdot\text{hr})$  and its selectivity was 20% at the 1% conversion level in Alptekin's study. No methanol was produced over silica. In this thesis, formaldehyde yields of 125 and 550  $\text{g}/(\text{kg}_{\text{cat}}\cdot\text{hr})$  were observed for silica and iron phosphate/silica, respectively. These yields are slightly less than reported by Alpetkin (1998), but still higher than reported for most other metal oxide/silica catalysts. In the present work, methanol was not detected over silica or silica-supported iron phosphate. Even in Alptekin's work, the methanol concentration in the reaction products was very low and poorly quantified.

The main goal of this work is to better understand the reaction network and reaction kinetics in this system. By knowing the important steps in the reaction network, one can theoretically design a better catalyst and optimize important reactions steps. Another objective is to provide information on surface active sites and active species. Experimental data were also collected for parameter evaluation and model comparison. A number of important observations were made during the experimental program and will be discussed in this chapter:

- Silica appears to be the active catalyst for methane oxidation. Addition of  $\text{FePO}_4$  modifies the properties of silica to improve yield of HCHO and significantly reduce the rate of conversion of CO to  $\text{CO}_2$ .
- Addition of  $\text{FePO}_4$  to silica doubles the number of oxygen chemisorption sites.
- Gas phase oxygen is required for methane oxidation.
- Effect of oxygen partial pressure in methane oxidation cannot be modeled by simple power law kinetics. The oxygen partial pressure effect in subsequent oxidation of methanol, formaldehyde, and CO can be described using a simple power law model.
- Reaction order for oxygen in reactions of methane, methanol, formaldehyde, and CO was always greater than zero (in the range of 0.5 to more than 1). This suggests that chemisorption of oxygen on the reduced sites occurs at a rate comparable to that of substrate oxidation, and may therefore limit the oxidation rate.
- Reaction orders for CO in CO oxidation are negative for silica, indicating some form of kinetic inhibition. The CO reaction order is zero for iron phosphate/silica.

- HCOOH was observed as an intermediate species in pulsed reaction experiments, and apparently reacts to form CO<sub>2</sub>.

## 6.2 Comparing SiO<sub>2</sub> and FePO<sub>4</sub>/SiO<sub>2</sub>:

Table 6.1 summarizes the results of the flow reactor studies in terms of activation energy, power law kinetics, conversion, and selectivity. Table 6.2 reports global reaction rates per gram of catalyst, reaction rates per oxygen chemisorption site (turn over frequency), and space-time yield of formaldehyde. In these tables, we can see that the reaction rates per gram and conversion are almost the same for both catalysts, with the exception that conversion of CO to CO<sub>2</sub> is much slower over FePO<sub>4</sub>/silica. The similarity of almost all reaction parameters implies that silica is the dominant catalyst and that addition of FePO<sub>4</sub> modifies this catalytic material in some respects. This is consistent with results reported for V<sub>2</sub>O<sub>5</sub> and MoO<sub>3</sub> supported on silica, Parmaliana et al. (1994). Note that Alptekin (1998) found that unsupported FePO<sub>4</sub> was capable of methane oxidation, but with much lower reaction rate and selectivity than silica-supported FePO<sub>4</sub>.

For methane oxidation, addition of FePO<sub>4</sub> results in a significant increase in the energy barrier for reaction (activation energy), leading to a lower reaction rate than observed for bare silica under identical conditions. Yet space-time yield of formaldehyde is higher because of the much higher formaldehyde selectivity. Improved yield is not caused simply by a reduction in the rate of formaldehyde oxidation, as kinetic parameters for this reaction are essentially identical over both catalysts. However, note that HCHO

Table 6.1 Comparison of results over silica and silica-supported iron phosphate.

Reaction	Catalyst	Reaction Conditions		Power Law Kinetics			Selectivity				
		T <sub>R</sub> (K)	GHSV(1/hr)	Ratio	n <sub>HC</sub>	n <sub>O<sub>2</sub></sub>	E <sub>a</sub> (kJ/mol)	HC Conv.%	CO	CO <sub>2</sub>	HCHO
CO oxidation	SiO <sub>2</sub>	673	40000	1	-0.27	0.8	56	5.2	0	100	0
	FePO <sub>4</sub> /SiO <sub>2</sub>	673	40000	1	-0.1	1.2	32	5	0	100	0
HCHO oxidation	SiO <sub>2</sub>	648	25000	0.1	0.8	0.69	111	2.6	25	75	0
	FePO <sub>4</sub> /SiO <sub>2</sub>	648	25000	0.1	0.8	0.64	100	2.8	40	60	0
CH <sub>3</sub> OH oxidation	SiO <sub>2</sub>	723	35000	1	0.43	0.4	133	3.9	11	7	82
	FePO <sub>4</sub> /SiO <sub>2</sub>	723	35000	1	1	0.8	88	3.3	4.25	5.25	90.5
CH <sub>4</sub> oxidation	SiO <sub>2</sub>	873	30000	1	0.9	2.1	142	11.3	35.4	59.1	5.5
	FePO <sub>4</sub> /SiO <sub>2</sub>	873	30000	1	0.66	2.2	202	6.7	51.8	11.7	40.5

3.5

Table 6.2 Comparison of Turnover Frequency (TOF) for Silica and Silica-Supported Iron Phosphate.

Reaction	Catalyst	Reaction Conditions		Rate mol/(g <sub>cat</sub> ·min)	TOF 1/sec.	STY g/(kg <sub>cat</sub> ·hr)
		T <sub>R</sub> (K)	GHSV (1/hr)			
CO oxidation	SiO <sub>2</sub>	673	40000	1.55E-04	0.93	0
	FePO <sub>4</sub> /SiO <sub>2</sub>	673	40000	1.50E-04	0.70	0
HCHO oxidation	SiO <sub>2</sub>	648	25000	2.16E-05	0.13	0
	FePO <sub>4</sub> /SiO <sub>2</sub>	648	25000	4.52E-05	0.21	0
CH <sub>3</sub> OH oxidation	SiO <sub>2</sub>	723	35000	4.55E-04	2.72	486
	FePO <sub>4</sub> /SiO <sub>2</sub>	723	35000	3.00E-05	0.14	583
CH <sub>4</sub> oxidation	SiO <sub>2</sub>	873	30000	1.64E-03	9.80	125
	FePO <sub>4</sub> /SiO <sub>2</sub>	873	30000	6.01E-04	2.79	550

oxidation experiments were conducted at a much lower temperature. As temperature increases, the rates over the two catalysts may not change by the same amount. Also note that the reaction rate is influenced by the fraction of oxidized sites on the surface, which is influenced not only by the main reaction but also by subsequent reactions of products. As temperature is increased the effect of these subsequent reactions of the fraction of oxidized or reduced sites may also vary considerably between the two catalysts.

The active site density, as measured by oxygen chemisorption, for precipitated silica was comparable with that reported by Arena et al. (1999). Precipitated silica can adsorb large amounts of oxygen atoms. Adding 2 wt.% FePO<sub>4</sub> doubled the site density. Table 6.3 summarizes the total active site density for silica and some silica-supported catalysts. As discussed in section 6.5, the enhanced yield of HCHO over FePO<sub>4</sub>/silica is related to the much higher oxygen chemisorption site density, and much lower rate of consumption of oxidized surface sites by CO for this catalyst.

Table 6.2 presents turnover frequencies for silica and silica-supported catalysts; the rate is definitely lower over FePO<sub>4</sub>/silica. Adding FePO<sub>4</sub> increases the number oxygen chemisorption sites from 2.79E-6 mol/g<sub>cat.</sub> over silica to 3.59E-6 mol/g<sub>cat.</sub> over silica-supported iron phosphate. Overall reaction rates (per gram) are very similar for oxidation of CO, HCHO, and methanol and thus TOF is lower over FePO<sub>4</sub>/silica because of the higher number of sites. The space-time yield of formaldehyde from methanol over FePO<sub>4</sub>/silica is very close to the space-time yield observed in methane oxidation. This again suggests that the measured rates of HCHO oxidation over the two catalysts do not

Table 6.3 Results Reported for the Total Active Site Density on Silica and Silica Supported Catalysts

Catalyst	Total Active Site Density (Atoms/m <sup>2</sup> )	Reference
SiO <sub>2</sub>	4.20E+15	This Work
SiO <sub>2</sub>	5.60E+14	Arena et. al. (1999)
SiO <sub>2</sub>	4.35E+15	Oyama et. al. (1989)
2wt.% FePO <sub>4</sub> /SiO <sub>2</sub>	7.50E+15	This Work
V <sub>2</sub> O <sub>5</sub>	3.20E+18	Oyama et. al. (1989)
1 wt.% V <sub>2</sub> O <sub>5</sub> /SiO <sub>2</sub>	3.60E+16	Reddy et. al. (1989)
1.4 wt.% V <sub>2</sub> O <sub>5</sub> /SiO <sub>2</sub>	4.40E+17	Oyama et. al. (1989)
3 wt.% MoO <sub>3</sub> /SiO <sub>2</sub>	5.50E+16	Reddy et. al. (1989)

tell the entire story; some other effect must cause HCHO to be more stable over FePO<sub>4</sub>/silica during methanol and methane oxidation.

### **6.3 Chemisorbed Oxygen:**

It was found in the pulse reaction studies that the reaction required the presence of gas phase oxygen and the solid catalysts, and therefore, required chemisorbed oxygen. Most likely, methane is actually activated by a reactive form of chemisorbed oxygen, because a surface devoid of chemisorbed oxygen is inactive. The gaseous oxygen replaces the surface oxygen as it is consumed. This situation appears to be similar to that of the redox or Mars and van Krevelen mechanism but is actually quite different. In both cases, reduced surface sites must be reoxidized. However, for true redox catalysts, hydrocarbon oxidation can proceed without the presence of gas phase oxygen. Lattice oxygen, oxide anions of the solid oxide itself, react with the hydrocarbon and in some cases are replenished by solid-state diffusion of oxygen anions from within the interior of the catalyst particles. Under steady state conditions (with gaseous oxygen present), the sites for hydrocarbon oxidation and catalyst reoxidation may not even be the same. Catalysts that require the presence of gas phase or chemisorbed oxygen are said to work by a concerted mechanism requiring adsorption of both reactants on the same or adjacent active sites.

A second important observation from the pulsed reaction experiments is the build up of species on the surface with time. Unconverted oxygen and methane exit the reactor

as distinct pulses, however reaction product concentrations in the effluent build up slowly with pulse number and are not observed as distinct pulses. This indicates slow desorption of products, and perhaps the need for build up of some concentration of carbon containing surface species for the formation of selective oxidation products to occur.

The effect of oxygen partial pressure on the methane oxidation rate is shown in Figure 6.1 for silica and silica-supported iron phosphate. For a reaction that can be modeled using simple power law kinetics these plots should be linear (with the slope giving the oxygen reaction order). Thus the curvature indicates more complex kinetic behavior such as a change in the rate-limiting step as oxygen partial pressure is increased, or some other effect that requires explicit consideration of the surface in the kinetic model. Alptekin (1998) reported a 0.3 order for oxygen but covered a much wider range of methane to oxygen ratio, from 1:1 to 17:1 with only four or five data points. At the high ratios reaction order in oxygen approaches zero leading his regression to produce a slope of 0.3. Arena et al. (1999) used half order kinetics in oxygen in a model assuming dissociative oxygen chemisorption on silica. For elementary chemisorption steps, oxygen dissociation will result in half order and chemisorption of molecular oxygen will give first order kinetics.

Activation of methane has long been thought to be the rate-controlling step in methane partial oxidation. However, the fact that apparent reaction order in oxygen is far from zero suggests that generation (or regeneration) of the active sites by oxygen chemisorption may occur at a comparable rate. The same can also be said for oxidation

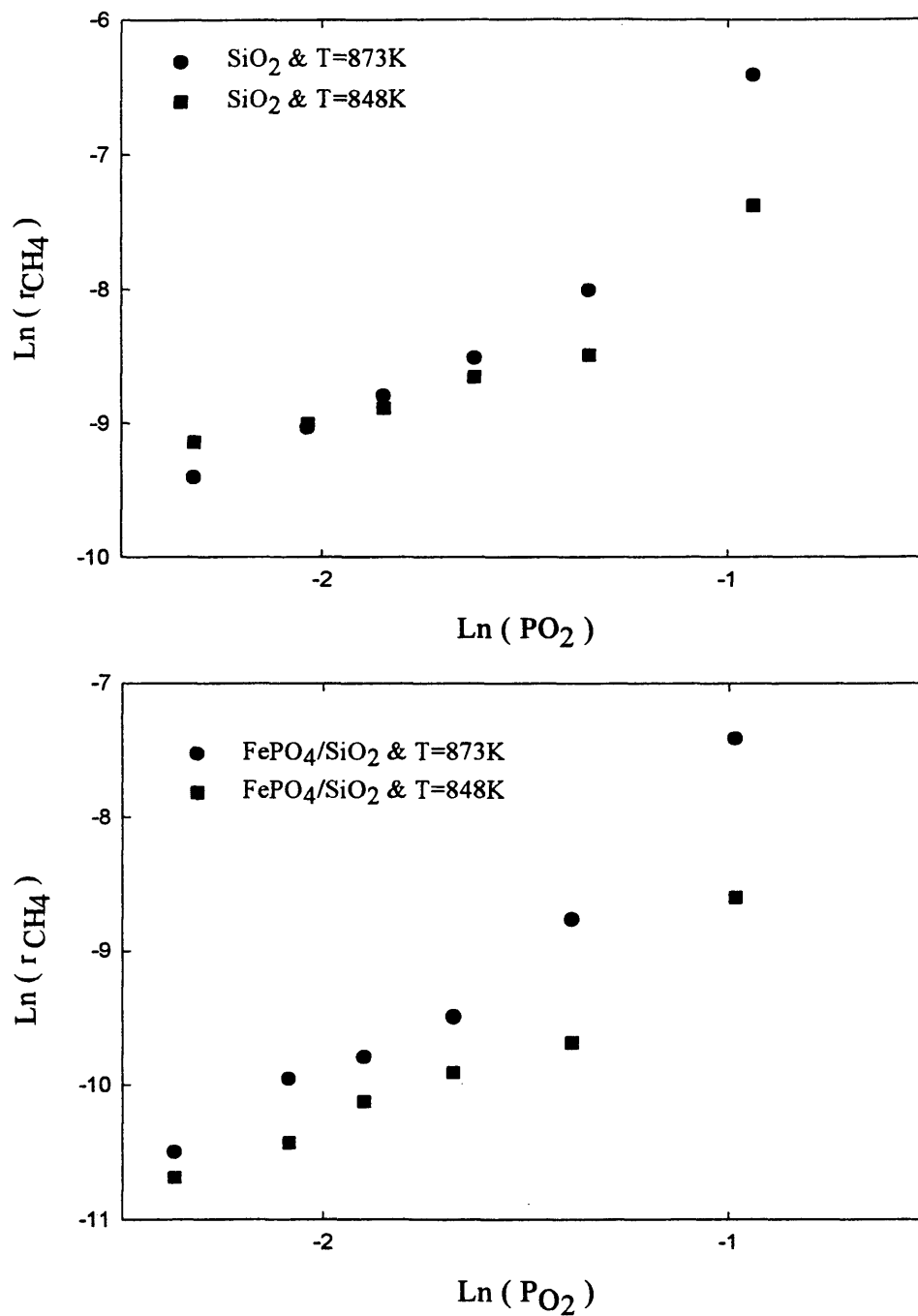


Figure 6.1 The effect of oxygen partial pressure on methane oxidation rate over silica and silica supported catalysts. GHSV= 30000 h<sup>-1</sup>, P<sub>O<sub>2</sub></sub> = 9-40 kPa @ P<sub>CH<sub>4</sub></sub>= 40 kPa.

of the intermediates methanol, formaldehyde, and CO. However, these intermediates may also be able to chemisorb on oxygen vacancy sites (reduced surface sites), which implies reaction with oxygen on an adjacent site. Note that methane activation most likely also requires adjacent sites as the reaction is thought to result in formation of a surface methoxide and a surface hydroxide. For silica, active sites are likely to be surface defects. Because of the requirement for adjacent sites, these defects are therefore concentrated as islands or lines of active centers. Oxygen can chemisorb as both molecular ( $O_2^-$  or  $O_2^{2-}$ ) and atomic forms ( $O^-$  or  $O^{2-}$ , the latter similar to lattice oxygen).

In this study, the  $P_{CH_4}/P_{O_2}$  ratio was kept between 1 and 4. Most of the data were acquired at a ratio of one for methane partial oxidation over  $FePO_4/SiO_2$ , and a ratio of two for  $SiO_2$ . The best HCHO yields were obtained at these methane to oxygen ratios in a previous study (Alptekin, 1998). In Figure 6.1, methane to oxygen ratio decreases with increasing oxygen partial pressure. The slope of the curve reaches a maximum at a ratio of 1:1. At this high oxygen partial pressure the surface is expected to be more highly oxidized, a condition shown to produce higher oxidation product yields. In fact, at the lowest methane-to-oxygen ratio conversion is much higher than at the lower ratios (about 6% versus less than 2%). As the oxidation products are much more reactive than methane, they will compete with methane for oxidized surface sites or perhaps compete with oxygen for reduced surface sites.

#### 6.4 Carbon Monoxide Inhibition:

CO<sub>2</sub> production rates from CO oxidation over silica and silica-supported iron phosphate are presented in Figure 6.2. CO<sub>2</sub> production increases with an increase of oxygen pressure. The CO<sub>2</sub> production rate is higher over silica, except for the highest oxygen partial pressure. On the other hand, the CO<sub>2</sub> production rate decreases when CO pressure is increased over silica, and stays almost constant over FePO<sub>4</sub>/SiO<sub>2</sub>. Silica exhibits an apparent negative reaction order in carbon monoxide, while the rate is zero order in CO for iron phosphate/silica. This negative order may be explained by competition between CO and O<sub>2</sub> for the active sites. That is, because an oxidized site is required to convert CO, as P<sub>CO</sub> increases at constant P<sub>O<sub>2</sub></sub> the number of oxidized sites can decrease resulting in a decreasing reaction rate or negative reaction order. The oxygen reaction order of approximately one is consistent with adsorption of oxygen being a slow step (relative to CO oxidation). Alternatively, CO can conceivably chemisorb on the same oxygen vacancy sites that are active for oxygen chemisorption. As P<sub>CO</sub> increases the number of sites occupied by CO increases and the number of oxidized sites able to oxidize CO decreases, again resulting in negative order in CO.

Addition of FePO<sub>4</sub> significantly reduces the rate of CO oxidation under almost all reaction conditions, while at the same time decreasing the degree of CO inhibition (reaction order is zero or less negative). If FePO<sub>4</sub> modifies the active sites so they are less reactive with CO, either for chemisorption on reduced sites or for oxidation on

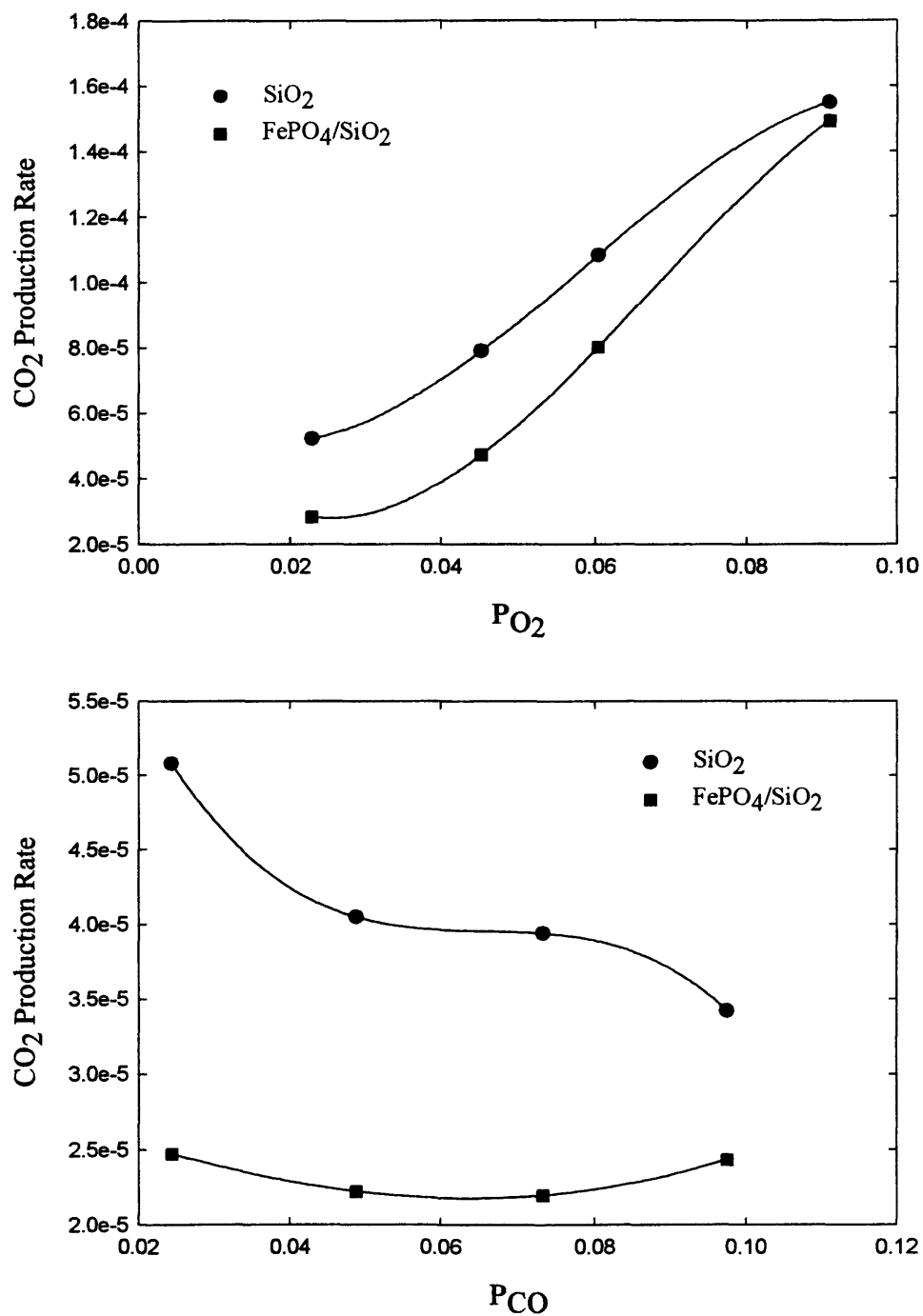


Figure 6.2 CO<sub>2</sub> Production rate (mol/(g.min)) as a function of the reactants partial pressure over silica and silica supported catalysts. GHSV= 40000 h<sup>-1</sup>, P<sub>O2</sub>=2-9 kPa @ P<sub>CO</sub>=9 kPa, P<sub>CO</sub>=2.5-10 kPa @ P<sub>O2</sub>=2.5 kPa, and T=673 K.

oxidized sites, this will reduce the self-inhibiting effect. Because the rate at which CO reacts is lower, oxygen can more easily compete.

### **6.5 Enhanced Formaldehyde Yield**

The enhanced formaldehyde yield over FePO<sub>4</sub> silica may be explained by two related factors. Just as the FePO<sub>4</sub> surface is less reactive with CO, it is less reactive with formaldehyde. These molecules can clearly adsorb at oxygen vacancy sites via the non-bonding orbitals of their oxygen atom, and might then react with adjacent oxidized sites. These molecules might also adsorb on oxidized sites, becoming more oxidized in the process. The results presented here are consistent with a situation where less adsorption and conversion of oxygenates takes place on a more highly oxidized surface. An important hypothesis arising from this study that might be tested in any future study is that oxidation of HCHO and CO require chemisorption of these molecules on reduced surface sites. Note that methane is unlikely to chemisorb on reduced sites, but will require a reactive oxygen site.

The FePO<sub>4</sub> silica surface is more highly oxidized because of the much higher concentration of oxygen chemisorption sites, and because of their apparently lower reactivity with CO. For silica, because CO conversion is faster and there are fewer sites, there are more reduced surface sites under methane oxidation conditions than for FePO<sub>4</sub> silica. The results taken together also suggest that the role of FePO<sub>4</sub> is to increase the rate

at which surface sites reoxidize, most likely because of the redox capability of the iron atom. Experiments directed at testing this hypothesis are discussed in the next section.

### **6.6 Adding Silver to Improve Surface Re-oxidation:**

In previous sections, it was proposed that the  $\text{FePO}_4$  silica catalyst is less active for CO oxidation and produces higher HCHO yield because the surface has a higher concentration of oxidized active sites. One way to test this hypothesis is to try and increase the number of oxidized sites, or increase the rate at which they are reoxidized, even further. Silver is well known to activate oxygen for dissociative chemisorption (Satterfield, 1989). Thus, silver (0.5 wt.%) was added to  $\text{SiO}_2$  and  $\text{FePO}_4/\text{SiO}_2$  to provide more oxygen adsorption sites and accelerate the catalyst surface re-oxidation. The results for these experiments are shown in Appendix B. The major effect of silver addition was observed on the global activation energy. Little change in reaction orders was observed. For both catalysts ( $\text{Ag-SiO}_2$  and  $\text{Ag-FePO}_4\text{-SiO}_2$ ), the activation energy was lowered, to 86 kJ/mol for  $\text{Ag-SiO}_2$  and to 120 kJ/mol for  $\text{Ag-FePO}_4\text{-SiO}_2$ . The comparison between these results and that for  $\text{SiO}_2$  and  $\text{FePO}_4/\text{SiO}_2$  are shown in Table 6.4. The product selectivity pattern for  $\text{Ag-FePO}_4\text{-SiO}_2$  is shown in Figure 6.3.

For both catalysts, addition of silver significantly increased formaldehyde yield and further inhibited CO conversion for the  $\text{FePO}_4/\text{silica}$  catalyst. Furthermore the same results (formaldehyde yield) were achieved at a lower temperature than that over the iron phosphate/silica. When the reaction was carried out over  $\text{Ag-FePO}_4\text{-SiO}_2$  at  $P_{\text{CH}_4}/P_{\text{O}_2}$

Table 6.4 Comparing Conversion-Selectivity and reaction rates for different Catalysts

Catalyst	Conversion		Selectivity		Rate mol/(g <sub>cat</sub> .min)	HCHO STY g/(kg <sub>cat</sub> .hr)	Power Low Kinetics		
	CO	CO <sub>2</sub>	HCHO	P <sub>CH4</sub>			n <sub>CH4</sub>	n <sub>O2</sub>	Ea (kJ/mol)
<b>R=1:1</b>	<b>T=575 C</b>		<b>GHSV= 30000/hr</b>		<b>P<sub>O2</sub>=40kPa</b>				
SiO <sub>2</sub>	6.6	14.1	72.1	13.8	0.000625	169	0.9	1.2	142
Ag/SiO <sub>2</sub>	6	10.7	65.9	23.4	0.000573	264	1.16	1.57	86
<b>R=1:1</b>	<b>T=575 C</b>		<b>GHSV= 60000</b>		<b>PO2=40kPa</b>				
FePO <sub>4</sub> /SiO <sub>2</sub>	2.04	8.8	50.7	40.5	0.000386	310	0.66	1.43	202
FePO <sub>4</sub> -Ag-SiO <sub>2</sub>	6.74	49.1	23	27.9	0.001274	700	0.87	1.29	120

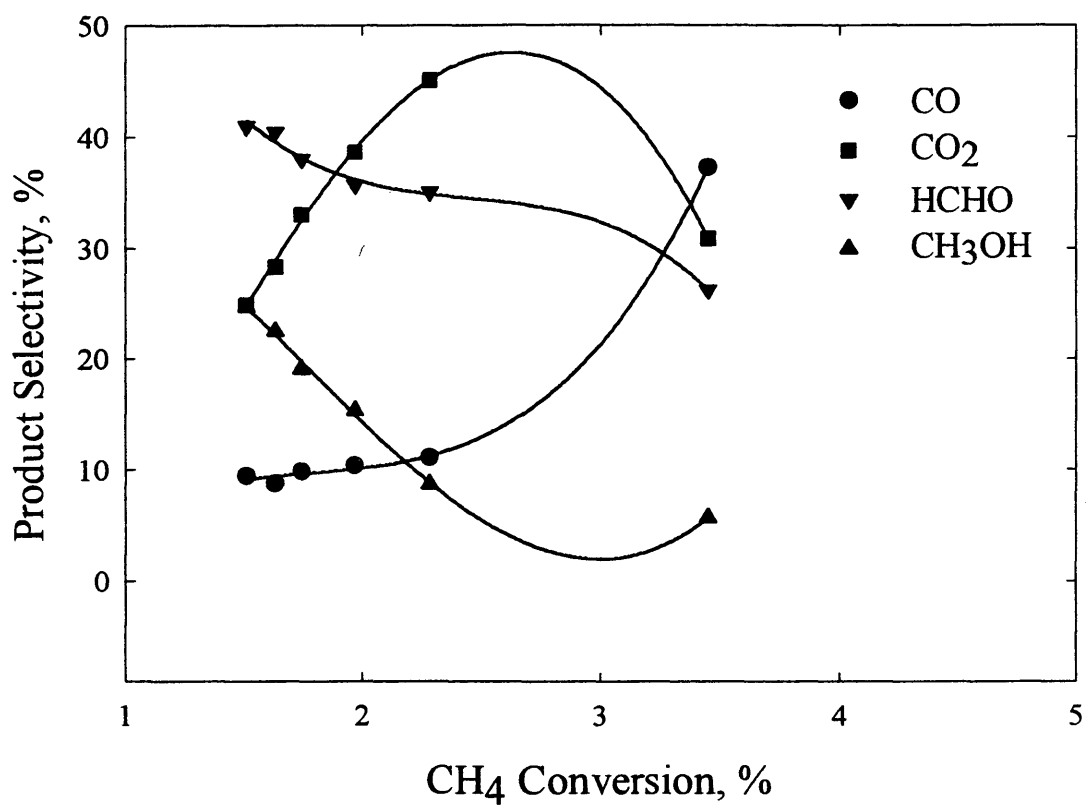


Figure 6.3 Product selectivity, % as a function of methane conversion, % for FePO<sub>4</sub>-Ag-SiO<sub>2</sub> Catalyst. GHSV= 12000-60000 h<sup>-1</sup>, P<sub>O<sub>2</sub></sub>= 17-26 kPa, P<sub>CH<sub>4</sub></sub>= 34-52 kPa, P<sub>CH<sub>4</sub></sub>/P<sub>O<sub>2</sub></sub>=2, and T=848-898 K.

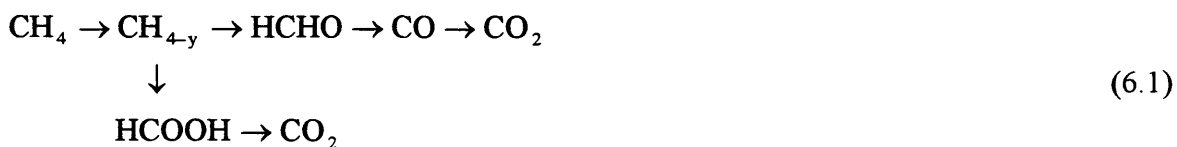
ratio equal 2, methanol was produced in measurable amounts. At low methane conversion, methanol selectivity reaches 25% (methanol STY=31 g/kg<sub>cat</sub>.hr). Thus, silver addition is consistent with the notion that higher oxygenate yields are obtained over catalysts with a high concentration of oxidized surface sites, and can be enhanced by modifications that enhance the rate of surface reoxidation. This result is also consistent with the hypothesis that chemisorption and oxidation of HCHO and CO, and perhaps also methanol, require the presence of reduced surface sites.

### **6.7 Formic Acid Intermediate and the Reaction Network**

A direct route from methane to carbon dioxide has been reported over several catalysts, Spencer and Periera (1989) and Alptekin (1998). In this study we also present evidence consistent with parallel conversion paths from HCHO to CO and to CO<sub>2</sub>. We also have shown that formic acid is produced in small amounts over silica and silica supported iron phosphate during pulsed reaction experiments. These experiments operate under transient conditions that sometimes reveal the presence of intermediates that are difficult to observe under steady state conditions. This is the first time that formic acid has been reported as an intermediate in methane partial oxidation. Some type of CH<sub>2</sub> species bonded to two surface oxygens was observed by Feil et. al. (1987), Machiels and Sleight (1982), and Busca (1989) in methanol FT-IR experiments. At that time it was suggested that this species is a weak type of formate.

From Figures 4.13 and 5.13, there is very little formic acid or CO<sub>2</sub> for the initial pulses, but the concentration of these species in the product increases with pulse number. CO<sub>2</sub> production and formic acid production increase in parallel, suggesting that formic acid is an intermediate in the direct route to CO<sub>2</sub>, either from methane or from formaldehyde (or both). Formic acid and formaldehyde production do not change in parallel, perhaps indicating that formic acid is formed directly from methane rather than from formaldehyde.

For formic acid formation directly from methane we have the following reaction network (water and oxygen are not included):



The species initially formed (CH<sub>4-y</sub>) from methane can be a methoxide (CH<sub>3</sub>-O). The methoxide then reacts with adjacent surface oxygen to form HCOOH and HCHO in parallel paths.

## CHAPTER 7

### MODELING METHANE PARTIAL OXIDATION

#### 7.1 Introduction:

Most kinetic studies of methane partial oxidation conducted previously were used to predict product-selectivity and activity-selectivity patterns. Spencer and Pereira (1987 and 1989) reported two pathways for methane oxidation; one is sequential from methane to formaldehyde, carbon monoxide, and in turn to carbon dioxide. They also observed a parallel direct path where methane is converted to carbon dioxide over  $\text{MoO}_3/\text{SiO}_2$  and  $\text{V}_2\text{O}_5/\text{SiO}_2$ . A global kinetic study was carried out to describe methane partial oxidation over both catalysts. The reactions were assumed to be first order in hydrocarbon and zero order in oxygen, and the catalyst surface was not considered explicitly in the model. The objective of that work was to predict product-selectivity and activity-selectivity patterns.

With the help of Spencer and Pereira, Amiridis et al. (1991) carried out a more complex micro-kinetic model to describe methane partial oxidation. The objective of this work was to formulate a reasonable reaction mechanism that captures important aspects of the surface chemistry, and to link methane partial oxidation kinetics to that observed for oxidation of subsequent gaseous products. Over both molybdate and vanadate catalysts, this model does not accurately predict the CO and CO<sub>2</sub> selectivity. Most likely, this is because of their assumption that the CO conversion rate is low and can be

neglected. The reaction network and the details of the Amiridis study were shown in Chapter 2.

A more simple but chemically sophisticated model was proposed by Arena et al. (1999). The main idea behind this work is the similarity of the methane and oxygen activation steps over silica and supported silica-based catalysts to a Mars and Van Krevelen mechanism (1954). In this study, the fractional density of reduced sites was related to the reactant pressure ratio ( $P_{\text{CH}_4}/P_{\text{O}_2}$ ). The methane oxidation reaction rate was then expressed as a function of the fractional site density and partial pressures at steady state. The explicit consideration of the surface oxidation state is a major improvement in this model over previous work. Unfortunately, the CO oxidation reaction was also neglected, and zero order for oxygen was assumed based on Amiridis et al. (1991). It should be mentioned that Amiridis and coworkers suggested a strong effect of CO adsorption on the surface chemistry, and noted that the rate constant for this step is kinetically significant especially over  $\text{V}_2\text{O}_5/\text{SiO}_2$ . Because CO is rapidly oxidized over silica and silica-supported catalysts, the CO oxidation reaction will impact the density of reduced surface sites, and hence the catalyst activity and selectivity in methane oxidation. Other product oxidation reactions also impact the density of reduced surface sites, but to a lesser extent than the CO oxidation reaction.

In this chapter, we present a model of the impact of all reactions occurring during methane oxidation on the fraction of oxidized surface sites. The modeling results are then considered in light of the observations discussed in Chapter 6.

## 7.2 Simple Models Comparison:

Before starting the modeling process, the similarity of the simple models presented previously in the literature will be demonstrated. In all of these models, under steady state conditions:

$$R_{CH_4} = R_{red} = R_{ox} \quad (7.1)$$

The rate of surface reduction ( $R_{red}$ ) and oxidation ( $R_{ox}$ ) are related to the fractional site density. Finding an expression for the site density as a function of the gaseous pressures is then the heart of this type of work.

The methane partial oxidation reaction rate expressions for some of these models are presented in the following sections.

### 7.2.1 Mars and Van Krevelen Model:

This mathematical model is proposed to describe hydrocarbon oxidation over redox catalysts. Methane partial oxidation can be broken into two general steps:



Where R is the hydrocarbon and M is the metal oxide.

At steady state, the rate of the reduction step equals the rate of the reoxidation step:

$$r = k_{red} * P_{HC} (1 - \theta_{red}) = k_{ox} * P_{O_2} * \theta_{red} \quad (7.3)$$

$\theta_{red}$  = Fraction of active sites in reduced state. Solving for  $\theta_{red}$  :

$$\theta_{\text{red}} = \frac{k_{\text{red}} P_{\text{HC}}}{k_{\text{red}} P_{\text{HC}} + k_{\text{ox}} P_{\text{O}_2}} \quad (7.4)$$

Substituting Eqn. (7.4) into the second equality of Eqn. (7.3) gives:

$$R_{\text{CH}_4} = \frac{k_{\text{red}} k_{\text{ox}} P_{\text{CH}_4} P_{\text{O}_2}}{k_{\text{red}} P_{\text{CH}_4} + k_{\text{ox}} P_{\text{O}_2}} \quad (7.5)$$

### 7.2.2 Arena Model:

The Arena model will be developed in the next section. The result is given here for model comparison:

$$R_{\text{CH}_4} = \rho_0^2 \frac{k_{\text{red}} * P_{\text{CH}_4}}{(1 + (\sqrt{k_{\text{red}} * P_{\text{CH}_4}} / \sqrt{k_{\text{ox}} * P_{\text{O}_2}}))^2} \quad (7.6)$$

It should be noted that all these models give almost the same results, in terms of their ability to fit methane partial oxidation data. Table 7.1 compare the methane reaction rate for the different expressions using data given in Arena et al. (1999). The rate constants used are  $k_{\text{ox}}$  and  $k_{\text{red}}$  equal to  $1.9\text{E}10$  and  $9.0\text{E}7 \text{ gmol}/(\text{s atm})^{-1}$ , respectively. Note that there is no difference between the rates predicted by the Mars and Van Krevelen model and the L-H Model. In fact, the concerted mechanism is also a type of L-H model where  $\text{CH}_4$  and  $\text{O}_2$  dissociation is assumed.

Table 7.1 Comparing Methane Reaction Rate (mol/(g.s)) for Different Models at T=600 °C.

$P_{CH_4}$ (atm)	$P_{O_2}$ (atm)	Arena	M&VK
0.342	0.020	4.25E-06	3.98E-06
0.342	0.044	4.23E-06	4.14E-06
0.342	0.171	4.16E-06	4.26E-06
0.079	0.171	9.77E-07	9.90E-07
0.162	0.171	1.99E-06	2.03E-06
0.342	0.171	4.16E-06	4.26E-06
0.674	0.171	8.09E-06	8.31E-06
0.973	0.171	1.16E-05	1.19E-05
1.214	0.171	1.43E-05	1.48E-05

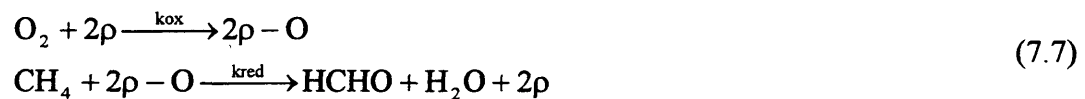
### 7.3 Mathematical Models:

At present a full, elementary reaction level model of  $CH_4$  oxidation over silica based catalysts is not possible. Any model of this type will have to account for the effect of oxygen partial pressure on the methane conversion rate and for CO inhibition. The models examined here are simply directed at correlating the fraction of reduced surface sites with reactant and product partial pressures. Two simple models will be used in the analysis of our experimental data. The first is used to predict the fractional density of reduced sites ( $\theta_{red}$ ) based on the inlet reactant ( $CH_4$  and  $O_2$ ) pressures. In the second, the effect of the gaseous product pressures ( $CH_4$ , HCHO and CO) on  $\theta_{red}$  are also included.

In this second approach, the product pressures are found experimentally rather than predicted by the model.

### 7.3.1 Reactants Pressure Effect on $\theta_{\text{red}}$ :

Methane activation has been thought to be the rate-controlling step. In the experimental section of this work, the importance of the surface re-oxidation step was revealed. The reaction network in this case will consist of the dissociation of oxygen and methane. Oxygen first dissociates on the active sites to provide the active species for methane activation. The two steps are represented as follow:



The rate expression for each step will be:

$$\begin{aligned} R_{\text{O}_2} &= k_{\text{ox}} P_{\text{O}_2} \theta_{\text{red}}^2 \\ R_{\text{CH}_4} &= k_{\text{red}} P_{\text{CH}_4} \theta_{\text{ox}}^2 \end{aligned} \quad (7.8)$$

Under steady state conditions:

$$R_{\text{O}_2} = R_{\text{CH}_4} \quad (7.9)$$

$$\theta_{\text{red}} = 1 - \theta_{\text{ox}} \quad (7.10)$$

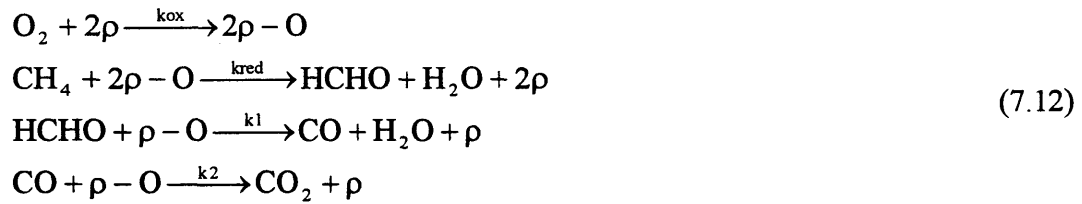
Substituting the rate expressions (7.8) in (7.9) and using (7.10), we get:

$$\theta_{\text{red}} = \frac{\sqrt{\frac{k_{\text{red}} P_{\text{CH}_4}}{k_{\text{ox}} P_{\text{O}_2}}}}{1 + \sqrt{\frac{k_{\text{red}} P_{\text{CH}_4}}{k_{\text{ox}} P_{\text{O}_2}}}} \quad (7.11)$$

Rate constants ( $k_{\text{red}}$  and  $k_{\text{ox}}$ ) and reactant inlet pressures are found experimentally in the flow reactor studies; the experimental data are given in Appendix C. Note that these studies were conducted under differential conditions where the assumption that reactant partial pressures do not change significantly down the length of the reactor can be made. The kinetic parameters are given in Table 7.2. The rate of surface reduction,  $k_{\text{red}}$ , is simply the rate of methane conversion. The rate of surface reoxidation is found using the quadrature technique from the CO and CH<sub>3</sub>OH oxidation experiments, and then extrapolated to the higher temperature of methane oxidation. The quadrature method presented by Gay (1971) is explained in appendix D. The use of this approach is discussed in more detail in the next section. The fractional density of reduced sites is then plotted as a function of the reactant inlet pressures. A log-log plot is used to find the order of dependence of  $\theta_{\text{red}}$  on  $P_{\text{CH}_4}$  and  $P_{\text{O}_2}$ . Note that this mathematical model was taken from Arena et al. (1999), but the model parameters are based on the data acquired in this work.

### 7.3.2 Effect of Reactions of Products on $\theta_{\text{red}}$ :

The reaction network below is an extension of the Arena model to include surface reduction by HCHO and CO. Methane and oxygen dissociation are the principal steps in this mechanism. The suggested reaction network is as follows:



The rate expression for each step will be:

$$\begin{aligned}
 R_{\text{O}_2} &= k_{\text{ox}} P_{\text{O}_2} \theta_{\text{red}}^2 \\
 R_{\text{CH}_4} &= k_{\text{red}} P_{\text{CH}_4} \theta_{\text{ox}}^2 \\
 R_{\text{HCHO}} &= k_1 P_{\text{HCHO}} \theta_{\text{ox}} \\
 R_{\text{CO}} &= k_2 P_{\text{CO}} \theta_{\text{ox}}
 \end{aligned} \tag{7.13}$$

Under steady state conditions:

$$R_{\text{O}_2} = R_{\text{CH}_4} + R_{\text{HCHO}} + R_{\text{CO}} \tag{7.14}$$

$$\theta_{\text{red}} = 1 - \theta_{\text{ox}} \tag{7.15}$$

Substituting the rate expressions (7.13) in (7.14) and using (7.15) we get:

$$\begin{aligned}
 0 = & (k_{\text{red}} P_{\text{CH}_4} - k_{\text{ox}} P_{\text{O}_2}) \theta_{\text{red}}^2 - (2k_{\text{red}} P_{\text{CH}_4} + k_1 P_{\text{HCHO}} + k_2 P_{\text{CO}}) \theta_{\text{red}} \\
 & + (k_{\text{red}} P_{\text{CH}_4} + k_1 P_{\text{HCHO}} + k_2 P_{\text{CO}})
 \end{aligned} \tag{7.16}$$

This quadratic equation can be solved for  $\theta_{\text{red}}$  :

$$\theta_{\text{red}} = \frac{-b \pm \sqrt{b^2 - 4ac}}{2a} \tag{7.17}$$

It is known that:  $0 < \theta_{\text{red}} < 1$ , then the positive root represents the fraction of reduced sites. The rate constants and gaseous pressures are evaluated experimentally; a summary of the kinetic parameters is given in Table 7.2 for both silica and iron phosphate/silica catalysts. The rate constants were found from the flow reactor studies. The observed rate constants for CO and HCHO oxidation ( $k_2$  and  $k_1$ ) are found at the reaction conditions then extrapolated to the methane partial oxidation conditions. This involves extrapolation to a significantly higher temperature and assumes that the reaction mechanism and rate determining step for CO and HCHO oxidation remains the same for reaction under the conditions of methane oxidation. Clearly extrapolation of a linear regression fit (the Arrhenius equation) to well beyond the experimental range is not justified for quantitative models of reaction kinetics. In the present context, the purpose of the model is merely to illustrate the impact of subsequent reactions on the surface oxidation state in a qualitative way. For this purpose, extrapolation can be justified when it is explicitly brought to the reader's attention. The reoxidation rate constant ( $k_{\text{ox}}$ ) was found by analyzing the CO and HCHO experiments. The quadrature method was then used to find  $k_{\text{ox}}$  at two temperatures, then an Arrhenius form was evaluated from these two points. Again, because of the illustrative rather than quantitative nature of the model, this approach can be justified.

Table 7.2 Kinetic Parameters For Methane Partial Oxidation

Catalyst	Rate Constant
SiO <sub>2</sub>	$k_{ox} = 3.86 \cdot \text{Exp.}(-4150/RT)$ $k_{red} = 2.76E4 \cdot \text{Exp.}(-142000/RT)$ $k_1 = 234920 \cdot \text{Exp.}(-111400/RT)$ $k_2 = 12.8 \cdot \text{Exp.}(-56090/RT)$
FePO <sub>4</sub> /SiO <sub>2</sub>	$k_{ox} = 7 \cdot \text{Exp.}(-17300/RT)$ $k_{red} = 8.3E9 \cdot \text{Exp.}(-202138/RT)$ $k_1 = 9.04E5 \cdot \text{Exp.}(-101000/RT)$ $k_2 = 1.5 \cdot \text{Exp.}(-31950/RT)$

#### 7.4 Methane Oxidation Over Silica:

The trends of  $\theta_{red}$  with partial pressures at  $T=600$  °C for both models are given in Figures 7.1 (reactant pressure dependence only) and 7.2 (with product pressure dependence). In Figure 7.1,  $\theta_{red}$  is low and has half order dependence on both  $P_{CH_4}$  and  $P_{O_2}$  (Figure 7.1.B). This plot essentially reproduces the results of Arena and coworkers, but uses our experimental rate constants rather than those developed by Arena et al. by fitting the model to their data. The low rate constant ratio ( $k_{red}/k_{ox} = 0.00004$ ) implies that the rate of re-oxidation is very high compared to the rate of reduction consistent with methane activation as the rate-limiting step.

When the product pressure effect on surface reduction was included (Figure 7.2),  $\theta_{\text{red}}$  is roughly two times larger and the order in methane partial pressure is 0.2. For oxygen, the dependence was 0.66. The inclusion of additional reducing species increases the degree of surface reduction. The rate constant ratio is much higher  $((k_{\text{red}}+k_1+k_2)/k_{\text{ox}} = 0.026)$ , hundreds of times the value for analysis with the inlet reactant pressures only. The rate of surface reoxidation is the same for both cases, but the combined rate of surface reduction is much higher and is more comparable to the oxidation rate. The inclusion of the reaction products and their impact on surface reduction in the model increases the fractional density of reduced sites, which means less oxidized surface sites available to activate methane. Figure 7.3 compares  $\theta_{\text{red}}$  for the two models.

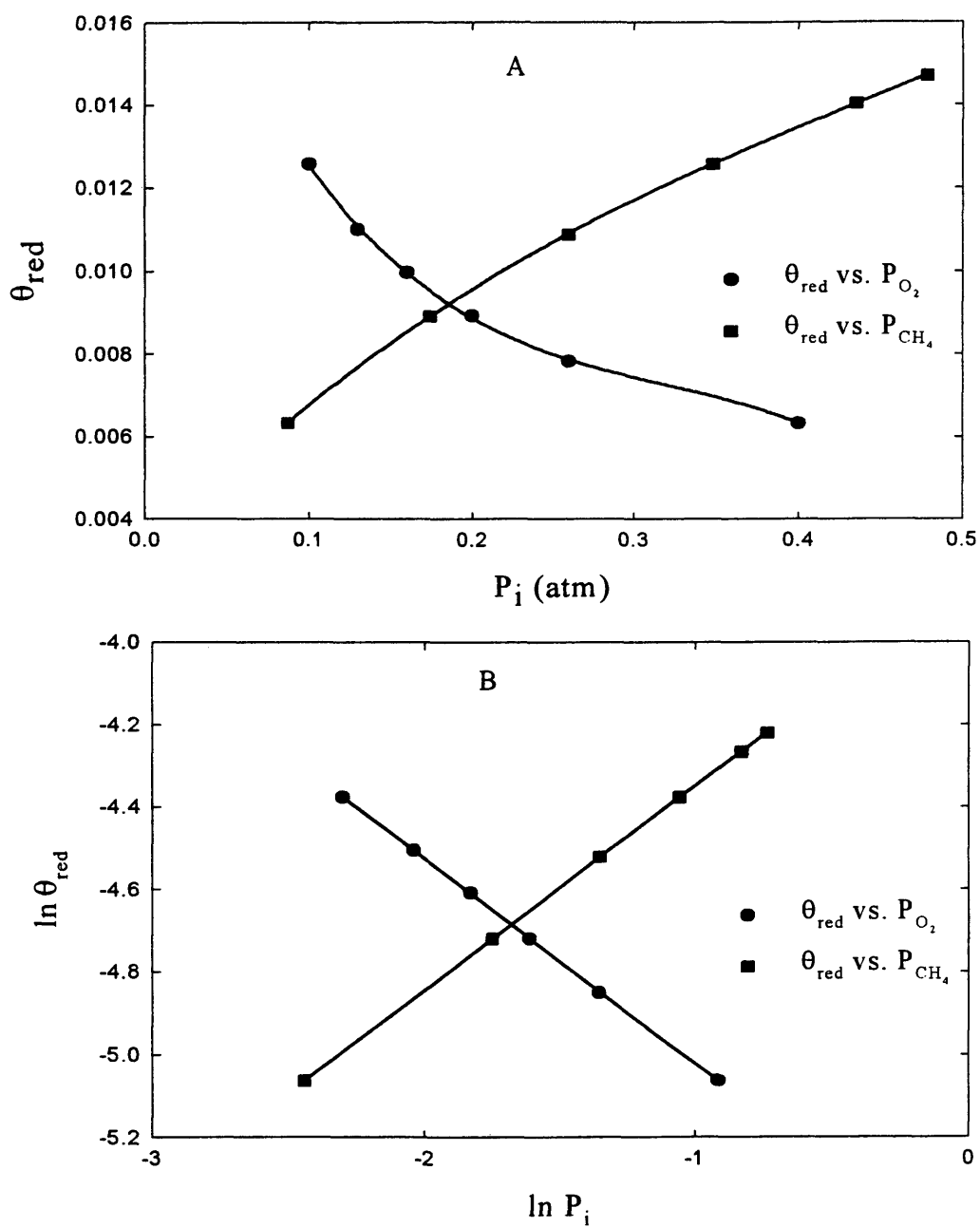


Figure 7.1 Methane partial oxidation over silica at  $T=873K$ :  
 (A) Fractional density of reduced sites versus inlet reactants pressure.  
 (B) Log-log plot to find  $\theta_{red}$  dependence on  $P_{CH_4}$  and  $P_{O_2}$ .

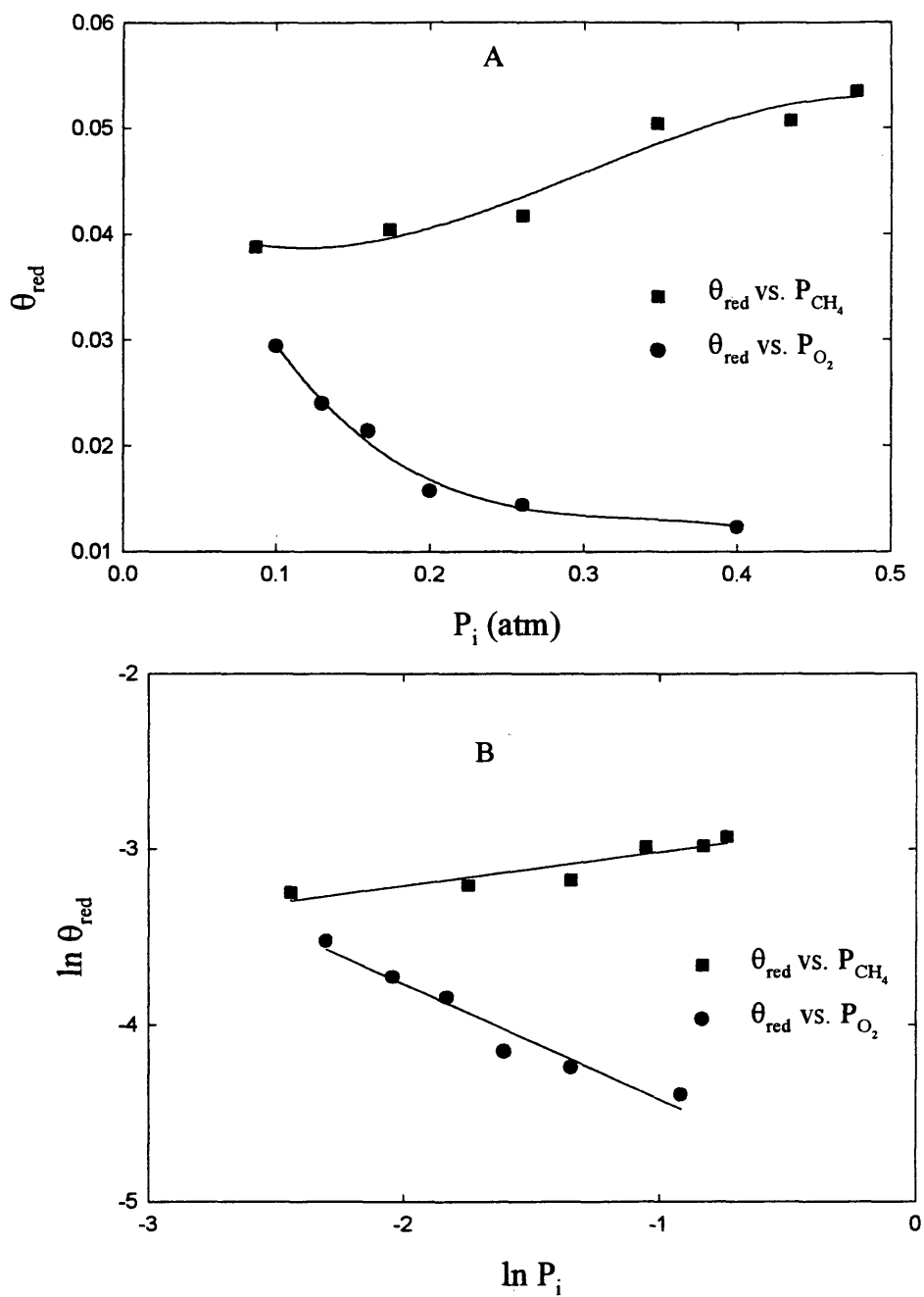


Figure 7.2 Methane partial oxidation over silica at  $T=873K$ :  
 (A) Fractional density of reduced sites versus products pressure.  
 (B) Log-log plot to find  $\theta_{red}$  dependence on  $P_{CH_4}$  and  $P_{O_2}$ .

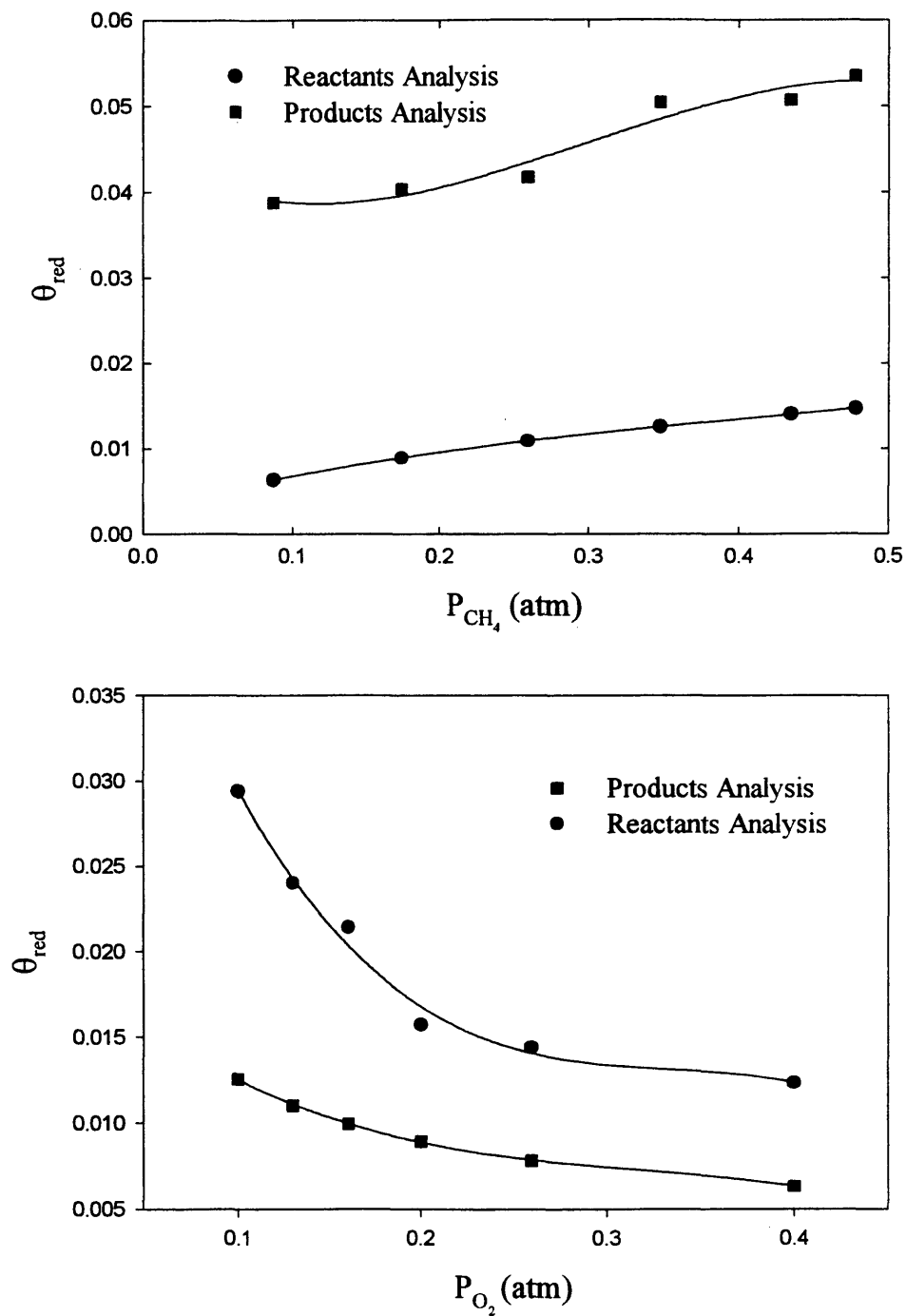


Figure 7.3 Comparing  $\theta_{red}$  when using the reactants and products pressure models.

### 7.5 Methane Oxidation Over Iron Phosphate/Silica:

Plotting  $\theta_{\text{red}}$  vs.  $P_{\text{CH}_4}$  and  $P_{\text{O}_2}$  gives half order dependence when using both the reactants model and the products models over  $\text{FePO}_4/\text{silica}$ . When compared to silica, the rate constant ratio  $k_{\text{red}}/k_{\text{ox}} = 0.01$  (reactants pressure model) is higher. Similarly  $(k_{\text{red}}+k_1+k_2)/k_{\text{ox}} = 0.166$  (model considering reaction of products), showing the large effect of the reaction products and their subsequent reactions on the catalyst surface. The overall rates of surface reduction and reoxidation are of the same order of magnitude in this case.  $\theta_{\text{red}}$  could reach as high as 40% for high methane to oxygen ratios, as seen in Figure 7.5. The presence of iron phosphate appears to make the surface much easier to reduce overall, based on this model. It should be noted that the presence of the 2wt.%  $\text{FePO}_4$  nearly doubled the total site density, so that under typical conditions there are many more oxidized surface sites present under reaction conditions for the  $\text{FePO}_4/\text{SiO}_2$  catalyst than for  $\text{SiO}_2$ .

### 7.6 Rate Constants Sensitivity Analysis:

A sensitivity analysis was performed by changing the rate constant for each step by 10% of its experimental value and observing the effect on  $\theta_{\text{red}}$ . Other rate constants were unchanged. For silica the most important reactions are surface re-oxidation and formaldehyde conversion to CO. A 10% change in  $k_1$  and  $k_{\text{ox}}$  (rate constant for

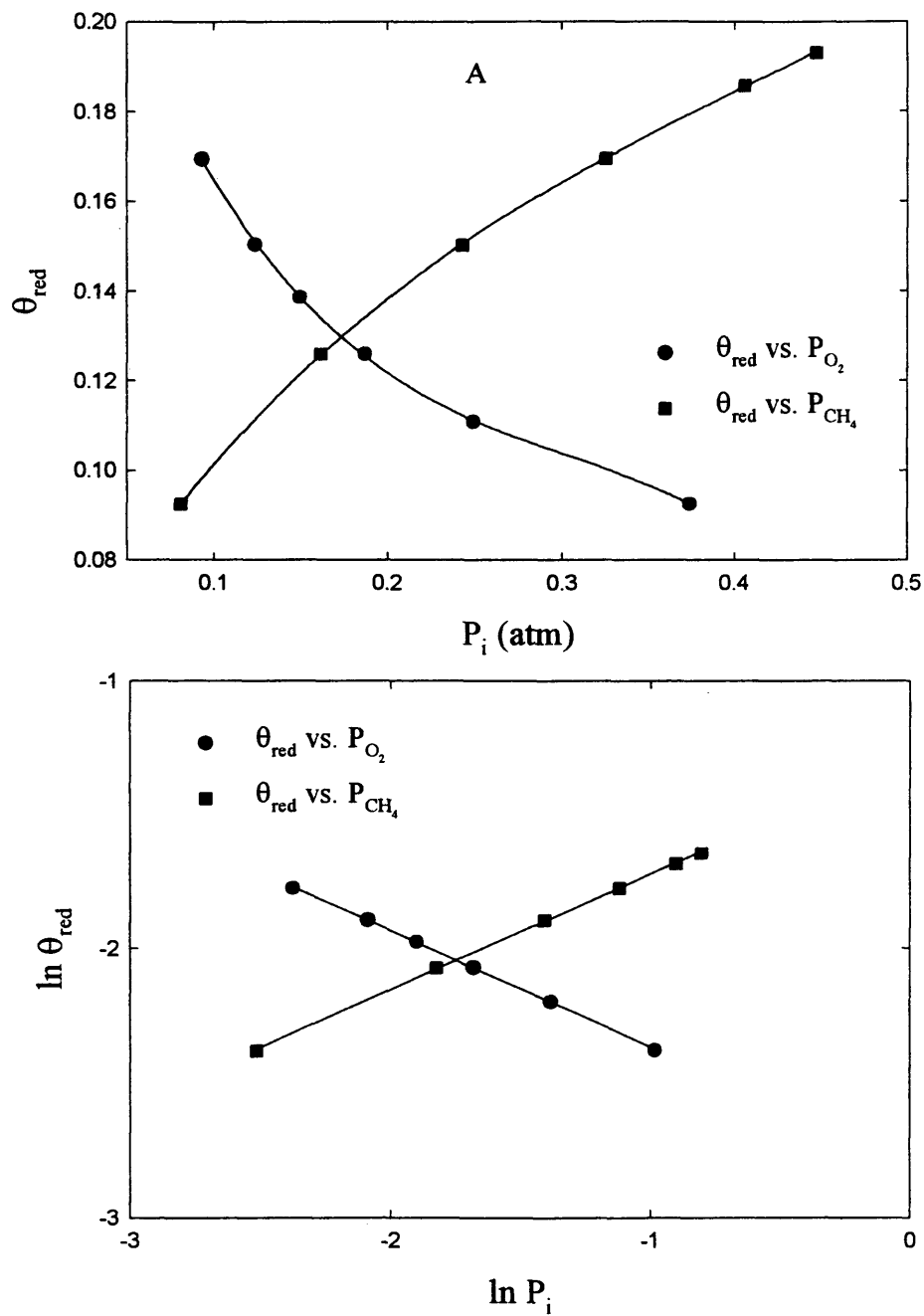


Figure 7.4 Methane partial oxidation over iron phosphate/silica at  $T=873\text{K}$ :  
 (A) Fractional density of reduced sites versus inlet reactants pressure.  
 (B) Log-log plot to find  $\theta_{\text{red}}$  dependence on  $P_{\text{CH}_4}$  and  $P_{\text{O}_2}$ .

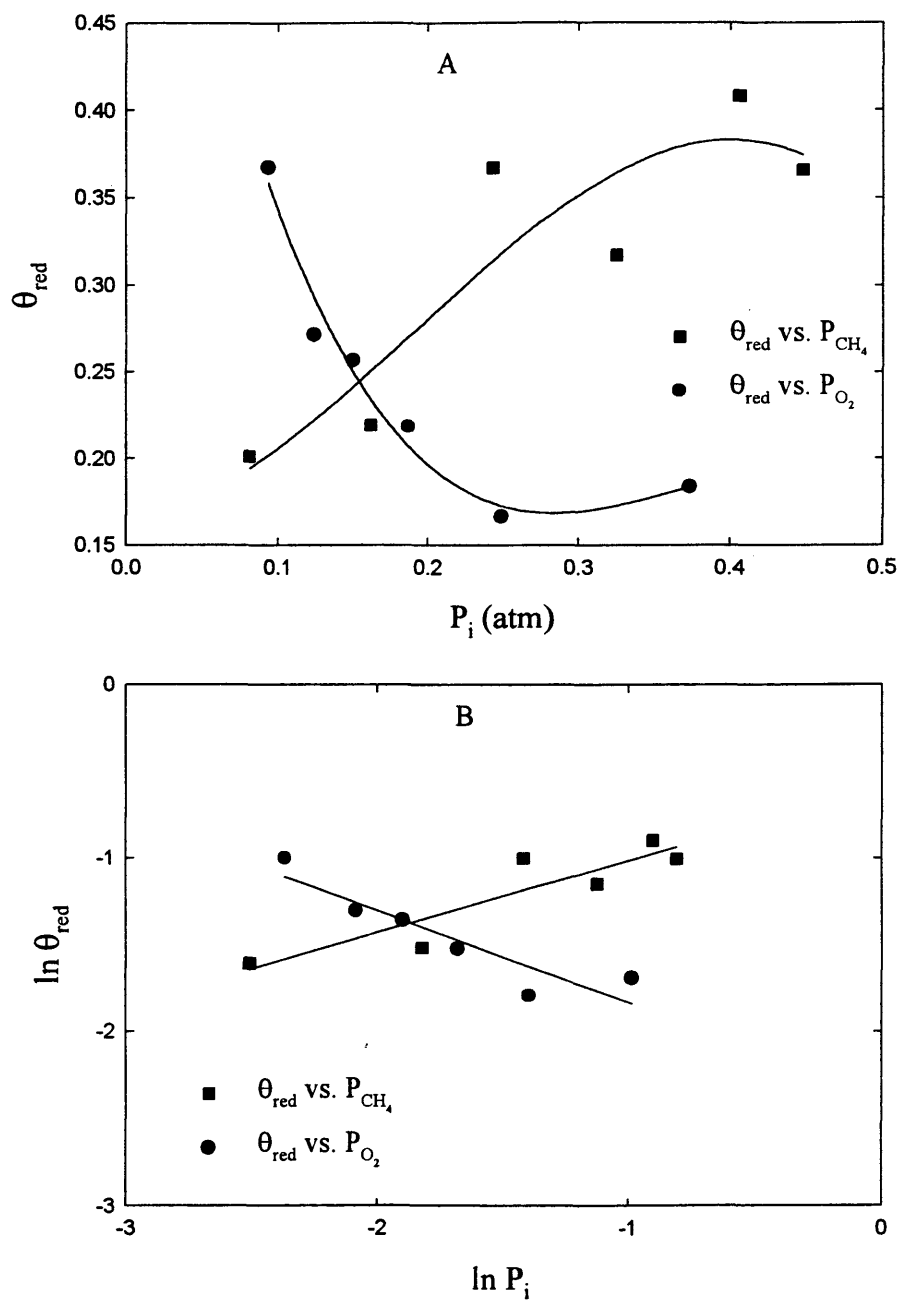


Figure 7.5 Methane partial oxidation over iron phosphate/silica at  $T=873K$ :  
 (A) Fractional density of reduced sites versus products pressure.  
 (B) Log-log plot to find  $\theta_{red}$  dependence on  $P_{CH_4}$  and  $P_{O_2}$ .

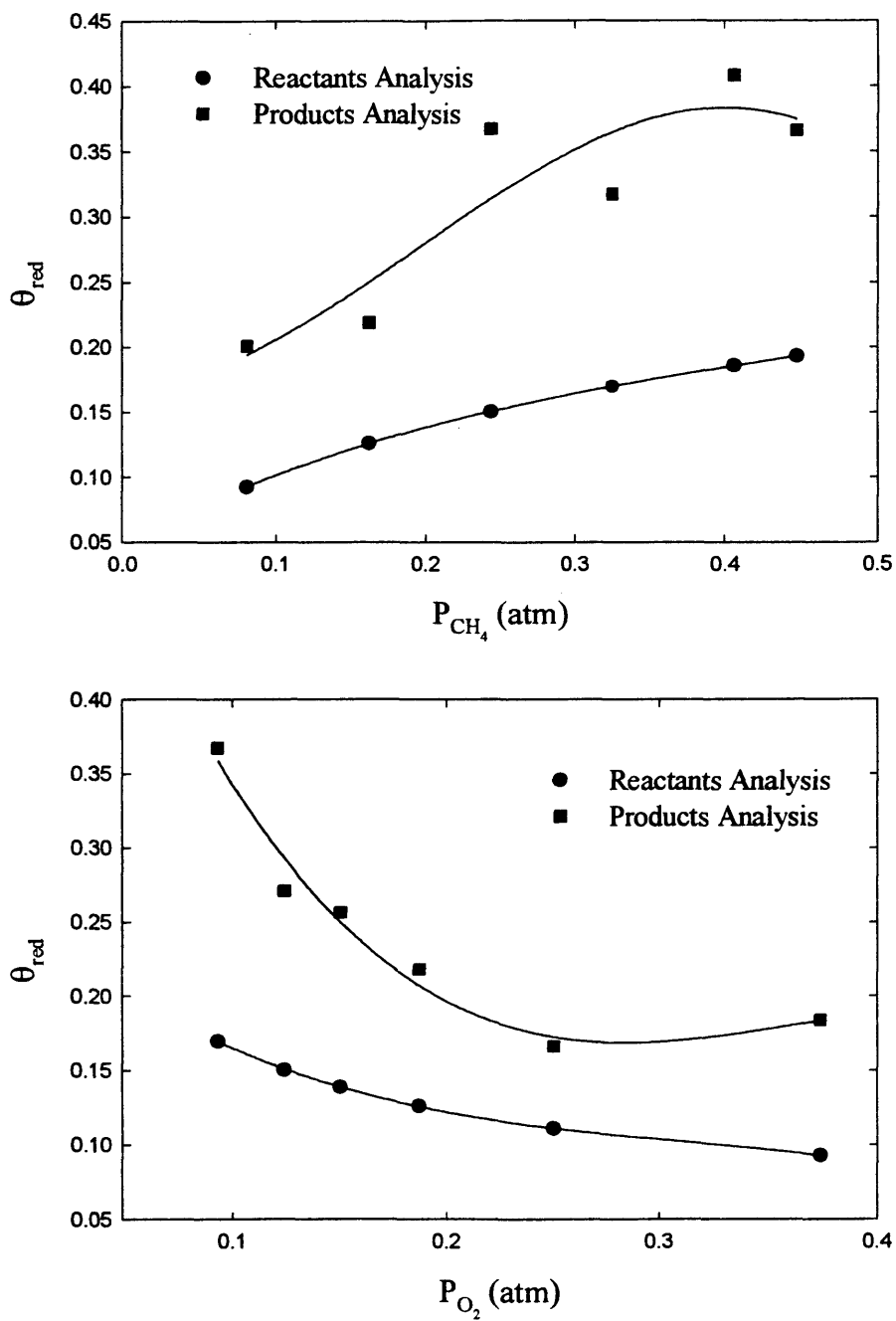


Figure 7.6 Comparing  $\theta_{red}$  when using the reactants and products pressure models.

formaldehyde oxidation and surface reoxidation, respectively) would impact the reduced site density by about 5%. A change in methane activation or CO oxidation rate constants had only a small effect on  $\theta_{\text{red}}$  (<1%). Over FePO<sub>4</sub>/SiO<sub>2</sub>, a 10% change in methane activation or surface re-oxidation rate constants would cause a 10% difference in  $\theta_{\text{red}}$  value. Here the two steps have comparable effects on the catalyst surface, and both could be rate controlling steps. Doubling rate constants for product oxidation (CO or HCHO) could cause up to a 50% change in the  $\theta_{\text{red}}$ . The sensitive nature of the catalyst surface to the reaction intermediates affects its activity.

## CHAPTER 8

### CONCLUSIONS AND RECOMMENDATIONS

#### 8.1 Conclusions:

1. The domination of the silica surface on the reaction network and most of the methane partial oxidation results confirms that silica is the main active catalyst. Addition of  $\text{FePO}_4$  modifies the properties of silica to improve yield of HCHO and significantly reduce the rate of conversion of CO to  $\text{CO}_2$ .
2. Gas phase oxygen is required for methane oxidation to occur, implying that chemisorbed oxygen rather than lattice oxygen is reacting.
3. In the direct route, it was discovered that formic acid is an intermediate that is oxidized to carbon dioxide as seen in the mass spectral analysis.
4. Global reaction order for oxygen is always significantly above zero, implying that active site reoxidation occurs at a rate comparable to that of methane (or other hydrocarbon) activation. Effect of oxygen partial pressure in methane oxidation cannot be modeled by simple power law kinetics. The oxygen partial pressure effect in subsequent oxidation of methanol, formaldehyde, and CO could be described using a simple power law model.
5. Reaction orders for CO in CO oxidation are negative for silica, indicating some form of kinetic inhibition. The CO reaction order is zero for iron phosphate/silica. This

result, and the stability of HCHO over a surface with a higher density of oxidized sites, suggests that oxidation of these compounds may require their chemisorption on oxygen vacancy sites.

6. The population of reduced sites on the catalyst surface during methane oxidation is significantly impacted by subsequent reactions of formaldehyde and CO, thus these reactions must be included in any kinetic model that explicitly includes surface sites.
7. The rates of surface reduction by oxidation and reduction are of the same order of magnitude, and therefore methane activation may not be the rate determining step.

It was hypothesized that increasing the rate of surface re-oxidation will enhance the catalyst performance and increase the desired products yield. Silver is known for its ability to adsorb oxygen, Satterfield (1981). Adding silver to iron phosphate/silica catalyst improved the yields to desired products. Methanol selectivity of 25% was achieved at low conversion. High formaldehyde yields are also reported at lower temperatures.

## **8.2 Recommendations:**

It is recommended to further study the catalyst surface re-oxidation step at low  $P_{\text{CH}_4}/P_{\text{O}_2}$  pressure ratios. The possibility of the change of the rate limiting step or the presence of more than one controlling step should be investigated. A more complex model that considers a change in the rate limiting step or accounting for more than one

controlling step is advised. The presence of two active oxygen species or active sites must be included.

In modeling methane partial oxidation, the carbon monoxide inhibiting effects must be included. Assuming that carbon monoxide oxidation rate was low is the reason of the discrepancy that occurs in carbon monoxide and dioxide selectivity in many methane partial oxidation models (Amiridis et al.(1991) and Arena et al. (1999)).

Adding silver to silica based metal oxide enhanced the catalysts activity and increased the desired products yield. In this work only very low loading of silver was used ( $Ag < 0.5\text{wt}\%$ ), different catalyst loading must be examined. Further more, high-pressure studies are also recommended.

## REFERENCES CITED

1. Adamson, A.W., "Physical Chemistry of Surfaces", John Wiley & Sons, NY, (1982).
2. Ai, M., *J. Catal.* **101**, 389 (1986).
3. Alptekin, G.O., "Methane Oxidation to Methanol and Formaldehyde Over Transition Metal Phosphates", **Ph. D. Thesis**, Colorado School of Mines (1998).
4. Alptekin, G.O., Herring, A.M., Williamson, D.L., Ohno, T.R., and McCormick, R.L., *J. Catal.* **181**, 104 (1998).
5. Amiridis, M.D., Rekoske J.E., Dumesic, J.A., Rudd, D.F., Spencer, N.D., and Pereira, C.J., *AICHE* **37**, 87 (1991).
6. Arena, F., Frusteri, F., and Parmaliana, A., *Appl. Catal. A: General* **197** (2000).
7. Asada, H., Nishizaki, M., and Morizawa, Y., *Surf. Sci.* **383**, 277 (1997).
8. Bett, J.A.S., and Hall, W.K., *J. Catal.* **10**, 105 (1968).
9. Bonnet, P., Millet, J.M.M., Leclercq, C., and Vedrine, J.C., *J. Catal.* **158**, 128 (1996).
10. Bonnet, P., and Millet, J.M.M., *J. Catal.* **161**, 198 (1996).
11. Boonrueng, S.K., "Sorption of NO By SiO<sub>2</sub> Supported 12-Tungstophosphoric Acid", **Master Thesis**, Colorado School of Mines (1998).
12. Borescov, G.K., Kolovertnov, G.D., Kefeli, L.M., Plyasove, L.M., Karakchiv, L.G., and Mastikhin, V.N., *Kinet. Catal.* **7**, 144 (1996).
13. Bradley, S.A., Gattuso, M.J., and Bertolacini, R.J., "Characterization and Catalyst Development", American Chem. Soc., DC, (1989).

14. Broadbelt, L.J., and Rekoske, J.E., *Chem. Eng. Sci.* **51**, 3337 (1996).
15. Brown, M.J., and Parkyns, N.D., *Catalysis Today* **8**, 305 (1991).
16. Bui, P.A., Vlachos, D.G., and Westmoreland, P.R., *Surf. Sci.* **385**, L1029 (1997).
17. Clarke, D.B., Lee D., Sandoval, M.J, and Bell, A., *J. Catal.* **150**, 81 (1994).
18. Chaix, L., and Domine, F., *J. Phys. Chem.* **101**, 6105 (1997).
19. Cheng, W., and Kung, H., "Methanol Production and Use", Marcel Dekker, Inc., NY, (1994).
20. Coltrin, M.E., Kee R.J., Rupley F.M., and Meeks, E., "SURFACE CHEMKIN-III", Sandia Report, Sandia National Laboratories, NM and CA, (1996).
21. Dumesic, J.A., Rudd, D.F., Aparicio, L. M., Rekoske J.E., and Trevino, A.A., "The Microkinetics of Heterogeneous Catalysis", American Chem. Soc., Washington DC, (1993).
22. Dunne, J.A., Rao, M., Sircar, S., Gorte, R.J., and Myers, A.L., *Langmuir* **13**, 4333 (1997).
23. Ebner, J.R, and Thompson, M.R., *Catalysis Today* **16**, 51 (1993).
24. Faraldos, M., Anderson, J.A., Banares, M.A., Fierro, J.L.G., and Weller, S.W., *J Catal.* **168**, 110 (1997).
25. Feil, F.S., Van Ommen, J.G., and Ross, J.R.H., *Langmuir* **3**, 668 (1987).
26. Fogler, H.S., "Elements of Chemical Reaction Engineering", Prentice Hall, 2<sup>nd</sup> Ed., NJ, (1992).
27. Fox, J.M., Chen, T., and Degen, B.D., *Chem. Eng. Progress.*, April, 42 (1990).

28. Gay, I., *J. Phys. Chem.* **75**, 10 (1971).
29. Gesser, H.D., Hunter, N.R., and Prakash, C.B., *Chem. Rev.* **85**, 235 (1985).
30. Golwasser M. R., and Trimm D., *Ind. Eng. Chem. Prod. Res. Dev.*, **18(1)**, 27 (1979).
31. Hall, T.J., Hargreaves, J.S.J., Hutchings, G.J., Joyner, R.W., and Taylor, S.H., *Fuel Proc. Technol.* **42**, 151 (1995).
32. Hattori, T., and Murakami, Y., *J. Catal.* **10**, 114 (1968).
33. Hickman, D.A., and Schmidt, L.D., *AICHE* **39**, 1164 (1993).
34. Jongsomjit, B., "Partial Oxidation of Methane over Vanadia/Silica Cogel Catalysts", **Master Thesis**, Colorado School of Mines, 1998.
35. Khan, M.M., and Somorjai, G.A., *J. Catal.* **91**, 263 (1985).
36. Klissurski, D., Rives, V., Abadzhieva, N., Pesheva, Y., Pomonis, P., Sdoukos, T., and Petrakis, D., *J. Chem. Soc., Chem. Commun.*, 1606 (1993)
37. Kobayashi, T., Nakagawa, K., Tabata, K., and Haruta, M., *J. Chem. Soc. Chem. Commun.* 1609 (1994).
38. Kung, H.H., *In. Eng. Chem. Prod. Res. Dev.* **25**, 175 (1986).
39. Levenspiel, O., "Chemical Reaction Engineering", John Wiley & Sons, NY, (1982).
40. Masel, R.I., "Principles of Adsorption and Reaction on Solid Surfaces", John Wiley & Sons, NY, (1996).
41. Mars, P., and Van Krevelen, D. W., *Chem. Eng. Sci.*, 3 (suppl.), 41 (1954).
42. Matsushima, T., Hashimoto, M., and Toyoshima, I., *J. Catal.* **58**, 303 (1979).

43. McCormick, R.L.; Alptekin, G.O., Herring, A.M., Ohno, T.R., and Dec, S.F., *J. Catal.* **172**, 190 (1997).
44. McCormick, R.L., and Alptekin, G.O., *Catal. Today* **55**, 269 (2000).
45. McCormick, R.L., Alptekin, G.O., Williamson, D.L., and Ohno, T.R., *Topic in catal.* **10**, 115 (2000).
46. Michalakos, P.M., Kung, M.C., Jahan, I., and Kung, H.H., *J. Catal.* **140**, 226 (1993).
47. Millet, J.M.M., Rouzies, D., and Vadrine, J.C., *App. Catal.* **124**, 205 (1995)
48. Millet, J.M.M., Virely, M., Forissier, M., Bussiere, P., and Vadrine, J.C., *Hyperfine Interactions* **46**, 619 (1989)
49. Muneyama, E., Kunishige, A., Ohdan, K., and Ai, M., *J. Catal.* **158**, 378 (1996).
50. Murakami, Y., Hattori, Tat., and Hattori, Tad., *J. Catal.* **10**, 123 (1968).
51. Nag, N., Chary, B., Mahipal, R., Rama RAO, and Subrahmanyam, S., *Appl. Catal.* **9**, 225 (1984).
52. Nag, N., Komandur, V.R., Chary, B., Rama RAO, and Subrahmanyam, S., *Appl. Catal.* **31**, 73 (1987).
53. Oyama, S.T., Went, G.T., Kenneth, B.W., Alexis, T.B., and Somorjai, G.A., *J. Phys. Chem.* **93**, 6786 (1989).
54. Pak, S., Smith, C.E., Rosynek, M.P., and Lunsford, J.H., *J. Catal.* **165**, 73 (1997).
55. Parkyns, N.D., Warburton, C.I., and Wilson, J.D., *Catalysis Today* **18**, 385 (1993).
56. Parmaliana, A., Frusteri, F., Mezzapica, A., Miceli, D., Scurrrell, M.S., and Giordano, N., *J. Catal.* **143**, 262 (1993).

57. Parmaliana, A., Sokolovskii, V., Mezzapica, A., Miceli, D., Arena, F., and Giordano, N., *J. Catal.* **148**, 514 (1994).
58. Pepera, M.A., Callahan, J.L., Desmond, M.J., Milberger, E.C., Blum, P.R., and Bremer, N.J., *J. Am. Chem. Soc.* **107**, 4883 (1985).
59. Poirer, M.G., Sanger, A.R., Smith, K.J., *Can. J. Chem. Eng.* **69**, 1027 (1991).
60. Pitchai, R., and Klier, K., *catal. Rev. Sci. Eng.* **28**(1), 13 (1986).
61. Richard, W.G., and Scott, P.R., "Structure and Spectra of Molecules", John Wiley & Sons, NY, (1985).
62. Ribeiro, F.H., Chow, M., and Dalla Betta, R.A., *J. Catal.* **146**, 537 (1994).
63. Rouzies, D., Millet, J.M.M., Siew Hew Sam, D., and Vedrine, J.C., *App. Catal.* **124**, 189 (1995).
64. Satterfield, C.N., "Hetrogeneous Catalysis In Industrial Practice", McGraw-Hill, 2<sup>nd</sup> Ed., NY, (1991).
65. Sica, A.M., Valles, E.M., and Gigola, C.E., *J. Catal.* **51**, 115 (1978).
66. Smith, J.M., "Chemical Engineering Kinetics", McGraw-Hill, 3<sup>rd</sup> Ed., Singapore, (1981).
67. Spencer, N.D., and Pereira, C.J., *J. Catal.* **116**, 399 (1989).
68. Spencer, N.D., *J. Catal.* **109**, 187 (1988).
69. Spencer, N.D., and Pereira, C.J., *AICHE* **33**, 1808 (1987).
70. Srivastava, R.D. Zhou, P., Stiegel G.J., Rao, V.U.S., and Cinquegrane, G, *J. Catal.*, 183 (1990).

71. St-Just, J., Basset, J. M., Bousquet, J., and Martin, G. A., *La Recherche* **21** (222), 730 (1990)
72. Sun, Q., Jehng, M., Hu, H., Herman, R.G., Wachs, I.E., and Klier, K., *J. Catal.* **165** 91 (1997)
73. Valden, M., Pere, J., Hirsimaki, M., Suhonen, S., and Pessa, M., *Surf. Sci.* **377**, 605 (1997).
74. Wang, Y., and Otsuka, K., *J. Catal.* **155**, 256 (1995).
75. Wang, Y., and Otsuka, K., *J. Catal.* **171**, 106 (1997).
76. Wang, Y., and Otsuka, K., *J. Molec. Catal.* **111**, 341 (1996).
77. Wang, Y., Hermam, R.G., and Klier, K., *Surf. Sci.* **279**, 33 (1992).
78. Weng, T., and Wolf, E.E., *App. Catal.* **96**, 383 (1993).

## APPENDIX A

CO Adsorption Experiments over  $\text{SiO}_2$  and  $\text{FePO}_4/\text{SiO}_2$

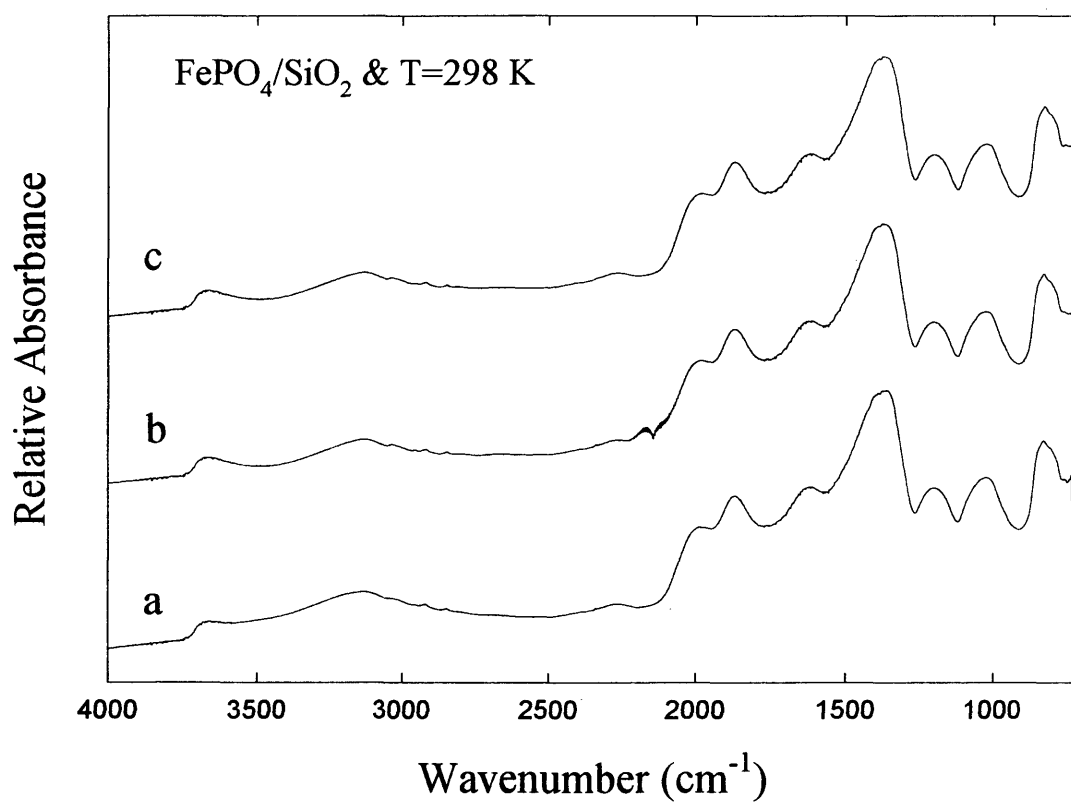


Figure A.1 IR Spectra for Carbon Monoxide adsorption over Silica Supported Iron Phosphate at T=298 K:

- a. Before adsorption, Ar was introduced for 1 hr.
- b. During adsorption, CO + O<sub>2</sub> was introduced for 1 hr.
- c. After adsorption, Ar was introduced for 1 hr.

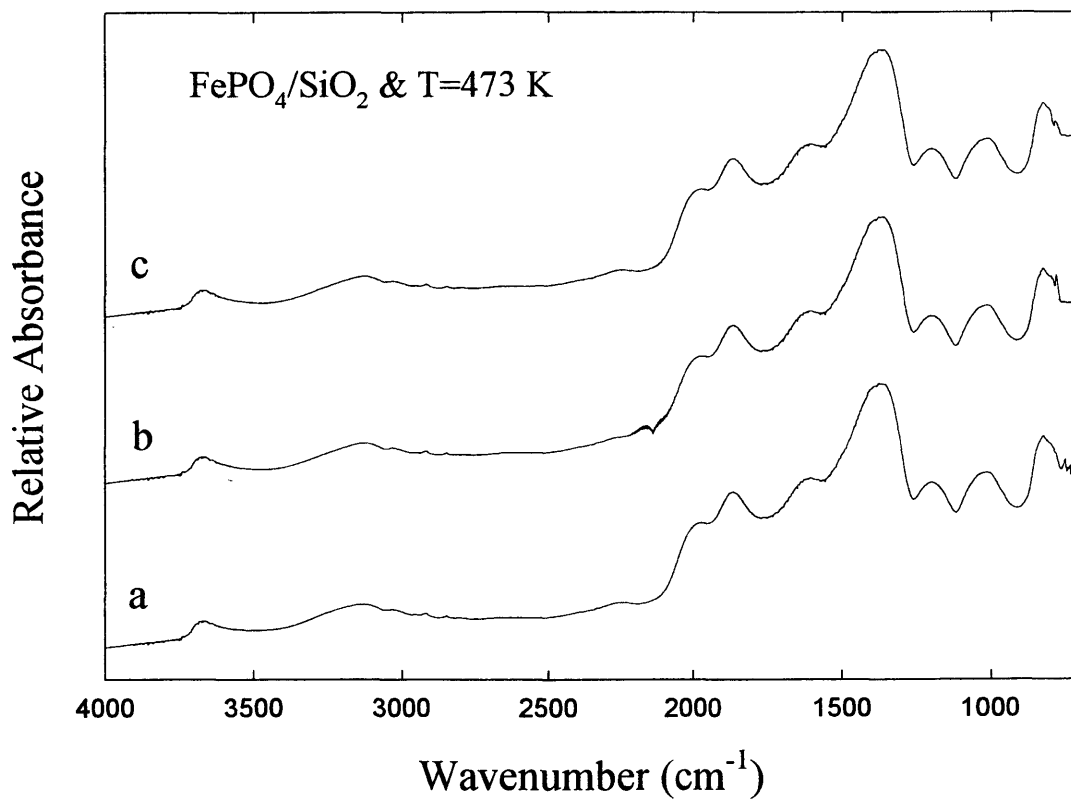


Figure A.2 IR Spectra for Carbon Monoxide adsorption over Silica Supported Iron Phosphate at T=473 K:

- a. Before adsorption, Ar was introduced for 1 hr.
- b. During adsorption, CO + O<sub>2</sub> was introduced for 1 hr.
- c. After adsorption, Ar was introduced for 1 hr.

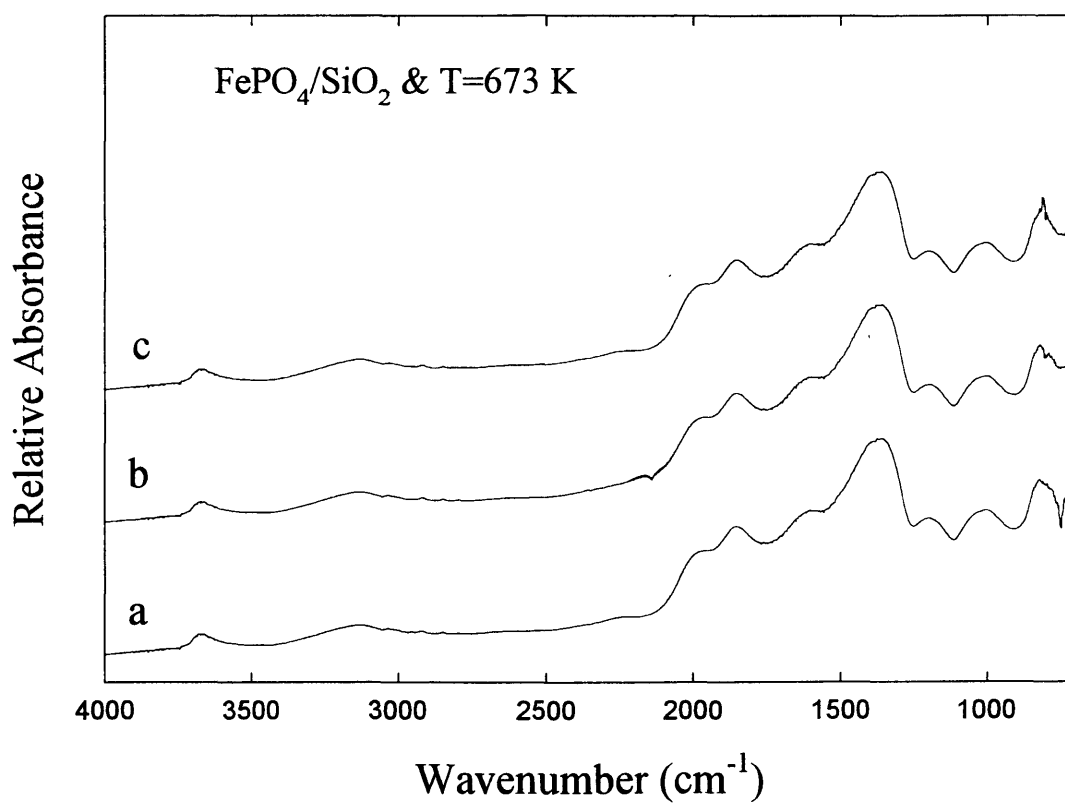


Figure A.3 IR Spectra for Carbon Monoxide adsorption over Silica Supported Iron Phosphate at T=673 K:

- Before adsorption, Ar was introduced for 1 hr.
- During adsorption, CO + O<sub>2</sub> was introduced for 1 hr.
- After adsorption, Ar was introduced for 1 hr.

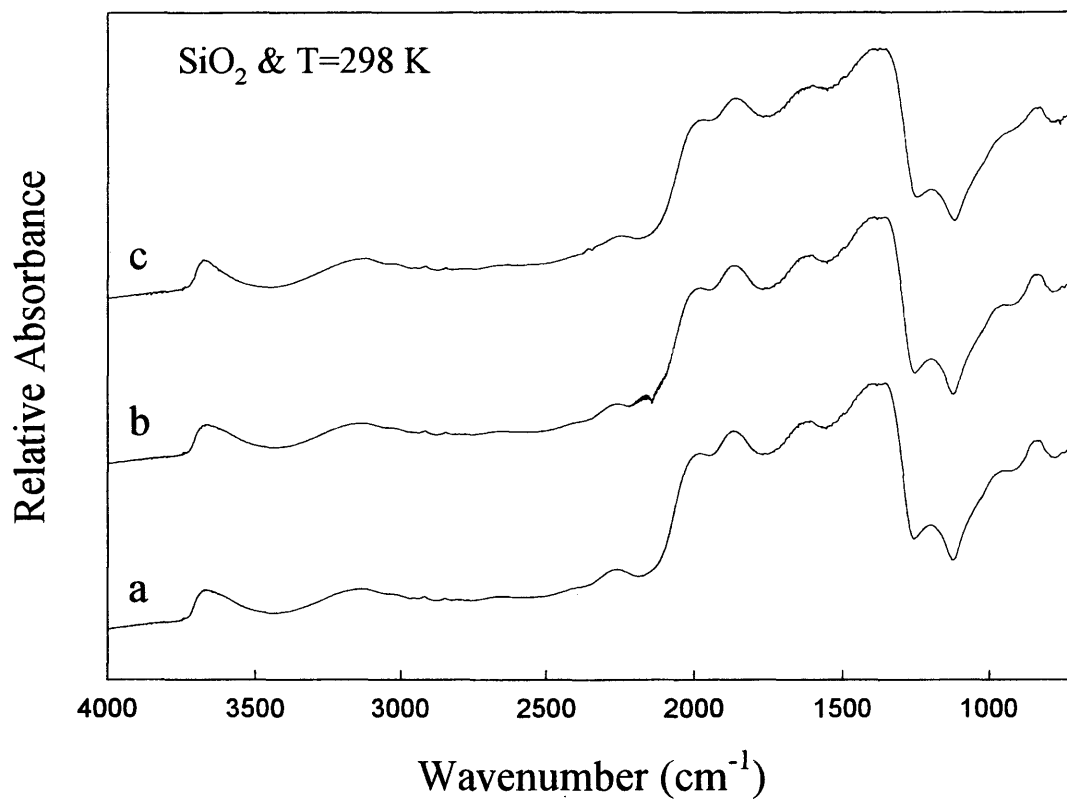


Figure A.4 IR Spectra for Carbon Monoxide adsorption over Silica at T=298 K:

- a. Before adsorption, Ar was introduced for 1 hr.
- b. During adsorption, CO + O<sub>2</sub> was introduced for 1 hr.
- c. After adsorption, Ar was introduced for 1 hr.

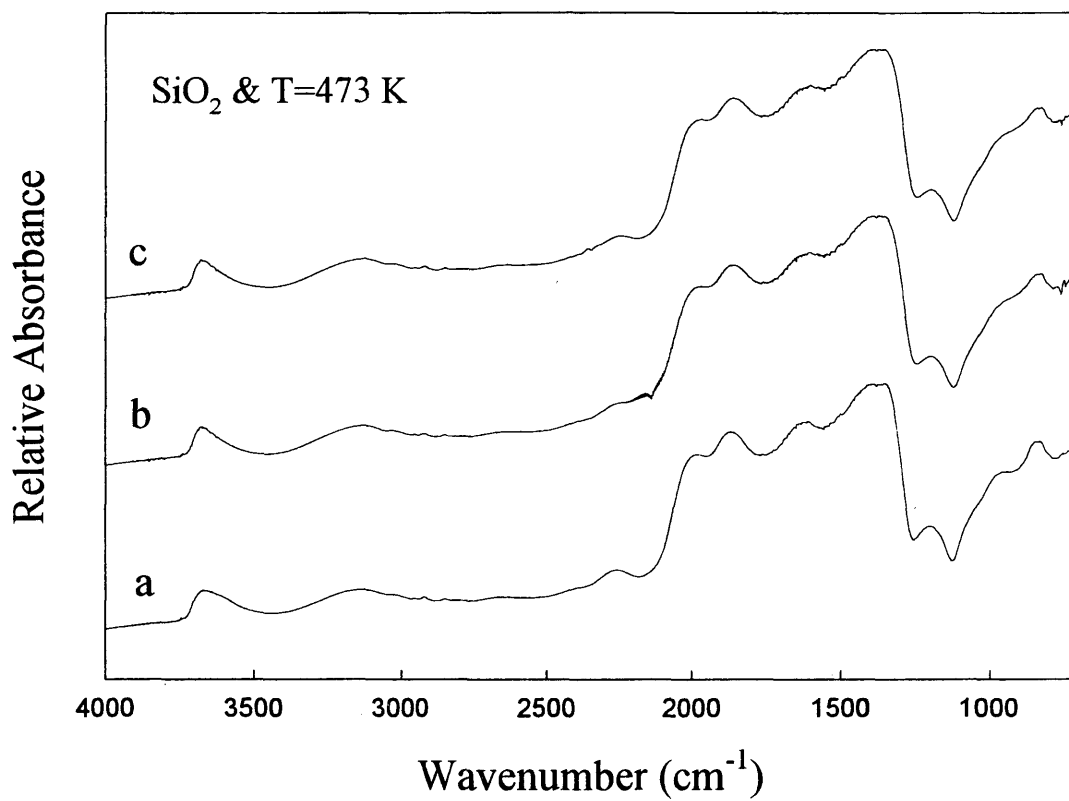


Figure A.5 IR Spectra for Carbon Monoxide adsorption over Silica at T=473 K:

- a. Before adsorption, Ar was introduced for 1 hr.
- b. During adsorption, CO + O<sub>2</sub> was introduced for 1 hr.
- c. After adsorption, Ar was introduced for 1 hr.

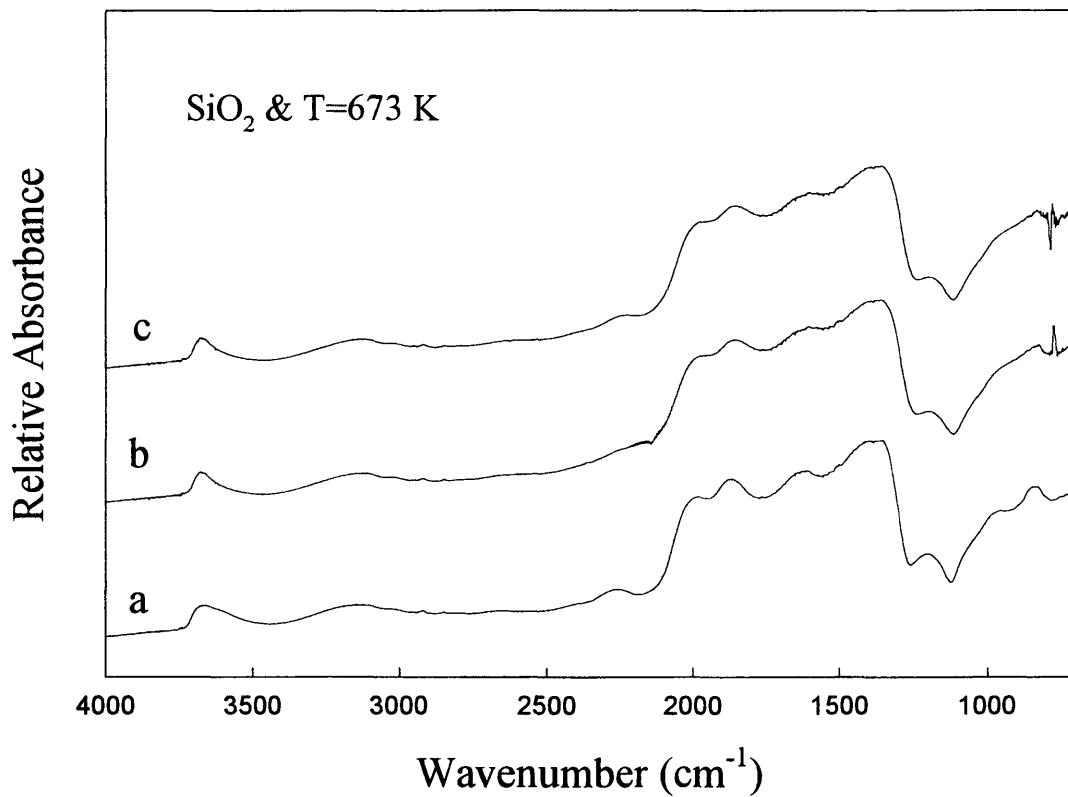


Figure A.6 IR Spectra for Carbon Monoxide adsorption over Silica at T=673 K:

- a. Before adsorption, Ar was introduced for 1 hr.
- b. During adsorption, CO + O<sub>2</sub> was introduced for 1 hr.
- c. After adsorption, Ar was introduced for 1 hr.

## APPENDIX B

Methane Partial Oxidation over Ag/SiO<sub>2</sub> and Ag-FePO<sub>4</sub>/SiO<sub>2</sub>

## **Methane Oxidation over Silver/Silica and Silver-Iron Phosphate/Silica Catalysts**

Silver was added to silica and iron phosphate/silica catalysts to accelerate surface reoxidation, proposed to be one of the controlling steps. The role of silver in oxygen adsorption and dissociation is well known in literature, Satterfield (1989).

### **B.1. Silver/Silica and Silver-Iron Phosphate/Silica Catalysts Preparation:**

Silver nitrate,  $\text{Ag}(\text{NO}_3)$  solution is used to impregnate the precipitated silica and iron phosphate/silica. First precipitated silica and iron phosphate/silica catalysts are prepared by the methods given in chapter 3. Then  $\text{Ag}(\text{NO}_3)$  is dissolved in deionized water to produce 0.5 wt.% silver solution. Impregnation is then followed by drying at 363 K and calcinations in air for 24 hrs at 973 K.

### **B.2. Catalyst Testing:**

Flow reaction studies were performed in a fixed-bed microreactor, shown in Figure 3.2. The reactor is a quartz tube, 30 cm long and 1.0 cm ID at the catalyst bed portion, mounted vertically in a tubular furnace. The catalyst samples is loaded into the reactor and covered with a layer of quartz beads to obtain a uniform gas distribution and a preheating zone. The exit diameter is decreased to 5 mm ID right after the quartz frit so the reaction products leave the heated zone more rapidly. Two K-type (chromel-alumel)

thermocouples, one placed in contact with the catalyst bed and the other right under the frit, are used to monitor the temperature.

The catalyst is heated in situ up to reaction temperature (723-923 K) in a helium flow (20 ml/min). To stay above the upper flammability limit methane is introduced into the reactor first and methane conversion is kept below 10% for all experiments reported.

Conversion and selectivity are defined as:

$$\text{Conversion} = \frac{\text{moles (HCHO + CO + CO}_2\text{) formed}}{\text{moles CH}_4\text{ fed}} \quad (3.1)$$

$$\text{Selectivity} = \frac{\text{moles HCHO formed}}{\text{moles (HCHO + CO + CO}_2\text{) formed}} \quad (3.2)$$

The overall carbon balance closures obtained are within 5 %.

The product stream is analyzed by an on-line Hewlett-Packard 5890 Gas Chromatograph (GC) equipped with a thermal conductivity detector (TCD). The flow reactor and GC system are shown in chapter 3.

### **B.3. Steady-State Reactor Results:**

Methane partial oxidation was carried out at T=848 K and atmospheric pressure. The effect of the reactant partial pressures is shown in Figure B.1 over Ag-SiO<sub>2</sub> and B.2 over Ag-FePO<sub>4</sub>/SiO<sub>2</sub>, methane partial pressure is varied between 9 to 50 kPa at constant oxygen partial pressure of 9 kPa, while oxygen pressure changed from 9 to 40 kPa at constant methane partial pressure (40 kPa). The gas hourly space velocity equal 30,000

$\text{hr}^{-1}$  and methane to oxygen ratio varied from 1 to 4. The reaction order for methane is  $0.16 \pm 0.05$  and  $0.87 \pm 0.1$  over  $\text{Ag-SiO}_2$  and  $\text{Ag-FePO}_4\text{-SiO}_2$ , respectively. On the other hand, the reaction order for oxygen is  $1.5 \pm 0.1$  and  $1.29 \pm 0.7$  over  $\text{Ag-SiO}_2$  and  $\text{Ag-FePO}_4\text{-SiO}_2$ , respectively. Figures B.3 and B.4 show the activation energy over both catalysts, over  $\text{Ag-SiO}_2$  the activation energy equals  $86 \pm 5$  kJ/mol and over  $\text{Ag-FePO}_4\text{-SiO}_2$ , equals  $120 \pm 9$  kJ/mol. Figures B.5 and B.6 present the product-conversion patterns. High methanol selectivity is observed over  $\text{Ag-FePO}_4/\text{SiO}_2$ . At low conversion,  $\text{CO}_2$  selectivity is relatively high suggesting a direct path from methane to carbon dioxide.  $\text{CO}$  selectivity is almost zero at this low conversion meaning it is mainly produced from formaldehyde oxidation. The reaction network can be presented as follow:



This network is the identical to that proposed for silica. Silver modifies the catalyst surface, may be by providing more OH groups that help in producing methanol.

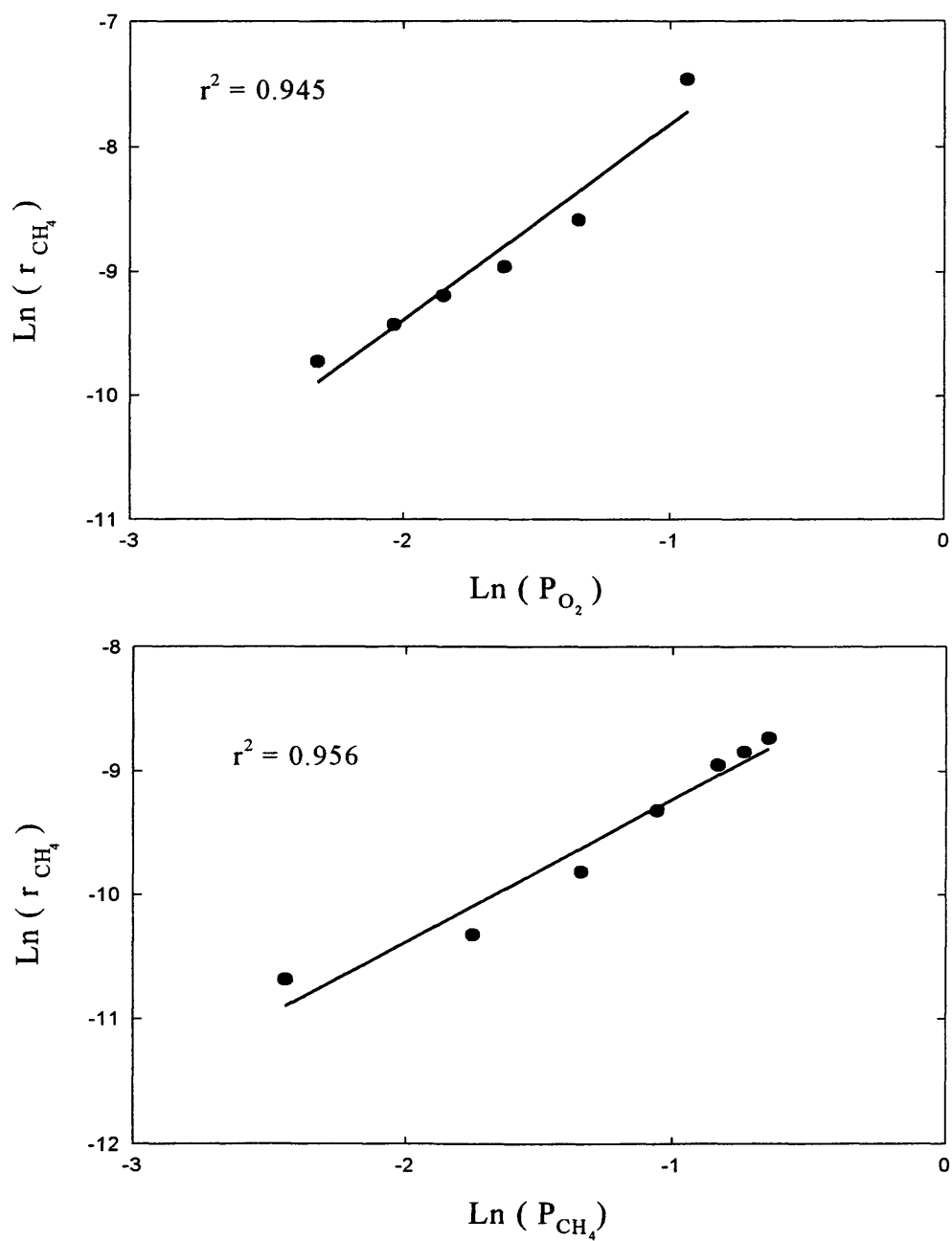


Figure B.1 Effect of reactants partial pressure on methane oxidation rate over silica. GHSV= 30000 h<sup>-1</sup>, P<sub>O<sub>2</sub></sub> = 9-40 kPa @ P<sub>CH<sub>4</sub></sub>= 40 kPa, P<sub>CH<sub>4</sub></sub> = 9-50 kPa @ P<sub>O<sub>2</sub></sub> = 9 kPa and T= 848 K.

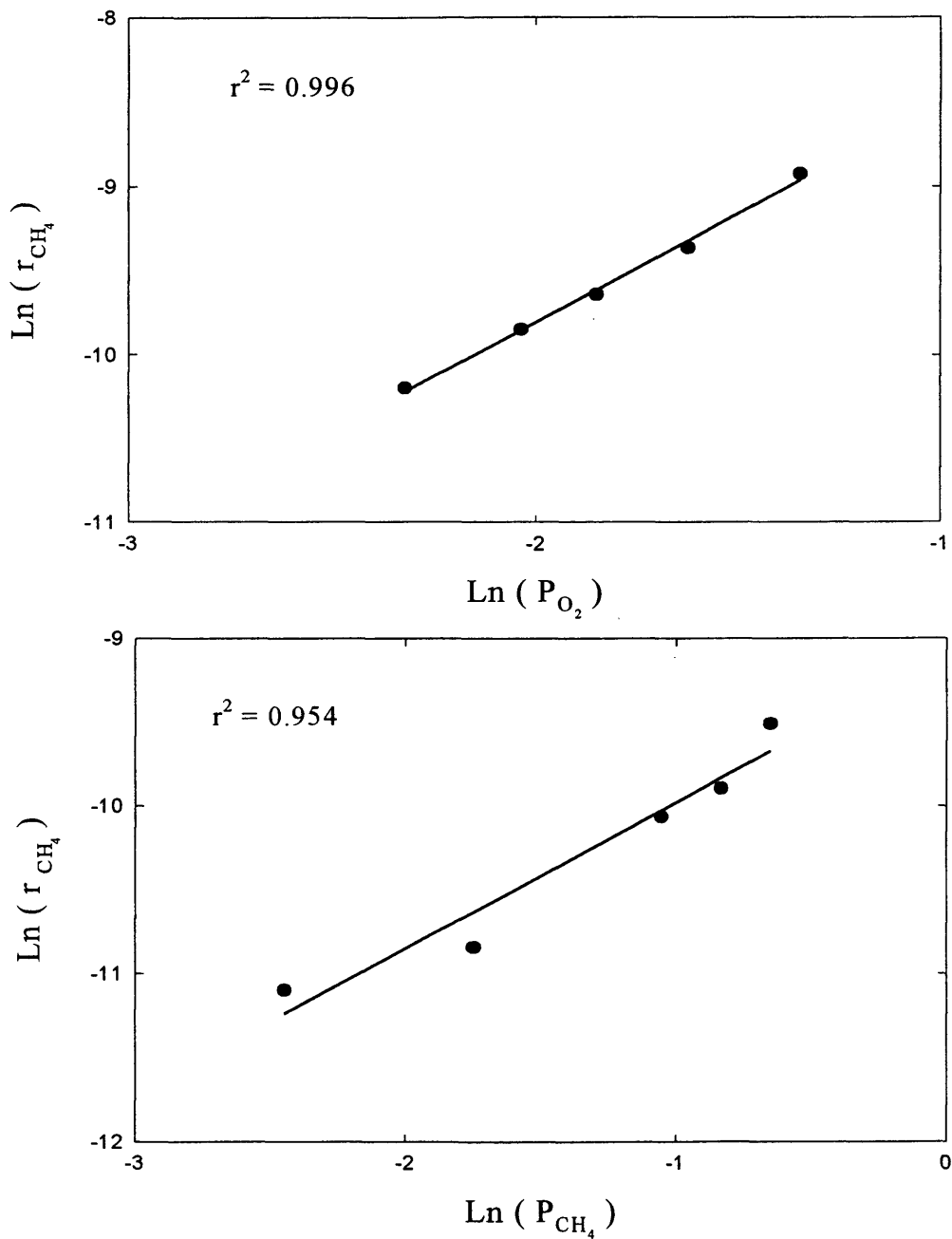


Figure B.2 Effect of reactants partial pressure on methane oxidation rate over silica supported iron phosphate. GHSV= 30000 h<sup>-1</sup>, P<sub>O<sub>2</sub></sub> = 9-40 kPa @ P<sub>CH<sub>4</sub></sub>= 40 kPa, P<sub>CH<sub>4</sub></sub> = 9-50 kPa @ P<sub>O<sub>2</sub></sub> = 9 kPa and T= 848.

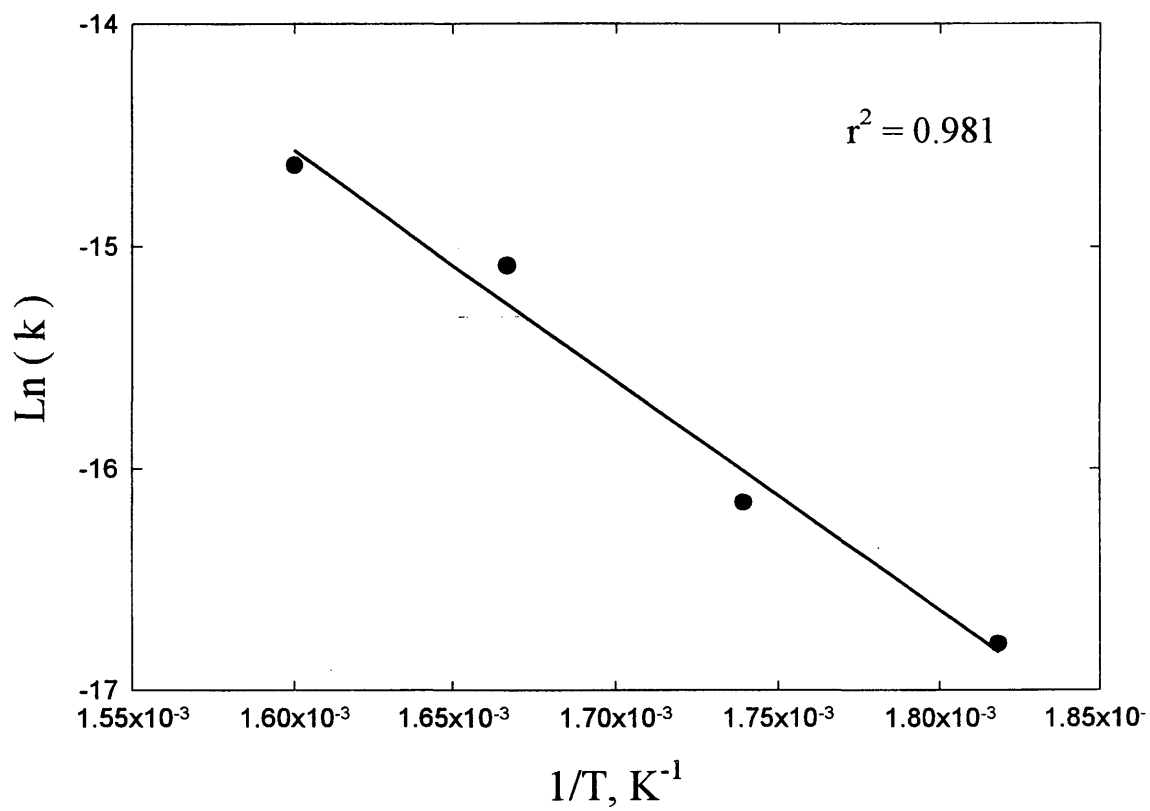


Figure B.3 Arrhenius plot for methane oxidation over silica.  $P_{\text{O}_2} = 20$  kPa,  $P_{\text{CH}_4} = 40$  kPa, and  $T = 823$ - $898$  K.

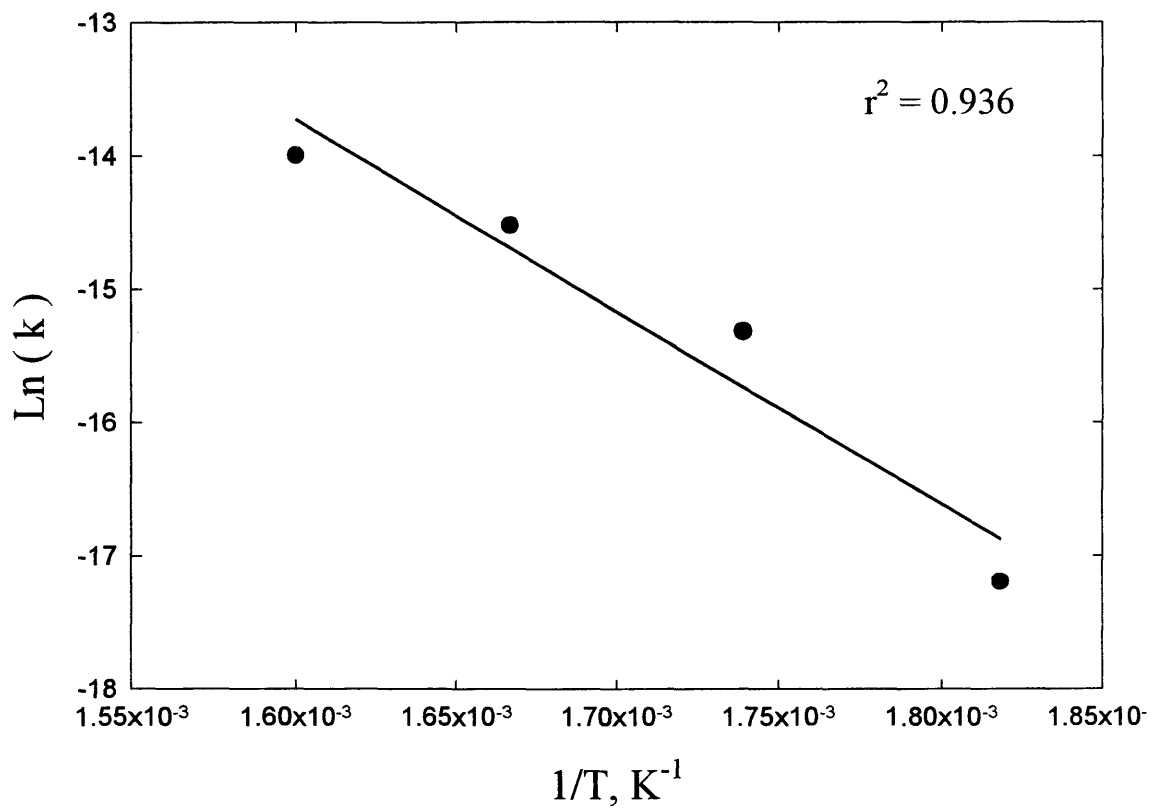


Figure B.4 Arrhenius plot for methane oxidation over silica supported iron phosphate.  $P_{\text{O}_2} = 20 \text{ kPa}$ ,  $P_{\text{CH}_4} = 40 \text{ kPa}$ , and  $T = 823\text{-}898 \text{ K}$ .

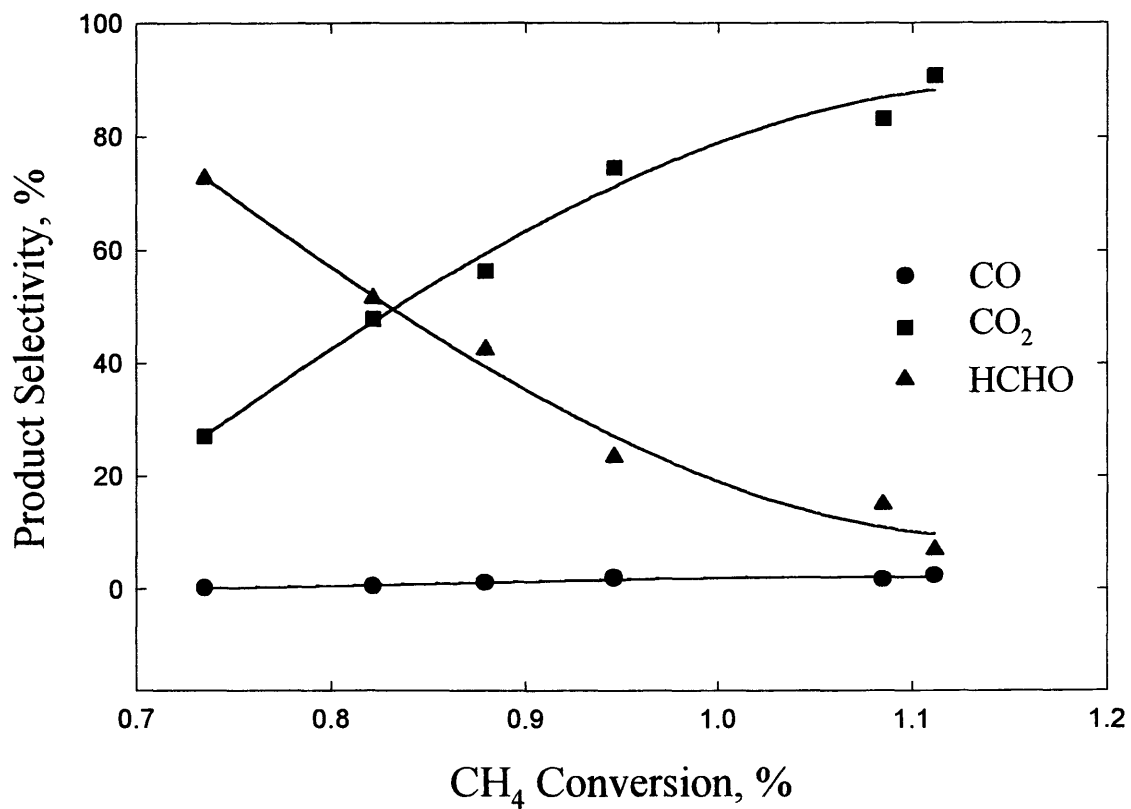


Figure B.5 Product selectivity (%) as a function of methane conversion (%) for silica. GHSV= 30000 h<sup>-1</sup>, P<sub>O<sub>2</sub></sub> = 20 kPa, P<sub>CH<sub>4</sub></sub> = 40 kPa, and T= 823-898 K.

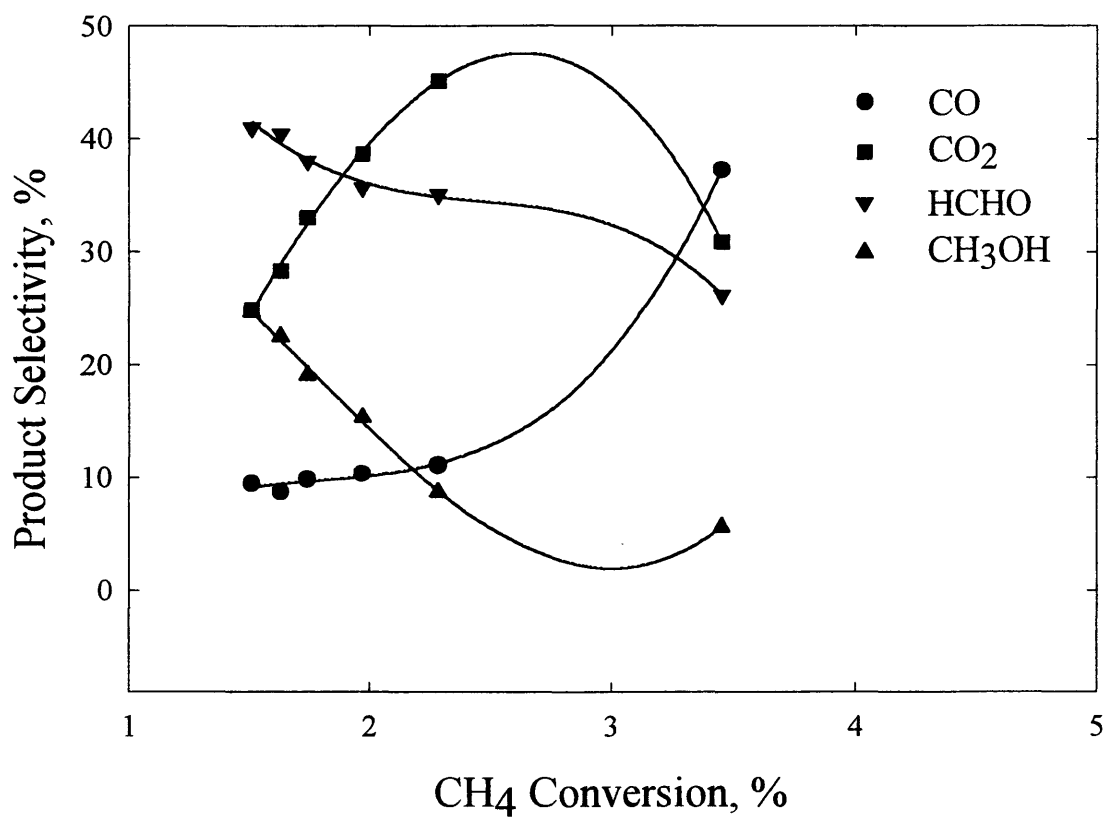


Figure B.6 Product selectivity (%) as a function of methane conversion (%) for silica supported iron phosphate. GHSV= 30000 h<sup>-1</sup>, P<sub>O<sub>2</sub></sub> = 20 kPa, P<sub>CH<sub>4</sub></sub> = 40 kPa, and T= 823-898 K.

**APPENDIX C**

**Experimental Data Used in Calculating Fractional Reduced Site Density**

Table C.1 Experimental Data Used in Calculating Fractional Reduced Site Density Over SiO<sub>2</sub> at T= 600 °C.

Conv.%	P <sub>CH<sub>4</sub>,in</sub>	P <sub>O<sub>2</sub>,in</sub>	P <sub>He</sub>	P <sub>CH<sub>4</sub>/P<sub>O<sub>2</sub></sub></sub>	Rate*	P <sub>CH<sub>4</sub>, out</sub>	P <sub>O<sub>2</sub>,out</sub>	P <sub>CO</sub>	P <sub>CO<sub>2</sub></sub>	P <sub>HCHO</sub>	P <sub>H<sub>2</sub>O</sub>
0.5	0.4	0.1	0.5	4	4.73E-05	4.04E-01	8.89E-02	5.16E-04	1.30E-03	2.43E-03	3.16E-03
0.7	0.4	0.13	0.47	3	6.62E-05	3.99E-01	1.14E-01	1.01E-03	1.70E-03	1.94E-03	1.18E-02
2.4	0.4	0.16	0.45	2.5	2.27E-04	3.47E-01	1.21E-01	1.73E-03	2.49E-03	1.52E-03	7.57E-02
5	0.4	0.2	0.4	2	4.73E-04	2.66E-01	1.44E-01	2.04E-03	3.06E-03	8.13E-04	1.84E-01
5.9	0.4	0.26	0.34	1.5	5.58E-04	1.95E-01	1.32E-01	1.84E-03	3.09E-03	6.14E-04	3.27E-01
6.8	0.4	0.4	0.2	1	6.43E-04	1.60E-01	1.87E-01	2.78E-03	5.07E-03	6.14E-04	4.45E-01
Conv.%	P <sub>CH<sub>4</sub>,in</sub>	P <sub>O<sub>2</sub>,in</sub>	P <sub>He</sub>	P <sub>CH<sub>4</sub>/P<sub>O<sub>2</sub></sub></sub>	Rate*	P <sub>CH<sub>4</sub>, out</sub>	P <sub>O<sub>2</sub>,out</sub>	P <sub>CO</sub>	P <sub>CO<sub>2</sub></sub>	P <sub>HCHO</sub>	P <sub>H<sub>2</sub>O</sub>
0.1	0.478	0.087	0.435	5.5	4.60E-04	4.58E-01	5.57E-02	8.96E-04	2.66E-03	5.55E-03	4.91E-03
0.6	0.435	0.087	0.478	5	3.03E-04	4.01E-01	5.22E-02	2.01E-03	3.54E-03	4.51E-03	5.59E-03
1.4	0.348	0.087	0.565	4	1.50E-04	3.31E-01	5.47E-02	3.44E-03	4.61E-03	4.68E-03	8.31E-03
1.8	0.26	0.087	0.652	3	8.79E-05	2.51E-01	5.31E-02	3.86E-03	4.93E-03	2.92E-03	9.06E-03
2.9	0.174	0.087	0.739	2	2.51E-05	1.62E-01	5.39E-02	4.88E-03	6.60E-03	2.80E-03	1.27E-02
4	0.087	0.087	0.826	1	2.08E-06	8.10E-02	4.76E-02	5.60E-03	7.23E-03	2.20E-03	2.93E-02

\* Methane Oxidation in mol/(g<sub>cat</sub>.s)

Pressure in Atmospheres

Table C.2 Experimental Data Used in Calculating Fractional Reduced Site Density over  $\text{FePO}_4/\text{SiO}_2$  at  $T=600\text{ }^\circ\text{C}$ .

Conv.%	$P_{\text{CH}_4,\text{in}}$	$P_{\text{O}_2,\text{in}}$	$P_{\text{He}}$	$P_{\text{CH}_4}/P_{\text{O}_2}$	Rate*	$P_{\text{CH}_4,\text{out}}$	$P_{\text{O}_2,\text{out}}$	$P_{\text{CO}}$	$P_{\text{CO}_2}$	$P_{\text{HCHO}}$	$P_{\text{H}_2\text{O}}$
0.5	0.374	0.0934	0.533	4	4.49E-05	3.92E-01	5.81E-02	1.45E-04	4.06E-04	1.34E-03	1.54E-02
0.6	0.374	0.124	0.502	3	5.56E-05	3.84E-01	9.18E-02	1.56E-04	6.28E-04	1.85E-03	1.93E-02
0.8	0.374	0.15	0.477	2.5	7.14E-05	3.90E-01	1.02E-01	3.51E-04	8.17E-04	1.96E-03	2.75E-02
1.2	0.374	0.187	0.44	2	1.09E-04	3.83E-01	1.34E-01	8.06E-04	1.10E-03	2.93E-03	3.88E-02
6.69	0.374	0.25	0.374	1.5	6.01E-04	2.47E-01	1.76E-01	7.61E-03	2.05E-03	7.83E-03	1.86E-01
10.86	0.374	0.374	0.25	1	9.75E-04	2.13E-01	1.32E-01	1.75E-02	3.70E-03	5.74E-03	3.78E-01
Conv.%	$P_{\text{CH}_4,\text{in}}$	$P_{\text{O}_2,\text{in}}$	$P_{\text{He}}$	$P_{\text{CH}_4}/P_{\text{O}_2}$	Rate*	$P_{\text{CH}_4,\text{out}}$	$P_{\text{O}_2,\text{out}}$	$P_{\text{CO}}$	$P_{\text{CO}_2}$	$P_{\text{HCHO}}$	$P_{\text{H}_2\text{O}}$
0.1	0.447	0.081	0.472	5.5	1.96E-06	4.48E-01	6.56E-02	0.00E+00	4.46E-04	7.12E-04	1.32E-02
0.25	0.406	0.081	0.531	5	1.46E-05	4.05E-01	5.07E-02	1.73E-05	2.99E-04	5.78E-04	1.23E-02
0.6	0.325	0.081	0.593	4	4.69E-05	3.27E-01	6.09E-02	1.25E-04	4.60E-04	1.38E-03	1.68E-02
0.95	0.244	0.081	0.675	3	9.26E-05	2.73E-01	4.04E-02	1.30E-04	2.77E-04	9.31E-04	1.07E-02
1.3	0.162	0.081	0.757	2	1.40E-04	1.17E-01	3.94E-02	1.39E-04	1.95E-04	5.87E-04	8.57E-02
1.85	0.081	0.081	0.827	1	2.17E-04	9.96E-02	4.38E-02	7.34E-04	5.71E-04	1.63E-03	2.66E-02

\* Methane Oxidation in  $\text{mol}/(\text{g}_{\text{cat}}\cdot\text{s})$ 

Pressure in Atmospheres

## APPENDIX D

### Numerical Quadrature Method

Gay (1970) presented the numerical quadrature method as a tool to analyze reaction kinetic experiments. The method is better explained via an example, consider the following first order reaction:



This system leads to the following differential equation (assuming plug flow reactor):

$$\frac{dC_A}{dt} = -kC_A \quad (D.2)$$

If equation (D.2) is multiplied by dt and integrated from 0 to any time t, one obtains:

$$C_A - C_{A0} = -k \int_0^t C_A dt \quad (D.3)$$

Where  $C_{A0}$  is the initial concentration of reactant A.

This integral can be evaluated for every experimental point by a graphical or numerical method then used to estimate k. let:

$$X = \int_0^t C_A dt \quad (D.4)$$

then,

$$C_A - C_{A0} = -kX \quad (D.5)$$

or,

$$k = \frac{C_{A0} - C_A}{X} \quad (D.6)$$